The spin evolution of accreting and radio pulsars in binary systems
Nielsen, A.B.

Citation

Nielsen, A. B. (2018, September 13). *The spin evolution of accreting and radio pulsars in binary systems*. Retrieved from https://hdl.handle.net/1887/65380

Cover Page

The handle http://hdl.handle.net/1887/65380 holds various files of this Leiden University dissertation.

Author: Nielsen, A.B.
Title: The spin evolution of accreting and radio pulsars in binary systems
Issue Date: 2018-09-13

Spin evolution of accreting and radio pulsars in binary systems

Ann-Sofie Bak Nielsen

Spin evolution of accreting and radio pulsars in binary systems

Proefschrift

ter verkrijging van
de graad van Doctor aan de Universiteit Leiden,
op gezag van Rector Magnificus prof. mr. C.J.J.M. Stolker,
volgens besluit van het College voor Promoties
te verdedigen op donderdag 13 September 2018
klokke 12.30 uur

door

Ann-Sofie Bak Nielsen

geboren te Odense, Denmark
in 1990

An electronic version of this thesis can be found at openaccess.leidenuniv.nl

To the women who inspire me.

Contents

1

Introduction

Neutron stars were mentioned for the first time by Baade & Zwicky (1934) as the end products of massive stars, after a supernovae explosion. The first pulsar was discovered in 1967, at Cambridge University, by Jocelyn Bell Burnell and Anothony Hewish (Hewish et al. 1968). This was, early on, used as the proof of the existence of neutron stars. The discovery led to the Nobel prize in physics awarded to Anthony Hewish and Martin Ryle in 1974. With the detection of the first pulsar followed multiple new discoveries, e.g. the double pulsar system, B1913+16, discovered by Russel Hulse and Joseph Taylor in 1974 (Hulse & Taylor 1975). This binary pulsar was used as an astrophysical laboratory to demonstrate the existence of gravitational waves. Indeed it could be shown that the orbital period of the binary was decaying, following the prediction of general relativity, due to loss of angular momentum carried away by gravitational waves. Russel Hulse and Joseph Taylor were awarded the Nobel prize in physics in 1993. Since these two ground breaking discoveries the pulsar zoo has been expanded to include accreting systems that show pulsations in X-ray and systems that show pulsations in both γ-rays and optical (Wijnands & van der Klis 1998; Shearer & Golden 2002; Smith et al. 2017). With this thesis I study some of the peculiar and puzzling behaviors we observe in binary systems with a pulsar.

1.1   Formation of neutron stars

Neutron stars are some of the most extreme objects in our Universe and they form through a violent process. Towards the end of the evolution of a high mass star, the star transforms silicon to iron in the core, and when the mass of the iron core exceeds the Chandrasekhar limit of $\lesssim 1.4\,M_\odot$, the core starts to collapse (Heger & Woosley 2003; Rosswog & Brüggen 2011). The initial collapse of the core happens so quickly that the outer layers of the star are not immediately affected. The core rebounds from the collapse and sends out a shock wave through the star. This shock wave is the supernova explosion, that disrupts the star, and it is only at this point that the outer layers of the star are affected (Rosswog & Brüggen 2011). The above is a rough description of a core-collapse supernova explosion. The remnants of these supernova explosions are either neutron stars or black holes. For the purpose of this thesis I will focus on neutron star remnants only.

Neutron stars formed in core-collapse supernova are thought to have a high initial spin, close to the break-up spin limit (Heger & Woosley 2003; Heger et al. 2004). Unevolved massive stars rotate fast, at around $200\,\mathrm{km\,s^{-1}}$ (Heger et al. 2004). The contraction of the core, leading up to the supernova explosion, leads to faster rotation, but other processes play a role in the rotation of the core, such as e.g. viscosity and the magnetic field, which leads to a loss of angular momentum (Heger & Woosley 2003). The initial spin of neutron stars are possibly as low as 7-140 ms (Migliazzo et al. 2002; Kramer et al. 2003). The typical size of a neutron star is assumed to be around 20 km in diameter and with a mass somewhere between 1.1-2.5 $M_\odot$, although for simplicity it is often assumed to be around the Chandrasekhar limit of $1.4\,M_\odot$ (Lattimer & Prakash 2007; Lorimer & Kramer 2012; Tauris 2016).

1.2   Pulsars

The zoo of pulsars spans several wavelength regimes, from γ-ray to radio. Common to all pulsars is the geometry of the neutron star. It has a magnetic field, which is misaligned with respect to the rotation axis (see Fig. 1.1). The offset between the magnetic field poles and rotation axis is the reason why we observe pulsations, as long as the emission cone is in our line of sight. The pulses are generated by the modulation of the emitted radiation and not created by distortions of the neutron star itself.

1.2.1   Accreting X-ray Pulsars

If a neutron star is formed in a binary system, with a non-degenerate companion star, it is possible that this system will become an X-ray pulsar binary (Frank et al. 2002). In some X-ray binaries the companion is able to transfer material onto the neutron star. This happens through one of two scenarios, either Roche lobe overflow or wind accretion. Roche lobe overflow, which is often the mechanism in
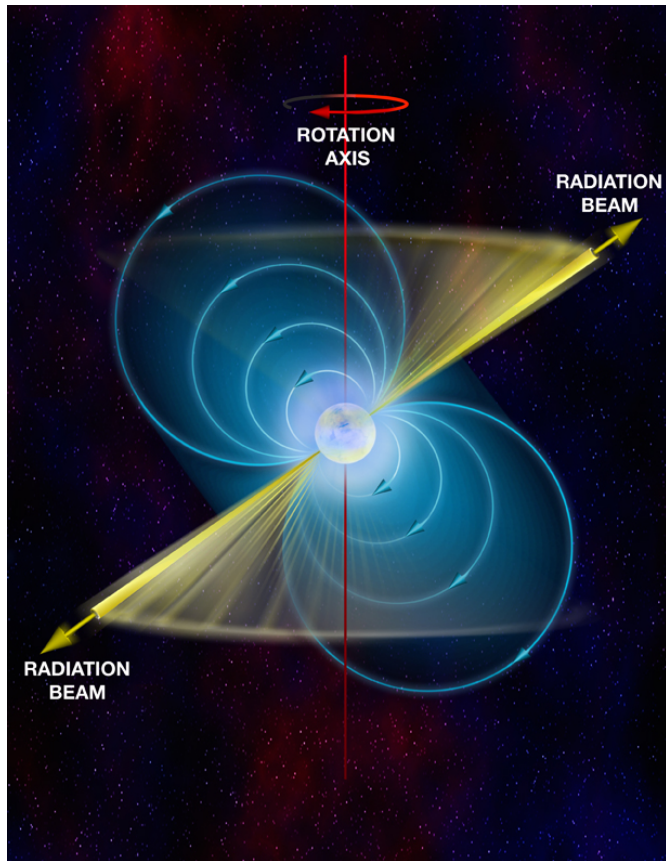
Figure 1.1: The basic geometry of a pulsar, where the magnetic field axis (north/south pole of the magnetic field) is misaligned with the rotational axis of the neutron star. Image credit: Bill Saxton, NRAO/AUI/NSF.

low mass X-ray binaries, can have three different causes: 1) the companion star expands on a nuclear evolution timescale, 2) the orbit shrinks, which is due to loss of angular momentum, by either magnetic breaking or gravitational radiation or 3) some other effects are present, e.g. mass ejection or spin-orbit coupling. Wind accretion happens when the donor star, during its stellar evolution, ejects some mass as a stellar wind, and parts of this material is captured by the neutron star and accreted onto the surface (Frank et al. 2002). Wind accretion is the accretion mechanism for pulsars in high mass X-ray binaries, and often also in symbiotic X-ray binaries. Due to the strong magnetic field of neutron stars, of $\sim 10^{7-15}$G, the accreted material will be channeled onto the magnetic poles of the neutron star, and material will fall on to the poles and not evenly spread out over the neutron star surface, creating hot spots. Due to the material falling onto the neutron star surface, energy is released, corresponding to ~ 200 MeV/baryon (Frank et al. 2002). If, as shown on Fig. 1.1, the magnetic axis and the rotation axis are misaligned, then it should be possible to detect the heated polar caps as X-ray pulses at a certain spin frequency. The accretion mechanism is though to be the driving force that spins up pulsars to milliseconds and reduce the magnetic field. It is not well known how the magnetic field decreases, but ideas range from simple decays to a burial of the magnetic field due to the accreted material (Taam & van den Heuvel 1986; Romani 1990; Cumming et al. 2001). Broadly speaking there are three types of X-ray pulsars; low mass X-ray binaries (LMXBs), high mass X-ray binaries (HMXBs) and intermediate mass X-ray binaries (IMXBs).

Low Mass X-ray Binaries

The first confirmed low mass X-ray binaries was discovered about ~ 50 years ago by Webster & Murdin (1972). Since then around 200 LMXBs have been discovered, however, pulsations are only observed in relatively few systems, which counts about 21 accreting millisecond X-ray pulsars (AMXPs), about 10 nuclear powered pulsars (powered by nuclear burning rather than accretion) and about 4 of the slower pulsars (e.g. 2A 1822−371, 4U 1626−67, GRO 1744−28 and Her X−1) (Wijnands & van der Klis 1998; Chakrabarty & Morgan 1998; Patruno & Watts 2012). The LMXB pulsar population is found to be in binaries with orbital periods between a few days, for the widest systems, to a few minutes, for the ultra compact systems (Patruno & Watts 2012). The companion mass in the LMXBs is $\leq 1.0\,\mathrm{M_\odot}$ (Xu & Li 2007). The accretion process in LMXBs occurs via Roche lobe overflow and the creation of an accretion disc. The donor star in LMXB systems varies from main sequence stars, white dwarfs (WDs) and brown dwarfs (BDs). The typical magnetic field for LMXB pulsars is around 10^{11-13} G for the slow spinning pulsars and 10^{8-9} G for the AMXPs.

The accretion disc mechanism

When accretion onto a neutron star happens via Roche lobe overflow (see Fig. 1.2), the binary orbit is close to circular and the orbital period is described by
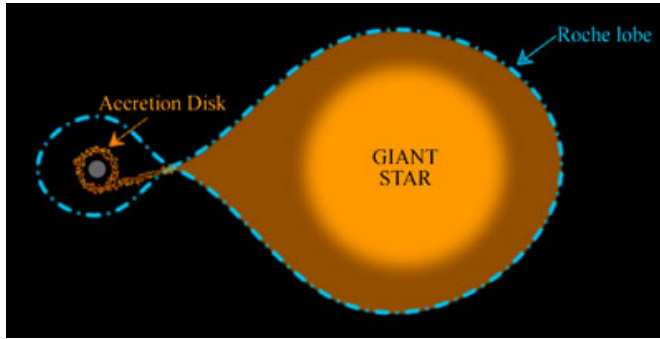
Figure 1.2: Roche Love overflow happens when the companion star expands beyond the Roche lobe, within which the material is gravitationally bound to the star. The overflow can then create an accretion disc around the neutron star. Image credit: Cosmos - Swinburne University.

keplerian motion:

$$P = 2\pi\sqrt{\frac{a^3}{GM_{tot}}} \tag{1.1}$$

where M_{tot} is the total mass of the two stars in the binary, a is the semi-major axis and G is the gravitational constant.

The Roche lobe overflow happens when the companion star fills out its Roche lobe and expands beyond the Roche lobe border, see Fig. 1.2. When the overflow happens, material is no longer gravitationally bound to the companion star, and it is free to pass through the first Lagrangian point and accrete onto the neutron star (Frank et al. 2002).

The material that is accreted carries a specific angular momentum, J. Due to the angular momentum, the material is not falling directly onto the neutron star, but settles in a disc around the neutron star. If gas pressure dominates the structure of the disc, then a geometrically thin and optically thick disc will be formed. This is known as an "α-disc" (Shakura & Sunyaev 1973; Ghosh & Lamb 1979). The optically thick and geometrically thin disc has a scale height, H, which is smaller than the radial extension of the disc. The viscosity (fluidity) of the α-disc is given by $\nu = c_s H$, where c_s is the speed of sound (Shakura & Sunyaev 1973). The disc rotates at a near Keplerian frequency,

$$\nu_K(r) = \frac{1}{2\pi}\sqrt{\frac{GM_{NS}}{R^3}} \tag{1.2}$$

M_{NS} is the mass of the neutron star and R is the radius of the gas element rotating in the disc. The accretion disc experiences turbulent viscosity and in that way the accretion disc losses energy through thermal emission and angular momentum is transported outwards. This will allow for material from the disc to spiral in towards the neutron star. The accretion flow in the inner regions of the

accretion disc is disrupted by the dipole magnetic field of the neutron star, which is described by $B \sim \frac{\mu}{R_{NS}^3}$, where μ is the magnetic moment. Accretion transfers angular momentum from the disc to the neutron star, and spins it up. The spin-up of a pulsar scales with the amount of mass that is accreted onto the star by $\dot{\nu} \propto \dot{M}_{acc}^{6/7}$, where $\dot{\nu}$ is the spin frequency derivative and $\dot{M}_{acc}$ is the rate at which the neutron star accretes material (Bildsten et al. 1997). For systems that become millisecond pulsars, the spin-up process is often referred to as the recycling scenario (Alpar et al. 1982).

Symbiotic X-ray Binaries

Symbiotic X-ray binaries (SyXBs) are a subclass of LMXBs, where the companion star is a post-main sequence low mass star (Kuranov & Postnov 2015). Most symbiotic X-ray binaries have a white dwarf (WD) primary star (Lü et al. 2012), however, a few systems do have a neutron star primary, e.g. GX 1+4 (See Chapter 3 of this thesis). The systems with a WD primary are only modest X-ray emitters (Corbet et al. 2008). SyXBs show flaring activity, which is typical for systems accreting from a stellar wind. This seems to be the case for e.g GX 1+4 (González-Galán et al. 2012; Kuranov & Postnov 2015).

High Mass X-ray Binaries

More than 100 high mass X-ray binaries are known in our Galaxy (Chaty 2011). HMXBs usually have a high mass OB type donor star, with a mass above $10\,M_\odot$ (Xu & Li 2007; Chaty 2011). Accretion in HMXBs typically happen through a slow and dense wind that the massive donor star expels. In rare occasions the HMXBs can form an accretion disc. A sub-class of HMXB are the so called Be X-ray binaries. They typically have a neutron star in a wide and eccentric orbit around a B0-B2e type star (this type of star show emission lines). The Be/X-ray binaries have a circumstellar disc or rather a de-cretion disc, where the neutron star passes through, and accretes material (Chaty 2011). In some Be/X-ray binaries the pulsar, is able to form and maintain an accretion disc, even after it leaves the de-cretion disc of the Be-star (See e.g. Chapter 4 of this thesis). The Be/X-ray binary pulsars typically exhibit type I and type II outbursts. The type I are periodic and come from the neutron star crossing the decreation disc. The type II outbursts are brighter and happen at any phase (Chaty 2011). There are about 50 known Be/X-ray binaries in our Galaxy.

Intermediate Mass X-ray Binaries

Intermediate mass X-ray binaries are systems with a donor star mass between the LMXBs and HMXBs, so about 1.0-10 $M_\odot$ (Xu & Li 2007). There are only very few IMXBs observed, due to mass transfer via Roche lobe overflow being

rapid and unstable for IMXBs. The instability is mostly due to the large mass ratio of the stars in the binary, which will lead to a common envelope and in-spiral phase (Xu & Li 2007). The mass transfer in IMXBs is so unstable and fast, that it is expected to happen on a dynamical/thermal timescale. The accretion is thought to occur via an accretion disc, as the donor stars in this mass regime are not able to create strong winds that could account for the X-ray emission from the pulsar (van den Heuvel 1975; Xu & Li 2007). There is some evidence that suggests, that some of the companion stars of LMXBs could originate from an IMXB donor star. This is due to high intrinsic luminosity of the current low mass donor star, and that it is simply easier for a higher mass donor star to keep the neutron star in a binary system after the supernova explosion (Podsiadlowski et al. 2002).

1.2.2 Radio Pulsars

Radio pulsars cover a variety of different sources from isolated slow pulsars to millisecond pulsars in binary systems. A typical way to classify radio pulsars is with the $P - \dot{P}$ diagram, which shows the spin period (P) vs. the spin period derivative ($\dot{P}$) of radio pulsars. In the top right corner of Fig. 1.3 the young pulsars are found. These are often isolated systems, and the spin of the young pulsars is thought to be close to their birth spin (Lorimer & Kramer 2012). The young pulsars often have a high spin down rate due to the loss of their rotational kinetic energy via electromagnetic wave radiation and relativistic particle outflow. They are thought to spin down and end up in the graveyard zone, where it is predicted by theoretical models that radio pulsars will not exist. If the pulsar is in a binary system, with a companion star that will evolve to fill its Roche lobe, then the pulsar could spin up to become a millisecond pulsar (MSP), as the ones seen in the lower left corner on Fig. 1.3. These do not only have a faster spin, they also have a lower magnetic field and are old systems (Smarr & Blandford 1976; Srinivasan & van den Heuvel 1982; Manchester 2017).

The radio MSPs are believed to have formed through a recycling scenario, where pulsars are spun up through accretion (and thus angular momentum transfer) onto the neutron star in a LMXB (Alpar et al. 1982; Bhattacharya & van den Heuvel 1991).

The age and magnetic field of the $P - \dot{P}$ diagram is inferred from $\tau \propto P/\dot{P}$ and $B \propto \sqrt{P\dot{P}}$. In Fig. 1.3 the spin down luminosity is also indicated, and this is usually given by $\dot{E} \propto \dot{P}/P^3$, which is the rate at which the rotational energy is lost (Lorimer & Kramer 2012). The initial spin periods of pulsars are related to the spin period of the progenitors core, which is not well known (Faucher-Giguère & Kaspi 2006).

1.2.3 Spiders & Recycled Pulsars

Part of the binary millisecond pulsar population are found to be in close binaries, with an orbital period (P_b) $\lesssim 24$ hr, and have relatively small companion stars (Chen et al. 2013). These systems are thought to ablate their companion star by
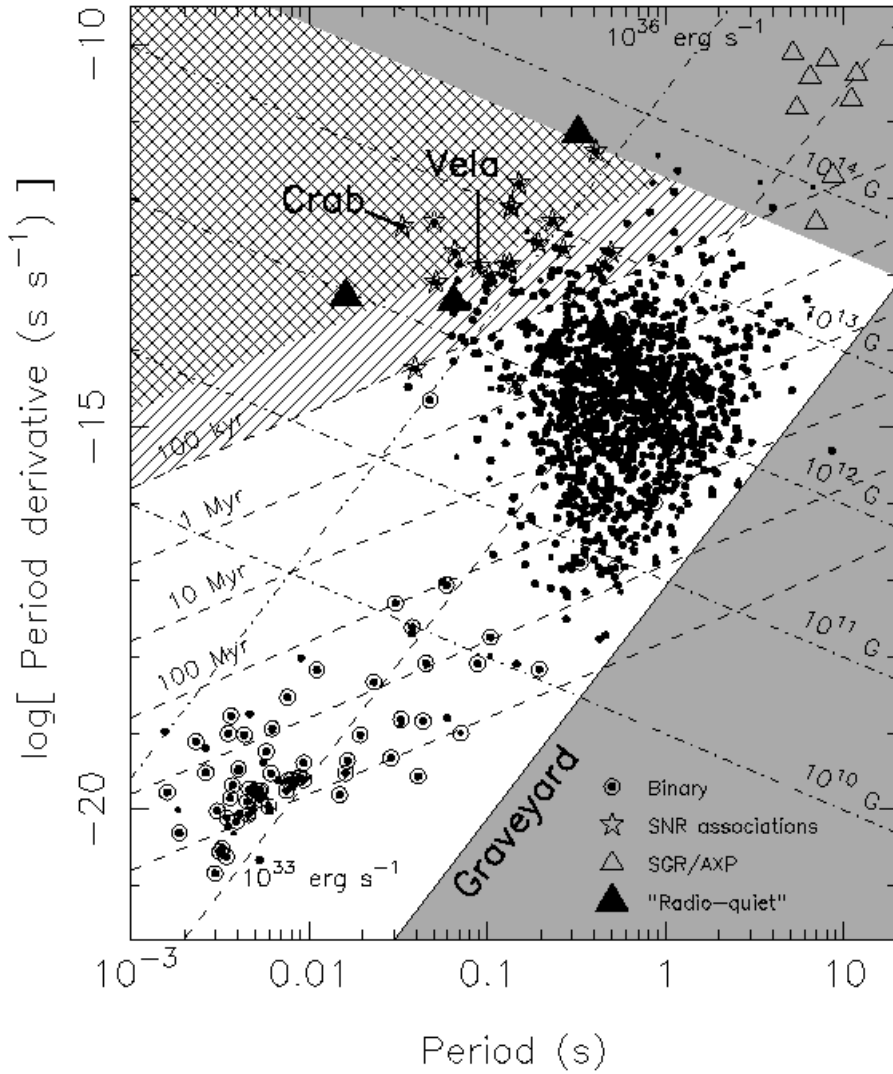
Figure 1.3: The P-$\dot{P}$ diagram of known radio pulsars. The upper area is occupied by the slow young radio pulsars and in the bottom left the old, recycled pulsars are shown. The dark grey areas are the graveyard zone for radio pulsars, within which very few radio pulsars are found. Image credit: Lorimer, D. & Kramer, M. - Handbook of Pulsar Astronomy, 2012

the pulsar electromagnetic radiation or the relativistic wind of the pulsar (Kiel & Taam 2013). The two types of spider systems, so called due to the ablation of the companion, are redback pulsars (RBPs) and black widow pulsars (BWPs). Some of the RBPs and BWPs show radio eclipses due to the outer layers of the companion star and the ablated material surrounding the companion star (Fruchter et al. 1988).

The general idea of the recycling mechanism is that pulsars in binary systems will, through accretion onto the neutron star, spin up the pulsar to millisecond spins. The spin-up happens through transfer of angular momentum in the accreted material. Furthermore, another part of the recycling scenario is that the magnetic field of the pulsar decreases (Alpar et al. 1982).

The spin period of recycled pulsars span 1.4-200 ms (Tauris 2016; Swiggum et al. 2015). The pulsar's spin is correlated with the mass of the companion star. The more massive and evolved the companion is when mass transfer begins, the slower the spin rate of the recycled pulsar will be. This is due to the mass transfer being much shorter for massive and evolved stars than for low mass stars (Tauris 2016).

Black Widow Pulsars

Black widow pulsars typically have small companion stars of less than $M_2 < 0.1\,M_\odot$ and a small magnetic field of $\sim 10^{8-9}$ G. The companion star is a semi-degenerate star, assumed to be similar to a brown dwarf (Chen et al. 2013). The first BWP was observed by Fruchter et al. (1988), since then about 40[1] systems have been found. The first two BWPs discovered, e.g. PSRs B1957+20 and J2051$-$0827, are unstable. The instability means that it is only possible to create a coherent, stable timing solution for short periods of time, months to years (Shaifullah et al. 2016; Lazaridis et al. 2011). There does, however, seem to be some BWPs that are stable, e.g. PSR J0023+0923, J2234+0944 and 2214+3000 (Arzoumanian et al. (2018) and Chapter 5 in this thesis).

Dependent on the size and configuration of the orbital period, the pulsar wind can interact with the ablated material form the companion star, and this produces an intra-binary shock, whose orientation can change with respect to the orbital phase. This is what creates the obscuration of the pulsed radio emission during the radio eclipses for some of the BWPs and RBPs (Roberts 2011).

Redback Pulsars

The first redback pulsar was found by D'Amico et al. (2001), and since then around 20 RBPs have been found. The RBPs have slightly larger companion masses than

---

[1]see e.g. `https://apatruno.wordpress.com/about/millisecond-pulsar-catalogue/` for both BWPs and RBPs.

the BWPs, of about 0.1-0.4 $M_\odot$ and the same low magnetic fields of about 10^{8-9} G (Chen et al. 2013). RBPs also differ from the BWPs with their less evolved companions. The companions are non-degenerate, suggesting that the RBPs are in the late stages of recycling (Roberts 2011). In 2009 a pulsar was discovered that linked the recycled pulsars to the LMXBs. It was PSR J1023+0038, which turned out to be a transitional system (Archibald et al. 2009; Roberts 2013). Transitional systems are binarys systems with a pulsar, that switch from being a LMXB to a radio pulsar in a cyclic way (Archibald et al. 2009; Papitto et al. 2013; Bassa et al. 2014; Roy et al. 2015). Observations from 2001 showed emission lines that indicated the presence of an accretion disc. In 2004 the emission lines were gone and radio pulsations were discovered (Roberts 2013).

1.3   Techniques

Timing of pulsars is a technique that tracks the time of arrivals (TOAs) of pulsars, recorded with an observatory, e.g. an X-ray or radio observatory, and then compares the TOAs with a predicted best-fit model (Lorimer & Kramer 2012; Desvignes et al. 2016). To track pulsations it is necessary to take into account the spin frequency of the pulsar (which is expressed as a Taylor series; $\nu(t) = \nu_0 + \dot{\nu}_0(t - t_0) + \frac{1}{2}\ddot{\nu}(t - t_0)^2...$ and to account for frequency dependent delays due to the ionized interstellar medium (IISM) (Lorimer & Kramer 2012).

1.3.1   Timing analysis

Timing analysis of pulsars is the essential tool in examining the basic properties (spin, orbital period, etc) of pulsars, and it is a tool that can help discover new properties of pulsars, and perhaps even gravitational wave signals (Lorimer & Kramer 2012; Janssen et al. 2015). When using timing analysis, several influences on the pulse time of arrival are taken into account, and propagation delays affecting the pulsar signal should be accounted for. First of all, the pulse time of arrivals need to be corrected to an inertial reference frame, to take the Earth movement around the Sun into account. The pulsar observations, both in X-ray and radio, are barycentered, meaning the pulsar position and movement is referred to the solar system barycenter. Furthermore, the planets in the solar system also have an effect on the signal we observe, and we need to correct the data for their relative positions to the solar system barycentre. Ephemerides for the planet positions are provided by the Jet Propulsion Laboratory (JPL). When the corrections are applied to the pulsar data, the data is folded to increase the signal to noise of the pulsations. So far, the above is valid for both X-ray and radio pulsars. However, to create TOAs for a radio pulsar it is necessary to cross-correlate the data with a template pulse profile. For X-ray pulsars a sinus curve, or harmonic decomposition of the signal, is used instead of a fixed template (Hartman et al. 2008). A harmonic decomposition will avoid that the phase and amplitude variability, observed in these pulsars, create artificial variations when creating the TOAs. Using a fixed profile for X-ray pulsars could thus introduce artificial variability in the TOAs.
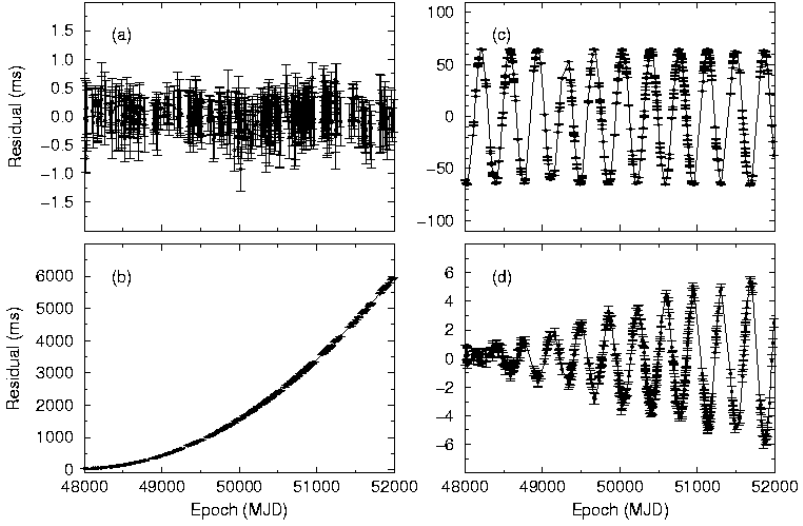
Figure 1.4: Residuals showing missing parameters from a timing solution, here PSR B1133+16 is used as an example. Panel *a* shows a perfect timing solution, with residuals having a Gaussian distribution around zero. Panel *b* shows a missing or underestimated $\dot{P}$. Panel *c* shows an off set in position, and panel *d* shows the effect of not taking the pulsars proper motion into account. Image Credit: Lorimer & Kramer (2012).

Radio pulsars have very stable pulse profiles, and it is thus a fixed template that is correlated to the data when creating the TOAs. The rotational phase of any pulsar is described by:

$$\phi(t) = \phi_0 + \nu_0(t - t_0) + \frac{1}{2}\dot{\nu}(t - t_0)^2 + \frac{1}{6}\ddot{\nu}(t - t_0)^3... \tag{1.3}$$

ϕ_0 it the pulse phase at time t_0, and the phase is measured in cycles. For any timing solution, the desired purpose is to be able to gain insight into the astrometric parameters (position, proper motion, parallax etc.), spin parameters (spin frequency and the derivatives of the spin frequency) and binary parameters (orbital period, eccentricity, semi-major axis etc.) (Lorimer & Kramer 2012). The aim is to find a phase-coherent timing solution, which accounts for all rotations of the pulsar between different observations. When using long observations, it is common that derivatives of parameters need to be included in the timing solutions. Incorrect timing solutions introduce systematic structures in the post-fit residuals, from which it is possible to detect which parameter is missing or needs to be adjusted, see Fig. 1.4.
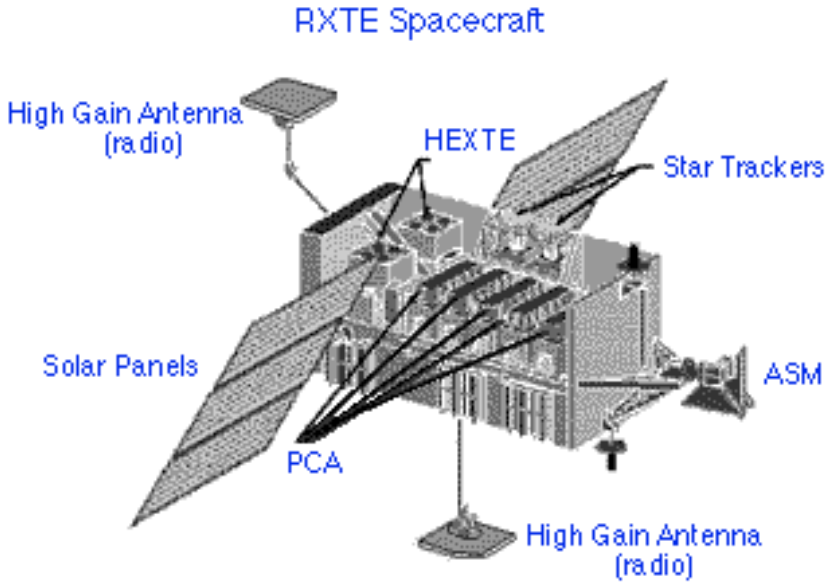
Figure 1.5: The Rossi X-ray Timing Explorer (*RXTE*) was an X-ray telescope which was active from 1995 to 2012. Image Credit: NASA.

1.4 Observatories

In this thesis data from several observatories has been used, and below is a short description of the different telescopes.

1.4.1 RXTE

The *Rossi X-ray Timing Explorer* (*RXTE*), see Fig. 1.5 , was a NASA controlled X-ray satellite, which was launched on 30. December 1995. The telescope could cover timescales of milliseconds to months and had a spectral range of 2-250 keV. *RXTE* was decommissioned in 2012. The telescope carried two pointed instruments. The proportional Counter Array (PCA), which had a collecting area of $6500\,\mathrm{cm^2}$ and which covered the low energy range of the telescope, 2-60 keV. The other pointed instrument was the High Energy X-ray Timing Experiment (HEXTE) which had a collecting area of $2\times800\,\mathrm{cm^2}$ and covered the upper range of the energy bands, 15-250 keV. In addition to this, *RXTE* also carried the All-Sky Monitor (ASM), which could scan about 80% of the sky at every orbit.

Figure 1.6: *XMM-Newton* is an ESA space telescope. It was launched in 1999 and is still operating. Image Credit: ESA.

1.4.2   XMM-Newton

The *X-ray Multi-Mirror Mission* (*XMM-Newton*) is an ESA controlled mission, launched on 10. December 1999 (see Fig. 1.6). There are three X-ray instruments on board *XMM-Newton* (RGS, EPIC-pn and EPIC-MOS) and an optical monitor (OM). The RGS consists of two Reflection Grating Spectrometer readout cameras and EPIC-MOS consists of two imaging detectors (MOS1 and MOS2), which are both CCD cameras, and MOS stands for Metal Oxide Semi-conductor. The EPIC-pn has an unobstructed beam and it uses pn CCDs. The EPIC cameras are able to perform sensitive imaging over the 30 arcmin telescope field of view and in the energy range of 0.15-15 keV. The OM instrument covers 160-550 nm and has a resolution down to magnitude +24.5. The telescope has a collecting area of 1475 cm^2 at 1.5 keV and 580 cm^2 at 8 keV. The relatively large collecting area and the ability to take long and uninterrupted exposures, make it a highly sensitive X-ray telescope.

1.4.3   Pulsar Timing Arrays

There are three collaborations around the world that aspire to observe gravitational waves using pulsar timing. Via precise timing of pulsars it should be possible to

detect signatures in the pulsar timing residuals which belong to gravitational waves crossing the pulsars (Desvignes et al. 2016). By using an array of pulsars, meaning different pulsars in different places on the sky, it should be possible to detect the characteristic quadrupolar, and higher order, angular signatures that gravitational waves crossing the sky exhibits. The quadrupolar behaviour of the gravitational wave signal should be distinguishable from the lower order terms that pulsars otherwise exhibit (Foster & Backer 1990). Furthermore, using an array of pulsars is expected to increase the signal to noise ratio of the gravitational wave signal in the timing residuals and by cross-correlating the signal between the pulsars in the array, it is possible to distinguish between the GW signal and other signals that may be present in the timing of the individual pulsars (Lentati et al. 2015).

The efforts to time an array of pulsars precisely is undertaken by the European Pulsar Timing Array (EPTA), North American Nanohertz Observatory for Gravitational Waves (NANOGrav) and the Parkes Pulsar Timing Array (PPTA), all three are collectively know as the International Pulsar Timing Array (IPTA). The EPTA uses five telescopes spread across Europe; the Effelsberg Telescope in Germany, the Lovell telescope at Jodrell Bank in the UK, the Nançay Radio Telescope in France, Westerbork Synthesis Radio Telescope (WSRT) in the Netherlands and the Sardinia Radio Telescope in Italy.

1.4.4   European Pulsar Timing Array Telescopes

The 5 telescopes used by the EPTA are very different telescopes. WSRT consists of 14 individual dish antennas, each with a diameter of 25 m, see panel a on Fig. 1.7, and was completed in 1970, with later upgrades. Twelve of the dishes are at permanent positions and at the eastern side of the telescope are two movable antennas. For the observations used in this thesis the WSRT had a frequency setup available of 345-1400 MHz. The total frequency range of WSRT is 120-8300 MHz.

The Effelsberg telescope is a 100 m single dish telescope, see panel b on Fig. 1.7. The telescope was first used in 1972 and has since then continuously been upgraded. The Effelsberg observes at a frequency of 300-9000 MHz, however, in this thesis it has been used at a configuration observing at 1400-2500 MHz.

The Nançay Radio Telescope was inaugurated in 1965 and is a transit instrument of the Kraus-type design, meaning it has two mirrors, a flat tilting primary mirror that is ten panels of 20 m long and 40 m tall (See panel c on Fig. 1.7). Its secondary mirror is 460 m south of the primary, which has the shape of part of a circle, which would have a radius of 560 m. The observing frequency of the telescope is 1060-3500 MHz and in this thesis the frequency range used is 1400-1500 MHz.

The Lovell telescope is the largest radio telescope at Jodrell Bank, and it is a single dish telescope with a diameter of 76.2 m. The telescope has been actively working since 1957 (See panel d on Fig. 1.7). The observing frequency spans
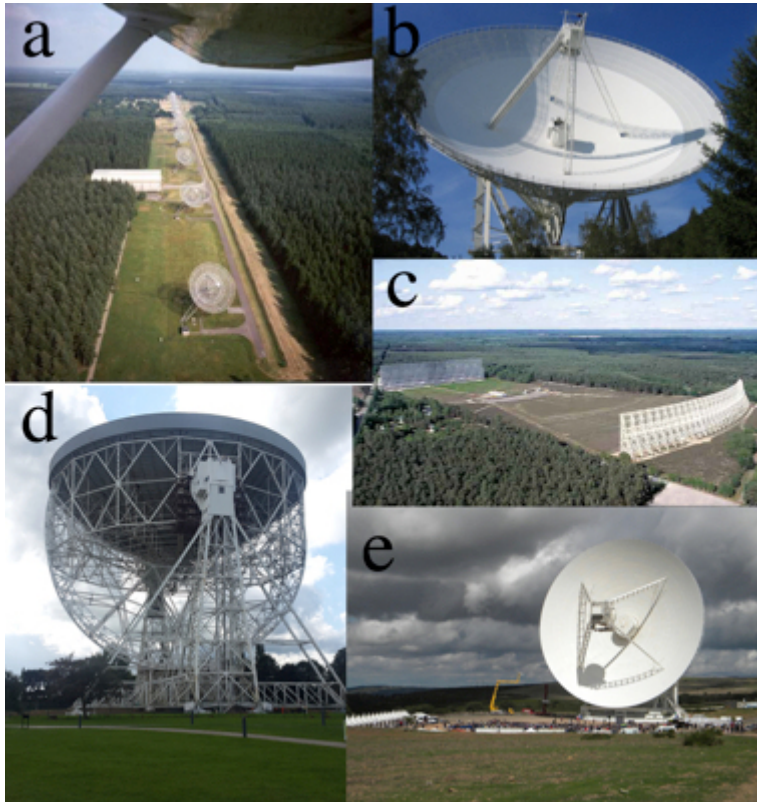
Figure 1.7: The European Pulsar timing array telescopes. a) The Westerbork Radio Synthesis Telescope, b) Effelsberg Radio Telescope, c) Nançay Radio Telescope, d) Lovell Telescope and e) The Sardinia Radio Telescope. Image credit: ASTRON (WSRT), EPTA (EFF), MPIfR BONN (Nançay), Private photo (Lovell), Sardinia Radio Telescope (SRT).

408-6000 MHz and the frequency setup used in this thesis was 1400-1500 MHz.

The last telescope of the EPTA is the Sardinia Radio Telescope (SRT), which was build in 2011 (See panel *e* on Fig. 1.7). It has a 64 m primary mirror and a 7.9 m secondary mirror. The frequency coverage is 300-1000 MHz.

1.5   This thesis

In this thesis I examine some of the peculiar behaviours that some pulsars show. I look at both accreting and radio pulsars in binary systems and try to give explanations to the behaviour of the different systems.

In Chapter 2 we look at the persistent low mass X-ray binary pulsar 2A 1822-371. It is an eclipsing system with an accretion disc corona and an orbital period of 5.57 hr. In this chapter we study the evolution of the pulsar and constrian the geometry of the system. We present a possible explanation for the orbital evolution of the system where we suggest that 2A 1822-371 is a source with a possible super-Eddington mass transfer rate. We used 13 years of *RXTE* data.

Chapter 3 is a study of whether there is pulse phase - flux correlation in the symbiotic X-ray pulsar GX1+4. A pulse phase - flux correlation has previously been found in accreting millisecond pulsars and in this chapter we thus tested if there is a smiliar correlation in binaries with high magnetic field and slow rotating pulsars. In this chapter we used *RXTE* data.

In Chapter 4 we examined the Be/X-ray transient 4U 0115+63 after the source had undergone a giant type-II outburst. The source did not immediately settle into its quiescent state, but instead it settled in a meta-stable plateau phase in which the luminosity then slowly decayed. *XMM-Newton* was used to observe the system during the meta-stable plateau phase and we found that there is an emitting region, suggesting a hot spot on the surface of the pulsar. The hot-spot was confirmed form the discovery of pulsations.

For Chapter 5 we examined three stable black widow pulsars, PSR J0023+0923, J2214+3000 and J2234+0944. The first BWPs observed have unstable timing solutions and show variability in the orbital parameters. In this chapter we present long-term timing solutions for the three stable BWPs, using four of the five EPTA telescopes. We discuss possibilities as to why these particular systems are stable and the first observed BWPs are unstable.

Bibliography

Alpar M. A., Cheng A. F., Ruderman M. A., Shaham J., 1982, Nature, 300, 728

Archibald A. M., et al., 2009, Science, 324, 1411

Arzoumanian Z., et al., 2018, preprint, (`arXiv:1801.01837`)

Baade W., Zwicky F., 1934, Physical Review, 46, 76

Bassa C. G., et al., 2014, MNRAS, 441, 1825

Bhattacharya D., van den Heuvel E. P. J., 1991, Phys. Rep., 203, 1

Bildsten L., et al., 1997, ApJ, 113, 367

Chakrabarty D., Morgan E. H., 1998, Nature, 394, 346

Chaty S., 2011, in Schmidtobreick L., Schreiber M. R., Tappert C., eds, Astronomical Society of the Pacific Conference Series Vol. 447, Evolution of Compact Binaries. p. 29 (`arXiv:1107.0231`)

Chen H.-L., Chen X., Tauris T. M., Han Z., 2013, ApJ, 775, 27

Corbet R. H. D., Sokoloski J. L., Mukai K., Markwardt C. B., Tueller J., 2008, ApJ, 675, 1424

Cumming A., Zweibel E., Bildsten L., 2001, ApJ, 557, 958

D'Amico N., Possenti A., Manchester R. N., Sarkissian J., Lyne A. G., Camilo F., 2001, ApJ, 561, L89

Desvignes G., et al., 2016, MNRAS, 458, 3341

Faucher-Giguère C.-A., Kaspi V. M., 2006, ApJ, 643, 332

Foster R. S., Backer D. C., 1990, ApJ, 361, 300

Frank J., King A., Raine D. J., 2002, Accretion Power in Astrophysics: Third Edition

Fruchter A. S., Stinebring D. R., Taylor J. H., 1988, Nature, 333, 237

Ghosh P., Lamb F. K., 1979, ApJ, 234, 296

González-Galán A., Kuulkers E., Kretschmar P., Larsson S., Postnov K., Kochetkova A., Finger M. H., 2012, A&A, 537, A66

Hartman J. M., et al., 2008, ApJ, 675, 1468

Heger A., Woosley S. E., 2003, in Ricker G. R., Vanderspek R. K., eds, American Institute of Physics Conference Series Vol. 662, Gamma-Ray Burst and Afterglow Astronomy 2001: A Workshop Celebrating the First Year of the HETE Mission. pp 214–216 (`arXiv:astro-ph/0206005`)

Heger A., Woosley S. E., Langer N., Spruit H. C., 2004, in Maeder A., Eenens P., eds, IAU Symposium Vol. 215, Stellar Rotation. p. 591 (`arXiv:astro-ph/0301374`)

Hewish A., Bell S. J., Pilkington J. D. H., Scott P. F., Collins R. A., 1968, Nature, 217, 709

Hulse R. A., Taylor J. H., 1975, ApJ, 195, L51

Janssen G., et al., 2015, Advancing Astrophysics with the Square Kilometre Array (AASKA14), p. 37

Kiel P. D., Taam R. E., 2013, Ap&SS, 348, 441

Kramer M., Lyne A. G., Hobbs G., Löhmer O., Carr P., Jordan C., Wolszczan A.,

2003, ApJ, 593, L31

Kuranov A. G., Postnov K. A., 2015, Astronomy Letters, 41, 114

Lattimer J. M., Prakash M., 2007, Phys. Rep., 442, 109

Lazaridis K., et al., 2011, MNRAS, 414, 3134

Lentati L., et al., 2015, MNRAS, 453, 2576

Lorimer D. R., Kramer M., 2012, Handbook of Pulsar Astronomy

Lü G.-L., Zhu C.-H., Postnov K. A., Yungelson L. R., Kuranov A. G., Wang N., 2012, MNRAS, 424, 2265

Manchester R. N., 2017, Journal of Astrophysics and Astronomy, 38, 42

Migliazzo J. M., Gaensler B. M., Backer D. C., Stappers B. W., van der Swaluw E., Strom R. G., 2002, ApJ, 567, L141

Papitto A., et al., 2013, Nature, 501, 517

Patruno A., Watts A. L., 2012, preprint, (arXiv:1206.2727)

Podsiadlowski P., Rappaport S., Pfahl E. D., 2002, ApJ, 565, 1107

Roberts M. S. E., 2011, in Burgay M., D'Amico N., Esposito P., Pellizzoni A., Possenti A., eds, American Institute of Physics Conference Series Vol. 1357, American Institute of Physics Conference Series. pp 127–130 (arXiv:1103.0819)

Roberts M. S. E., 2013, in van Leeuwen J., ed., IAU Symposium Vol. 291, Neutron Stars and Pulsars: Challenges and Opportunities after 80 years. pp 127–132 (arXiv:1210.6903)

Romani R. W., 1990, Nature, 347, 741

Rosswog S., Brüggen M., 2011, Introduction to High-Energy Astrophysics

Roy J., et al., 2015, ApJ, 800, L12

Shaifullah G., et al., 2016, MNRAS, 462, 1029

Shakura N. I., Sunyaev R. A., 1973, A&A, 24, 337

Shearer A., Golden A., 2002, in Becker W., Lesch H., Trümper J., eds, Neutron Stars, Pulsars, and Supernova Remnants. p. 44 (arXiv:astro-ph/0208579)

Smarr L. L., Blandford R., 1976, ApJ, 207, 574

Smith D. A., Guillemot L., Kerr M., Ng C., Barr E., 2017, preprint, (arXiv:1706.03592)

Srinivasan G., van den Heuvel E. P. J., 1982, A&A, 108, 143

Swiggum J. K., et al., 2015, ApJ, 805, 156

Taam R. E., van den Heuvel E. P. J., 1986, ApJ, 305, 235

Tauris T. M., 2016, Mem. Soc. Astron. Italiana, 87, 517

Webster B. L., Murdin P., 1972, Nature, 235, 37

Wijnands R., van der Klis M., 1998, Nature, 394, 344

Xu X.-J., Li X.-D., 2007, A&A, 476, 1283

van den Heuvel E. P. J., 1975, ApJ, 198, L109

CHAPTER 2

The X-ray Pulsar 2A 1822-371 as a Super Eddington source

The low mass X-ray binary 2A 1822-371 is an eclipsing system with an accretion disc corona and with an orbital period of 5.57 hr. The primary is an 0.59 s X-ray pulsar with a proposed strong magnetic field of $10^{10} - 10^{12}$ G. In this chapter we study the spin evolution of the pulsar and constrain the geometry of the system. We find that, contrary to previous claims, a thick corona is not required, and that the system characteristics could be best explained by a thin accretion outflow due to a super-Eddington mass transfer rate and a geometrically thick inner accretion flow. The orbital, spectral and timing observations can be reconciled in this scenario under the assumption that the mass transfer proceeds on a thermal timescale which would make 2A 1822-371 a mildly super-Eddington source viewed at high inclination angles. The timing analysis on 13 years of *RXTE* data show a remarkably stable spin-up that implies that 2A 1822-371 might quickly turn into a millisecond pulsar in the next few thousand years.

2.1   Introduction

2A 1822-371 is a persistent eclipsing low mass X-ray binary (LMXB) with a 0.59 s accreting X-ray pulsar (Jonker & van der Klis 2001). The neutron star primary accretes material from a $0.62\,M_\odot$ Roche lobe filling main sequence star (Harlaftis et al. 1997), and the system has a binary orbit of 5.57 hr (Hellier et al. 1990; Parmar et al. 2000; Jonker & van der Klis 2001). White et al. (1981) showed that the partial eclipses of the system are best explained by the presence of an accretion disk corona (ADC). The eclipses are clearly seen because the system is being viewed almost edge on at an inclination angle of 81-84° (Heinz & Nowak 2001; Jonker et al. 2003a; Ji et al. 2011), which was found through modelling of the light curve (Heinz & Nowak 2001). As shown by Heinz & Nowak (2001) the eclipse of 2A 1822-371 is a narrow peak in the light curve, however, most of the light curve, about 80 % of the orbit, is obscured. White & Holt (1982) suggested that the ADC is formed by evaporated material in the inner accretion disc due to radiation pressure from the X-rays produced by the neutron star. The accretion disc is thought to be optically thick and the ADC appears so extended that it is not completely blocked by the companion star. Indeed the companion seems to eclipse about 50% of the total light emitted (Mason & Cordova 1982; Somero et al. 2012). The magnetic field of 2A 1822-371 was inferred twice from the presence of cyclotron resonance scattering features (crsf). Sasano et al. (2014) reported results obtained with *Suzaku* and suggested a crsf at 33 keV which would correspond to a magnetic field of B$\sim$2.8$\times$10^{12} G. This, however, was in disagreement with the later findings of Iaria et al. (2015) who interpreted *XMM-Newton* spectral data as showing a crsf at around 0.7 keV (and an inferred magnetic field of B$\sim$8.8$\times$10^{10} G).

The intrinsic X-ray luminosity (L_X) of 2A 1822-371 is currently not well constrained. The first source of uncertainty comes from the distance, which is not well known although it was estimated to be around 2-2.5 kpc based on modelling of infrared and optical observations (Mason & Cordova 1982).
Mason & Cordova (1982) estimated the luminosity to be $L_X \sim 1.1 \times 10^{35}\,(d/1kpc)$ which, for a distance of about 2.5 kpc is $\sim$10^{36} erg s^{-1}. Since the pulsar is seen edge-on, its optical to X-ray luminosity ratio is $L_{\rm opt}/L_X \sim 15 - 65$. This value is very anomalous among LMXBs, which have a typical ratio of the order of $\sim$1000. The binary also shows a very large orbital period derivative of $\dot{P}_{orb}$=1.5-2.1$\times$10^{-10} s s^{-1} (implying a very fast orbital expansion Burderi et al. 2010; Jain et al. 2010; Iaria et al. 2015), and thus it has been suggested that the binary is undergoing a highly non-conservative mass transfer, with the neutron star accreting at the Eddignton-limit and the rest of the material expelled from the donor star via radiation pressure (e.g., Iaria et al. 2015). This also suggests the possibility that 2A 1822-371 is an Eddington limited source Jonker et al. (2003a) which would then be compatible with one of the magnetic field estimates inferred from the crsf (i.e., $B = 8.8\times10^{10}$ G). Another peculiar phenomenon in 2A 1822-371 is the fast spin up of the system, which gives an extremely short spin-up timescale of order 7000 yr (Jonker & van der Klis 2001). When looking at the ensemble of slow accreting pulsars in LMXBs, the short spin-up timescale of 2A 1822-371

is not unique. Indeed short timescales have previously been observed in LMXB pulsars such as 4U 1626-67 and GX 1+4, both of which show torque reversals (Bildsten et al. 1997; Jonker & van der Klis 2001). The accretion torque reversal is a still poorly understood phenomenon that occurs in some accreting pulsars and that causes a switch from a spin-up to a spin-down (and vice-versa). One possible interpretation of torque reversals is a transition between a Keplerian and a sub-Keplerian flow in the inner portion of the accretion disk (e.g., Yi et al. 1997).

The spin evolution of 2A 1822-371 can therefore be explained with two different scenarios: either the system has started accreting very recently (if the currently observed spin-up truly represents the secular evolution of the neutron star spin) or, alternatively, what we are observing is simply a short-term effect with the current spin up that will be possibly balanced by an episode of spin-down in the next future. The latter scenario would make 2A 1822-371 similar to the other high field LMXB pulsars like 4U 1626-67 and GX 1+4. In those two systems, the phenomenon of torque reversals occurs on timescales of years. Other pulsars, such as Her X-1, Cen X-3 and Vela X-1 (the latter two are high mass X-ray binaries) show variations on shorter timescales of days to a few years (see for example Fig. 6 in Bildsten et al. (1997)). Since several other LMXB pulsars show changes in their spin frequency derivative, we investigate here whether long-term spin-up in 2A 1822-371 is really stable or if there are underlying detectable fluctuations related to accretion torque variations.

A second problem is that, at least in the (low magnetic field) accreting millisecond pulsars, measuring the spin frequency derivative is sometimes complicated by the presence of timing noise in the X-ray time of arrivals of pulsations (Hartman et al. 2008; Patruno et al. 2009). It has, however, been observed that at least in some accreting millisecond pulsars, a large part of timing noise is correlated to variations in flux (Patruno et al. 2009, 2010; Haskell & Patruno 2011). One plausible interpretation of the flux-phase correlation is that the hot spot is moving on the pulsar surface in response to variations of the mass accretion rate. In high field accreting pulsars like 2A 1822-371 the presence of such correlation has never been reported and it is currently unclear whether such effects might be present in these systems too. For example, the stronger magnetic field of the neutron star in 2A 1822-371 might prevent a drift of the hot spot when the accretion rate varies. However, strong timing noise has been observed in the accreting X-ray pulsar Terzan 5 X-2 (Patruno et al. 2012a), which is an 11 Hz accreting pulsar with a magnetic field of the order of $10^9 - 10^{10}$ G, which is substantially stronger than the typical field observed in accreting ms pulsars ($B \sim 10^8$ G). Therefore it might be possible that the same phenomenon is present in 2A 1822-371 and in this work we plan to investigate this. There are therefore two questions that need to be addressed for 2A 1822-371:

1. Is the previously measured spin frequency derivative the true one or its measurement is affected by the presence of timing noise?

2. Does the (true) spin frequency derivative represent the long term spin evo-

lution of the neutron star?

In this chapter we use archival data from the *Rossi X-ray Timing Explorer* (*RXTE*), collected over a baseline of 13 years, to try to answer the aforementioned questions.

Furthermore, it has been suggested that the ADC forms an optically thick region around the neutron star (White & Holt 1982; Parmar et al. 2000; Iaria et al. 2001), with optical depth $\tau \sim 9 - 26$, which implies that most of the light coming from the pulsar is heavily scattered. However, at such large optical depths the coherent pulsations cannot preserve their coherence. Iaria et al. (2013) first noticed this problem and suggested that the Comptonised component is produced in the inner regions of the system which are never directly observed. Then only a small fraction ($\sim 1\%$) of the total light produced is scattered along the line of sight of the observer with an optical depth $\tau \sim 0.01$. This geometry, although possible, requires some fine tuning of the optical depth. Furthermore, to preserve the coherence of the pulsations, the whole (optically thick) Comptonization region needs to rotate with the neutron star. A third question that needs to be answered is therefore whether it is possible to keep a simple geometry of the system, with an ADC, and still obtain a spectrum compatible with $\tau \sim 1$.

In section 2.2 we present the observations and the data reduction procedure, in section 2.3 we show our results on the timing analysis, e.g. the spin evolution and flux-phase correlation, and in section 2.4 we discuss the implications of our finding and we extend previous models for 2A 1822-371 .

2.2   X-Ray Observations

We have used data taken over a baseline of 13 years, between 28 June 1998 and 30 November 2011. All observations were taken with the Proportional Counter Array (PCA) on board the *RXTE* (Bradt et al. 1993; Jonker & van der Klis 2001). *RXTE*/PCA consists of five xenon/methane proportional counter units, which are sensitive in the range of 2-60 keV (Jahoda et al. 2006). We chose science event files with a time resolution of 2^{-16}s (Event_16us), 2^{-13}s (Event_125us) and 2^{-20}s (GoodXenon) for the timing analysis whereas we selected Standard 2 data with 16 s time resolution to construct the X-ray lightcurve. The lightcurve is reconstructed in the 2–16 keV energy range and the X-ray flux is first averaged for each observation (ObsID) and then normalized in Crab units (see Fig. 2.4). A detailed description of this standard procedure can be found in van Straaten et al. (2003). The timing analysis is performed by selecting the absolute energy channels 24 to 67 that correspond approximately to an energy range of $\approx$9-23 keV. This range was chosen because the pulsation have the highest signal to noise ratio (S/N) as reported by Jonker & van der Klis (2001). The data was barycentered with the FTOOL *faxbary* by using the JPL DE405 Solar System coordinates and the most precise astrometric position found by *Chandra* observations, RA: 18:25:46.81 and DEC: -37:06:18.5 (Burderi et al. 2010) with an error of 0.6" (90% uncertainty circle of the *Chandra* X-ray absolute position). The barycentered data was then epoch folded in pulse profiles of 32 bins over either 1500 s, or the total length of the

data segment, which usually corresponds to 3000 s. We then cross-correlated each pulsation with a sinusoid at the spin frequency of the pulsar and generated a set of time of arrivals (TOAs). We selected only pulsations with a S/N larger than 3.1σ, defined as the ratio between the pulse amplitude and its 1 sigma statistical error. The value of 3.1σ is selected to account for the number of trials, i.e., we expect less than 1 false pulse detections among the 281 pulse profiles generated over the entire 13 year baseline. We looked for the presence of a 2nd harmonic which was detected only is a small subset of data segments and thus we do not consider it any further in the forthcoming timing analysis.

The ephemeris used in the epoch folding are composed by an initial pulse frequency from Jonker & van der Klis 2001 and Jain et al. 2010 and an orbital solution from Iaria et al. 2011. The orbital solution corresponds to a Keplerian circular orbit with a constant orbital period derivative. Since the data contains large data gaps we split it in 20 segments that could be potentially phase connected, meaning that our time baseline for each different segment spans typically a few days, see table 2.1. With the S/N criterion discussed above, we found significant pulsations in 15 out of 20 data segments. In this work we have used TEMPO2 version 2012.6.1 and kept the orbital values fixed throughout the analysis.

2.3   Results

Pulsations are found in the first 15 data segments described in table 2.1. In the last 5 data segments the S/N found was lower than the selected 3.1σ for most of the pulsations, thus leaving us with too few or no pulsations to perform the timing analysis. In table 2.1 we provide the 95% confidence upper limit of the fractional amplitude of the pulsations in these 5 data segments. All these upper limits are consistent with the fractional amplitude found in the first 15 data segments.

2.3.1   Spin Evolution

In two out of fifteen data segments the pulse time of arrivals of the neutron star required a spin frequency derivative. The χ^2 and degrees of freedom (dof) for the fits to all 15 data segments are given in table 2.1. The errors on the spin frequency were calculated by using standard χ^2 minimization techniques and by multiplying them by the square root of the reduced χ^2. The errors on the spin period is found from: $\sigma_P = \sigma_\nu (\frac{1}{\nu})^2$.

The collection of all spin frequencies (see Table 2.1) is then fitted with a linear function to determine the long-term spin frequency derivative over the entire baseline of the observations. The fit gives a reduced χ^2 of 1909 for 11 dof. This indicates that the fit is not statistically acceptable (p-value< 0.05%) and the bad fit is caused by several points that are clearly off the linear relation (see lower panel of Fig. 2.1). The best-fit linear slope that we find corresponds to a spin up of $\dot{\nu}=7.6(8)\times10^{-12}\,\mathrm{Hz\,s^{-1}}$ for the period ranging from June 1998 to November 2011, comparable to what has recently been found by Chou et al. (2016).

The bad fit to the spin frequencies shows that, although there is no evidence

Table 2.1: Overview of the data used throughout this chapter. The data are taken with *RXTE*, and in this data, segments 3, 9, 10, 13, 14, 15 represent data not analysed before in the literature Jain et al. (2010); Somero et al. (2012); Jonker & van der Klis (2001). The errors reported in the parentheses correspond to 1σ statistical errors. The χ^2 and dof given in the table is for the TEMPO2 spin frequency fit to the data. The 95% upper confidence limit is only given for the data segments were there were not found any significant pulsations (significance limit was 3.3σ).

#	ObsId	T_{start}	T_{end}	Upper limit (%)	PEPOCH	Spin frequency (ν_0)	Spin period (P_s)	χ^2	dof
1	30060	50992.8210	50993.9805		50993.1873	1.6860862(6)	0.593089449(2)	28.49	6
2	30060	51018.2434	51019.6464		51018.9449	1.6860957(3)	0.593086159(9)	63.30	17
3	50048	52031.5426	52032.8178		52032.1105	1.6866984(4)	0.59287742(3)	35.43	13
4	50048	52091.4522	52101.4647		52096.4049	1.6867365(2)	0.59286083(7)	47.41	12
5	70036	52435.4107	52435.7670		52435.5174	1.6869332(2)	0.59279212(5)	25.54	8
6	70037	52488.3701	52495.9115		52491.9201	1.68697104(4)	0.5927784(2)	100.13	26
7	70037	52503.3513	52503.9363		52503.5256	1.686980(2)	0.59277526(5)	21.77	8
8	70037	52519.1659	52519.5110		52519.3091	1.686988(4)	0.59277244(1)	42.79	6
9	70037	52547.3079	52547.8544		52547.3944	1.6870063(10)	0.59276601(4)	26.31	9
10	70037	52608.1849	52608.3845		52608.2072	1.686879(8)	0.59281075(3)	11.22	2
11	70037	52882.0214	52882.2226		52882.3290	1.687240(4)	0.59268391(2)	8.81	3
12	70037	52883.1514	52885.1249		52883.4896	1.6869901(8)	0.59277171(3)	20.55	2
13	80105	52896.2822	52896.4384		52896.2556	1.687243(3)	0.59268286(9)	11.12	4
14	96344	55880.6677	55884.8487		55882.5852	1.6891897(2)	0.59199982(6)	85.27	17
15	96344	55888.5020	55895.6318		55891.8696	1.689204448(8)	0.591994464(3)	23.85	7
16	60042	52138.7535	52141.8115	2.1	-	-	-	-	-
17	60042	52138.7535	52141.8115	2.1	-	-	-	-	-
18	50048	51975.7203	51976.1843	0.7	-	-	-	-	-
19	70037	52432.3887	52432.7906	0.6	-	-	-	-	-
20	70037	52724.7351	52724.7545	0.5	-	-	-	-	-
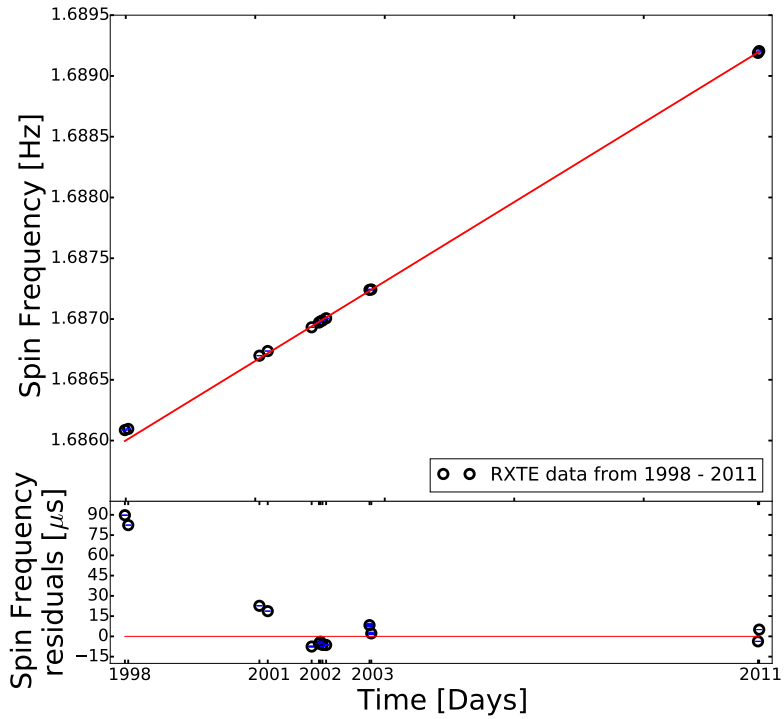
Figure 2.1: The longterm spin up over a time period of 13 years. The black points show the data used in this chapter and listed in table 2.1. The red line is a fit to the data from this chapter and it gives the spin up of the pulsar of $\dot{\nu}$=7.57(6)$\times 10^{-12}\,\mathrm{Hz\,s^{-1}}$. This figure is plotted with errors on all points, seen in blue. Most of the errors are, however, so small that they are not visible on the plot.
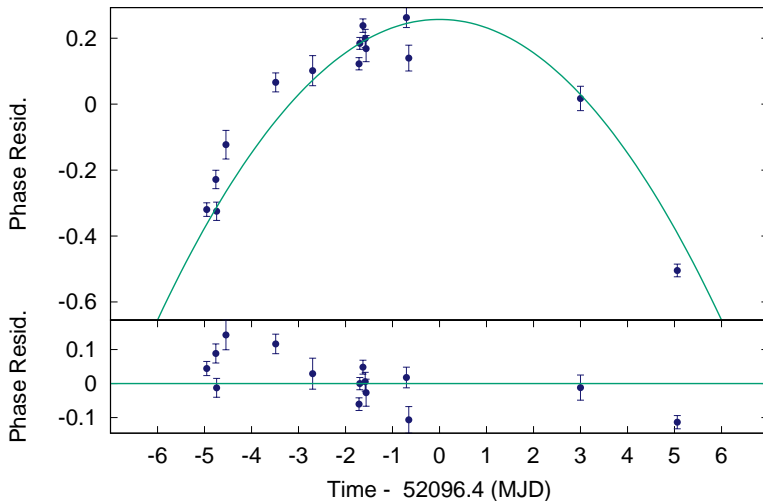
Figure 2.2: The pulse phase residuals before a spin frequency derivative is fitted for (top panel) and after (lower panel). The parabola is a clear evidence of the presence of a spin frequency derivative.

for a change in sign of the spin frequency derivative, some fluctuations are present in the data. We thus explored to what extent the magnitude of the accretion torque vary with time and whether *small/short-term* torque reversals are present in the data. First, in the data segments 4 and 6, it was possible to phase-connect the pulsations and we thus have a direct measure of the spin frequency derivative. Such spin frequency derivative is measured for a time interval of 10 and 8 days (for segment 4 and 6, respectively). The two spin up values found are $\dot{\nu}=6.7(4)\times 10^{-12}\,\mathrm{Hz\,s^{-1}}$ for segment 4 and $\dot{\nu}=8.2(5)\times 10^{-12}\,\mathrm{Hz\,s^{-1}}$ for segment 6 which are both within 1σ from the long-term linear trend seen in the 13-year long baseline.

The pulse phase residuals with respect to a constant spin frequency model can be seen for the data segment 4 in the top panel of Fig. 2.2. In the lower panel of the same figure we show the pulse phase residuals with respect to a spin frequency derivative model. The parabolic trend seen in the top panel of Fig. 2.2 is a clear signature of the presence of a frequency derivative.

2.3.2   Spin period derivative vs. time

To estimate the magnitude of the spin fluctuations we calculated the spin period derivative between each consecutive data point, i.e., we determined the slope between each pair of points, and plotted them versus time, see Fig. 2.3. The errors
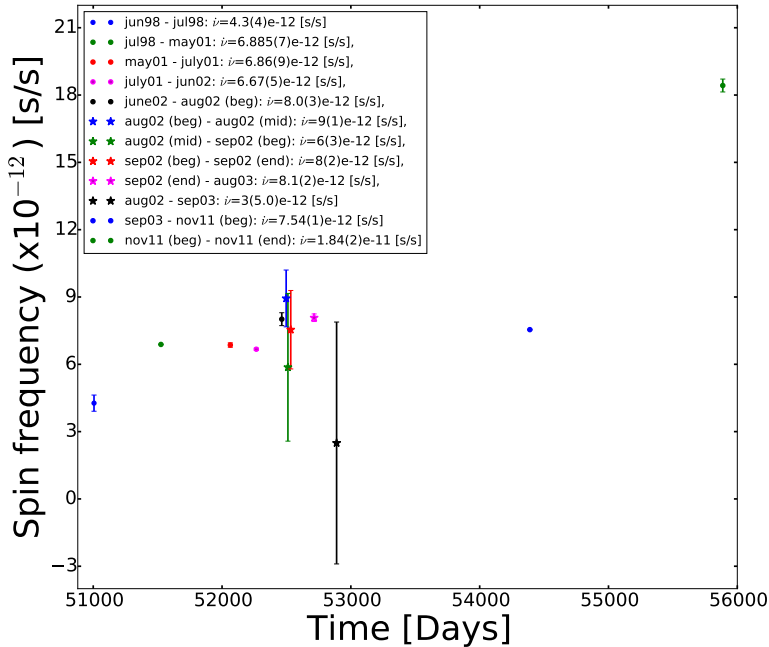
Figure 2.3: The spin period derivative change between the individual observations from Fig. 2.1. It is clearly seen that most of the observations coincide, and there is a close to constant development in the spin period derivative. However, there are a few points that are off, e.g. in 2003 and 2011.

on the spin period derivatives are found by taking the maximum and minium slope between the spin periods in Fig. 2.1. It is clear that most of the points in Fig. 2.3 are roughly consistent with a single constant spin period derivative with small variation of less than a factor 2 over the whole baseline with the exception of an outlier in the last data segment taken in 2011. In that case the spin frequency derivative is consistent with having increased by a factor 3 during the last month of the observations.

The 2–16 keV X-ray flux shows a variation of less than a factor 2 during that same month (see Figure 2.4) and no average variation when compared to the average X-ray luminosity of the previous years.

2.3.3   X-Ray Flux-Phase Correlation

2A 1822-371 is a persistent source that shows little variability in X-ray flux. In all our observations the X-ray flux varies by less than a factor of 2 with respect to the average value. Therefore even if a flux-phase correlation is present in 2A 1822-371 we expect little or no variation in the X-ray pulse phases. Nonetheless we inspected the data for the presence of such correlation, since it is the first time
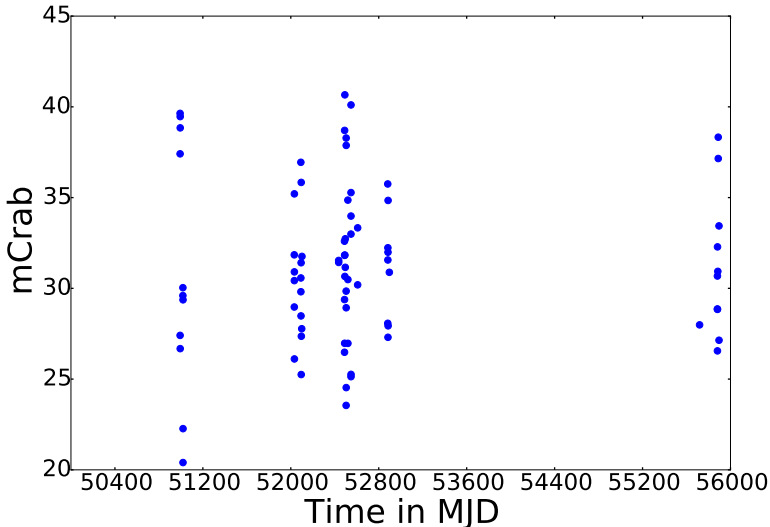
Figure 2.4: 2–16 keV X-ray lightcurve of 2A 1822-371. Each data point represents an ObsID average flux. The overall intensity of the light curve is fairly constant over the span of the observations used in this chapter, with variations of less than a factor 2 in 13 years of observations.

that such a test is performed in such a high field accreting pulsar.

We follow the procedure outlined in Patruno et al. (2009, 2010) i.e., we minimize the χ^2 of a linear fit to the X-ray flux vs. pulse phase. If there is a significant correlation then this might indicate the existence of some mechanism that determines the pulse phase variations in addition to genuine neutron star spin variations. Such mechanism for example can be the motion of the hot spot on the surface of the pulsar (Patruno et al. 2009, 2010).

We fit the data with a linear correlation

$$\phi = a + b\,F_x \tag{2.1}$$

where ϕ is the pulse phase and F_x the X-ray flux. If there is a correlation, b should be significantly different than zero. However, in all our 15 data segments, the b coefficient is consistent with zero within the statistical errors as can be seen in table 2.2.

2.3.4   Fractional Amplitude vs. cycles

We tested whether there was a correlation between the fractional amplitude of the pulsations and the eclipses with the purpose of testing whether we can actually directly see the surface of the neutron star when there is no eclipse.

On Fig. 2.5 we report the results of the data analyzed from 2002 and 2011. The fractional amplitude definition is the same as the one used in Patruno et al. (2010). When pulsations are not detected we provide 95% confidence level upper

Table 2.2: The A and B value for the Flux-Phase correlation fits for the individual data segments.

# segment	a	b
1	-0.08(10)	0.001(2)
2	0.20(3)	-0.0087(7)
3	0.2(1)	-0.007(4)
4	0.81(6)	-0.03(2)
5	0.08(7)	-0.003(2)
6	0.004(40)	-0.0001(15)
7	0.19(5)	-0.008(2)
8	-0.22(5)	0.010(2)
9	0.12(5)	-0.005(2)
10	-0.5(1)	0.019(4)
11	-1.8(2)	0.080(7)
12	0.11(8)	-0.004(3)
13	0.4(1)	-0.012(3)
14	-0.07(5)	0.002(2)
15	-1.20(7)	0.033(2)
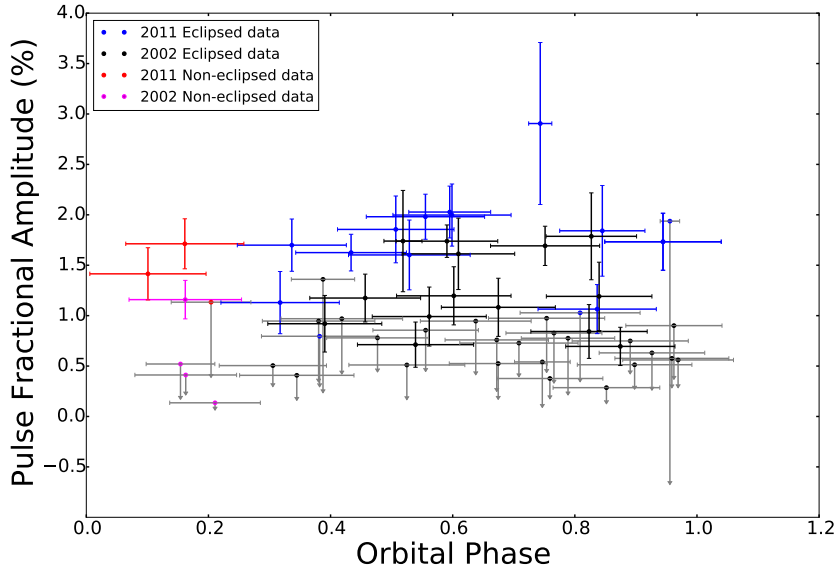
Figure 2.5: The fractional amplitude of eclipsed data and the non-eclipsed data vs. the cycle of the pulsar. The Eclipse fractional amplitudes are seen in blue/black (2011 and 2002 data), and the non-eclipsed fractional amplitudes are seen in red/pink (2011 and 2002). The non-eclipsed data is assumed to be 0.05-0.25 cycle, and the rest of the cycle is assumed to be a part of the eclipse. The eclipse is defined with a zero point at T_{ASC}.

limits. The red and pink points on Fig. 2.5 are the data from the non-eclipsed part of the lightcurve, and the blue and black points are from the eclipsed part of the orbit. We use T_{asc} as our reference orbital phase zero (i.e., the beginning of the cycle) and we thus expect that the non eclipsed data are between cycle 0.05-0.25. We further use the fact that the rest of the cycle is partially eclipsed. Note some other authors use a different definition of eclipse, for example Heinz & Nowak (2001), define the eclipse to be only the portion of the lightcurve that shows a deep dip (Hellier et al. 1990; Heinz & Nowak 2001). In any case, Fig. 2.5 shows that there is no detectable difference between the fractional amplitudes for the eclipsed and non eclipsed data in any orbital phase interval.

2.4 Discussion

In this chapter we have found a long-term spin frequency derivative of $\dot{\nu}=7.6(8)\times 10^{-12}\,\mathrm{Hz\,s^{-1}}$, and a short term spin frequency derivative of $\dot{\nu}=(6\text{--}8)\times 10^{-12}\,\mathrm{Hz\,s^{-1}}$, in two phase connected data segments. The long-term spin up is consistent with that reported by Chou et al. (2016), Iaria et al. (2015), Jain et al. (2010) and Jonker & van der Klis (2001). We find no evidence for torque reversals and few variations in the accretion torque, limited to fluctuations of less than a factor two with the exception of the last data segment in 2011, where the spin up requires an increases by a factor 3 with respect to the overall long-term spin frequency derivative. There is no corresponding increase in the X-ray flux (in the 2–16 keV band) at the time of the spin-up increase. Finally, no evidence for a phase-flux correlation and no strong variations in the X-ray flux of the source are found.

   Previous papers have suggested different models and parameters for 2A 1822-371. A summary of some of the most recent papers is found in table 2.3. The data examined in this chapter span a baseline of about 13 years, from 1998 to 2011. In the following sections we will try to explain the long-term spin evolution with a self consistent model that can explain the measured strength of the magnetic field, the neutron star spin frequency derivative and the mass transfer rate. Then we will move on to comment on the different possible magnetic fields reported by Iaria et al. (2015) and Sasano et al. (2014). We then proceed to discuss whether the observed spin frequency derivative reflects a secular spin up that will continue in the future, or whether we are indeed just observing a short-term spin up that will change sign and or magnitude in the future.

2.4.1 Long term spin evolution

The large spin up of 2A 1822-371 implies a very short spin-up time scale of about $\nu/\dot{\nu} \approx 7000\,\mathrm{yr}$. This is an extremely short time scale for a system that should take several million years to spin up (Bhattacharya & van den Heuvel 1991). The relatively constant spin up implies no variation in the accretion torques acting upon the neutron star at least down to timescales of 8-10 days. However, as shown in Section 2.3.1 the linear fit to the spin frequency vs. time gives a very large χ^2

which implies that the spin frequency is not increasing linearly with time. This would be expected in case of constant accretion torque, but the observed flux has an rms fluctuation of the order of 4.4 mCrab, suggesting that accretion torques do indeed vary slightly with time. The strongest evidence for this comes from the last data point in 2011 where the spin up increase by a factor 3. Accretion theory predicts that the strenght of the spin up should scale with the amount of mass accreted according to the following relation (see e.g., Bildsten et al. 1997):

$$\dot{\nu} \propto \dot{M}^{6/7}. \tag{2.2}$$

If the mass accretion rate is related to the X-ray luminosity (and thus the X-ray flux) with the usual relation $L_X \approx \eta c^2 \dot{M}$ then we should expect $\dot{\nu} \propto F_X^{6/7}$. Therefore a $3\times$ larger $\dot{\nu}$ should imply a $\approx 3\times$ larger X-ray flux. However, the average 2–16 keV X-ray flux is not varying, on average, by this amount and therefore this probably means that the 2–16 keV X-ray flux is not a good tracer of the instantaneous mass accretion rate. Such possibility has been proposed to explain the behaviour of a number of other LMXBs (van der Klis 2001).

We now wish to test if we can find a self consistent model that explains the observed spin parameters of 2A 1822-371. First, let's define the co-rotation radius as that point in the accretion disk where matter has the same angular velocity of the neutron star:

$$R_{CO} = \left(\frac{GM_{NS}}{4\pi^2\nu^2}\right)^{1/3} \tag{2.3}$$

Then, following Ghosh & Lamb (1979), we can define the magnetospheric radius as the point where the ram pressure of the disk plasma equals the magnetic pressure:

$$R_m = \xi R_A = \xi \left(\frac{\mu^4}{2GM_{NS}\dot{M}^2}\right)^{1/7} \tag{2.4}$$

Such definition has some issues since it is derived by equating the dipolar magnetic field pressure to the ram pressure of a spherically symmetric free falling gas. The factor $\xi \approx 0.5$ is typically used to account for the disk geometry instead of the spherical symmetry of the free falling gas. Several works (Aly 1985; Lovelace et al. 1995, Goodson et al. 1997) have demonstrated that the magnetospheric-disk interaction will quickly generate an azimuthal field component that causes many field lines to open and reconnect at infinity. D'Angelo & Spruit (2010, 2012) have thus derived a different version of the magnetospheric radius which accounts for this differences. The magnetospheric radius thus obtained however, is not substantially different from the expression above and since we are giving only an order of magnitude estimate of the quantities we will continue to use the definition above. This makes also the comparison with other works more direct, since they mostly rely on the definition of magnetospheric radius given by Ghosh & Lamb (1979)

From the table 2.3, we can see that a few parameters reported in the literature (e.g., B, L_x, $\dot{P}_s$, etc.) are not consistent with each other and sometimes some reported values are even inconsistent from a physical point of view. For example,

Table 2.3: The different parameters in the most recent published papers on 2A 1822371. The papers are JvdK2001 = Jonker & van der Klis (2001), Jain2010=Jain et al. (2010),BU2010=Burderi et al. (2010), Bay2010=Bayless et al. (2010), Ia2011= =Iaria et al. (2011), Som2012=Somero et al. (2012), Sas2014=Sasano et al. (2014) & Ia2015=Iaria et al. (2015)

Parameter	JvdK2001	Jain2010	Bay2010(UV/Optical)	Sas2014	Ia2015
$\dot{\nu}$ (Hz/s)	$(8.1\pm0.1)\times10^{-12}$	$(7.06\pm0.01)\times10^{-12}$	-	$(6.9\pm0.1)\times10^{-12}$	$(7.25\pm0.08)\times10^{-12}$
$\dot{P}_{Spin}$ (s/s)	$-2.85(4)\times10^{-12}$	$-2.481(4)\times10^{-12}$	-	$-2.43(5)\times10^{-12}$	$-2.55(3)\times10^{-12}$
L_X (erg/s)	$10^{36}-10^{38}$	$(2.38-2.96)\times10^{38}$	$\sim10^{37}$	$\sim10^{37}$	1.26×10^{38}
$\dot{M}(M_\odot/yr)$	-	$(4.2-5.2)\times10^{-8}$	6.4×10^{-8}	-	-
$M_{NS}(M_\odot)$	1.4	1.4	1.35	1.4	1.61-2.32
B (G)	10^8-10^{16}	$(1-3)\times10^8$	-	2.8×10^{12}	$8.8(3)\times10^{10}$
Pulse Amp	0.25-3%	-	-	$\sim\pm5\%$	$\sim0.75\%$
$P_{orb}/\dot{P}_{orb}$ (yr)	-	$(4.9\pm1.1)\times10^6$	$(3.0\pm0.3)\times10^6$	-	-
P_s (s)	0.59325(2)	0.5926852(21)	-	0.592437(1)	0.5928850(6)
Time span	1996-1998	1998-2007	1979-2006	2006	1996-2006

magnetic field strengths as large as 10^{16} G have been discussed by Jonker & van der Klis (2001), by using the relation between B and μ, which, can only be used when $R_m < R_{CO}$, since there will be no accretion if the magnetospheric radius is outside of the co-rotation radius (with the exception of accretion induced by magnetic diffusivity, see e.g.,Ustyugova et al. (2006)). For 2A 1822-371, the co-rotation radius is at ≈ 1200 km, so that any magnetospheric radius larger than this value cannot be inferred by using Eq. 2.3. With a B field of 10^{16}G one would indeed obtain a magnetospheric radius of 10^6 km for a luminosity of 10^{36}erg s^{-1}.

Since we know $\dot{\nu}$ we can use the relation for the X-ray luminosity to find the mass accretion rate ($\dot{M}$) (Frank et al. 2002):

$$\dot{M} = \frac{L_X R_{NS}}{GM_{NS}} \qquad (2.5)$$

This assumes that the X-ray luminosity does trace the instantaneous mass accretion rate, which is, however, not the case in 2A 1822-371 as we have shown above. To obtain an expression for μ that we have used in Eq. 2.4 we use the angular acceleration as a function of $\dot{M}$, $\dot{\Omega} = 2\pi\dot{\nu} = \frac{\dot{M}\sqrt{GM_{NS}R_m}}{I}$ which gives:

$$\dot{\nu} \approx 4.1 \times 10^{-5} \dot{M} \, M_{NS}^{1/2} \, R_m^{1/2} \, I^{-1} \mathrm{Hz/s}. \qquad (2.6)$$

In the above equation we use the measured long-term $\dot{\nu}$, and we assume a neutron star mass of $1.4\,M_\odot$, a neutron star radius of 10 km, the moment of inertia ($I = 10^{45}\,\mathrm{g\,cm^2}$, ξ=0.5. We assume $1.4\,M_\odot$ in the above, even though Iaria et al. (2015) find the mass of the neutron star to be $(1.69\pm0.13)\,M_\odot$ and find the companion mass to be $(0.46\pm0.02)\,M_\odot$, within the limits given by Muñoz-Darias et al. (2005).

We can see that the models that satisfy the condition $R_m < R_{CO}$ are those where the luminosity is in excess of the Eddington limit. However, it is not known if the star really does accrete at near the Eddington limit. The observed X-ray luminosity is only $L_X \approx 10^{36}(d_2)^2$erg s^{-1} assuming a (poorly constrained) distance of 2 kpc. The best distance approximation is between 1-5 kpc (Mason & Cordova 1982; Parmar et al. 2000) which however, would shift the luminosity by less than an order of magnitude. The most compelling evidence that the X-ray luminosity is indeed higher than the observed value is that the ratio $L_x/L_{opt} \approx$15-65 and not 500-1000 as observed in other LMXBs (Griffiths et al. 1978; Bayless et al. 2010; Somero et al. 2012; Iaria et al. 2015). This means that either the optical luminosity is much larger than expected or that only a small $(1 - 10\%)$ of the total X-ray luminosity of the source is effectively observed.

A source accreting at the Eddington rate requires a mass accretion rate of $\dot{M} \sim 10^{-8} M_\odot$/yr. This is 2 orders of magnitude larger than what is expected from binary evolution models under the assumption that the donor is a main sequence star that started Roche lobe overflow with a mass $\lesssim 1\,M_\odot$ and that the binary evolution is driven by angular momentum loss via magnetic braking (Podsiadlowski et al. 2002). Since 2A 1822-371 is a persistent source, the mass accretion rate (from the disk to the neutron star) must be equal (or very close to) the mass transfer

rate (from the donor to the accretion disk). Therefore in this model the system will only survive for about 1 Myr.

It is interesting to compare the behaviour of 2A 1822-371 with that of Terzan 5 X-2, another pulsar that is in many ways similar to 2A 1822-371. Terzan 5 X-2 is an 11 Hz accreting pulsar which is accreting from a sub-giant companion ($M \gtrsim 0.4\,M_\odot$) in a relatively large orbit (orbital period of 21 hr). The neutron star has a dipolar magnetic moment in the range of $\mu \simeq 10^{27}$-$10^{28}\,\mathrm{G\,cm^3}$ (Cavecchi et al. 2011; Papitto et al. 2011; Patruno et al. 2012b). This system has a clear spin-up of $\dot{\nu} \sim 10^{-12}\,\mathrm{Hz\,s^{-1}}$, and it appears to be evolving towards a millisecond pulsar in a very short timecale of a few tens of million years (Patruno et al. 2012b). Both 2A 1822-371 and Terzan 5 X-2 seem to be at odd with the very long phases that binaries with similar spin and orbital parameters spend in Roche lobe contact, which can last for about 1 Gyr or more. (Patruno et al. 2012b) proposed that Terzan 5 X-2 is in an exceptionally early RLOF phase although the reason why we are witnessing this unlikely event remains an open problem. Indeed observing two pulsars being recycled in an early RLOF phase in the relatively small population of LMXBs is unlikely. This means that the exceptionality of Terzan 5 X-2 cannot be due to chance alone and there must be a common evolutionary process that creates this kind of accreting pulsars. By using the proper motion, the radial velocity and the current position of 2A 1822-371, it is possible to find the original position and give an estimate of the age of the system. Maccarone et al. (2014) found 2A 1822-371 to likely originate from close to the Galactic center, and reported an age of about 3–4 Myr, which indeed makes the system very young (Maccarone et al. 2014) (although there is a quite big uncertainty due to the poorly constrained distance of the system). This may support the analogy that the system is similar to Terzan 5 X-2 and they both are in an early Roche lobe overflow phase.

2.4.2   Torque reversal

2A 1822-371 share a few common features with other accreting pulsars, besides Terzan 5 X-2. Short spin-up time scales are seen also in the ultra-compact binary 4U 1626-67 (Chakrabarty et al. 1997) which has $\nu/\dot{\nu}$=5,000 yr (Chakrabarty et al. 1997; Beri et al. 2014). 4U 1626-67 is a quite different binary from 2A 1822-371 since it is an ultra compact system ($P_{\mathrm{orb}} \approx 42$ min), the companion star is not a main sequence star, but rather a degenerate He or CO white dwarf, and the neutron star has a spin of 7.66 s. The system was originally discovered in 1972 by Giacconi et al. (1972). Torque reversal of the system was observed for the first time in 1990, where the system was found to be spinning down rather than up, as previously observed (Chakrabarty et al. 1997; Beri et al. 2014).

The torque reversal phenomenon is not very well understood since it is unclear what its origin is and what triggers it. However, the accretion torque in 4U 1626-67, no matter the sign of the spin frequency derivative, is very steady on timescales of years, which means that the accretion is almost certainly from an accretion disk. Chakrabarty et al. (1997) even found that the pulsar seems to be accreting steadily during spin-down. The first phase of spin-up lasted for at least 13 yr, the spin-down then lasted about 18 yr, and in 2008 4U 1626-67 began spinning up again

(Beri et al. 2014). In 4U 1626-67 the torque reversals are accompanied by sudden variations in the X-ray luminosity (Chakrabarty et al. 1997). A decrease in X-ray flux was seen when the neutron star moved from a spin-up to spin-down phase, and again there was an increase by a factor 2 in the X-ray flux with the second torque reversal (Beri et al. 2014). The very short spin-up timescale found for 2A 1822-371 is thus not incompatible with the notion that this system too will show a torque reversal somewhere in the near future.

2.4.3   Accretion Disc Corona

From the spectral analysis of 2A 1822-371 and from the shape of the eclipses it is evident that there is some extended X-ray emitting region around the pulsar, often assumed to be the ADC, that scatters the light originating on the pulsar (White & Holt 1982; Heinz & Nowak 2001; Iaria et al. 2013).

   One possible scenario is that an extended Comptonizing region is in fact the accretion curtain as it falls towards the neutron star, and it is possible that the emission we see is actually produced by photons upscattered through this curtain. To investigate this more quantitatively, we build a toy model for the spectrum, in which the underlying emission from the star (which we assume to consist of a blackbody and Comptonized hard X-ray component) is upscattered by hot electrons in the infalling accretion curtain. We use the method and code of D'Angelo et al. (2008) to produce the final Compton upscattered spectrum. We start with an initial input spectrum (assumed originating from the stellar surface) of a blackbody plus an additional power-law component with a cutoff at high energies. We then use this as a seed photon spectrum to generate an output spectrum as a result of inverse Compton upscattering through a hot (e.g. $\gtrsim$ 10keV) thermal electron cloud.

   To model this process we use a Monte Carlo Compton scattering code, whose details are described in Giannios & Spruit (2004). Briefly, the code works by using the seed photon spectrum as the initial photon energy distribution, and then calculating the outcome (final photon energy and direction) of a seed photon inverse Compton scattering off a hot electron. The electron cloud energy distribution is assumed to be thermal, and the temperature of the cloud is an input parameter of the simulation. The cloud is assumed to be isotropically surrounding the source of seed photons, and the probability of scattering depends mainly on the optical depth of the electron cloud (another input parameter).

   The model thus has six free parameters, four for the input spectrum: the blackbody temperature ($t_{\rm bb}$), the power-law slope (Γ) and cut-off energy (E_c), the relative strength of the blackbody to power law (N), and two for the Comptonizing cloud: its temperature (T_e) and optical depth (τ). We vary these parameters in order to explore the range of temperatures and optical depths for the electron cloud that could be made consistent with the observed X-ray spectrum.

   The requirement of an ADC has been introduced in the literature to explain the excess of light seen during the eclipses, with the X-ray flux never reaching a

value of zero as expected from a full eclipse. The X-ray flux is seen hovering at around 50% of its non-eclipse value. Furthermore the very long duration of the partial eclipses (about 80% of the orbit) requires an extended source surrounding the central X-ray source (White & Holt 1982; Hellier et al. 1990). The ADC was suggested to be formed from evaporated material in the accretion disk (White & Holt 1982). Shakura & Sunyaev (1973) suggested that the central source of X-ray binaries could evaporate material from the disk, and that if the material does not escape the system, it could form a corona-like cloud around the central source. White & Holt (1982) showed that the central source is always obscured if the inclination angle of the system is more than $60°$, which is compatible with what is observed for 2A 1822-371, with an inclination angle of $i =82.5°\pm1.5°$ (Heinz & Nowak 2001). As we have shown in section 2.3.4 this scenario is compatible with the behaviour of the pulsed fraction as a function of the orbital phase. Indeed the fractional amplitude of the pulsations is consistent with being constant regardless of the orbital phase of the binary. This implies that the neutron star is obscured by some material throughout the orbit. Another important point is that the fractional amplitude of the pulsar does not vary with the depth of the eclipses. This does support the idea that the surface of the neutron star is never observed and that the pulsations we do see are indeed scattered through some medium, e.g., an ADC or an accretion stream.

Iaria et al. (2001, 2015) and Parmar et al. (2000) previously suggested that the ADC must be optically thick. This was also discussed by Heinz & Nowak (2001), and Iaria et al. (2013), who stated that an optically thick ADC is not consistent with the pulsations observed. To explore the possibilities for a lower value for the optical depth we explored the parameter space for the optical depth, the power law index and the electron temperature of the Compton up-scattering cloud. We found it possible to create an input spectrum, that, sent through the Compton up-scattering cloud, would be similar to the fitted spectrum with a high optical depth used by Iaria et al. (2015). This can be seen on Fig. 2.6, where the red line is the fit used by Iaria et al. (2015), the blue line is the input spectrum we created, using both a power law and a black body, and the black line is the output spectrum after the input spectrum has been sent through a Compton cloud.

The blue line on Fig. 2.6 corresponds to a power law index of $\Gamma = 1$, electron temperature of $E_c = 10\text{keV}$ and optical depth of $\tau = 1$. Our test of the optical depth should be taken only as a proof of principle, that a model spectra with a black body and a power law can recreate the spectra observed *even if the optical depth is small*. The quality of the spectra and its match with the spectra found for example by Iaria et al. (2015) is judged by eye and by the normalized root mean square deviation which we find to be 28%.

The limits for the electron temperature is $3 < T_e < 15\,\text{keV}$, the power law index limits are $0.5 < \Gamma < 1.5$ and the acceptable range of optical depth is $0.01 < \tau < 3$. Within these limits the spectra are reasonably reproduced with a much lower optical depth that is thus compatible with the presence of pulsation without requirement an optically thick Comptonization region plus an optically thick scattering ADC as suggested in Iaria et al. (2013). These results are also
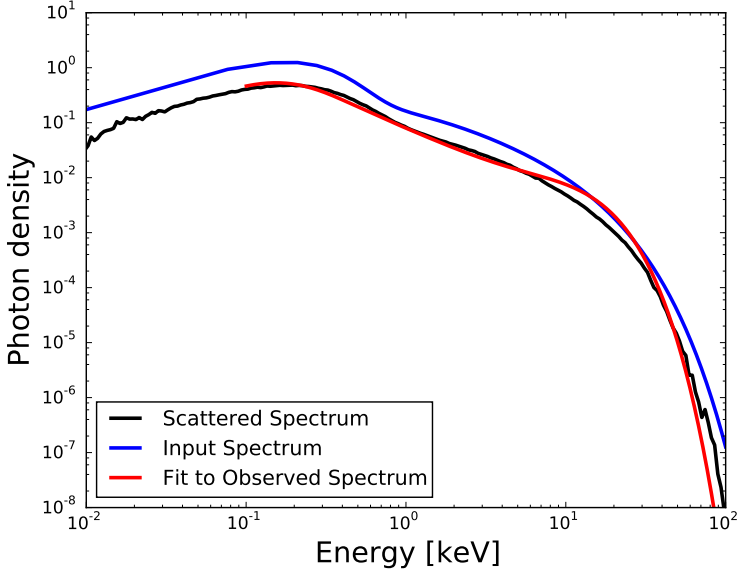
Figure 2.6: The black line represents the best simulated spectrum. The black line is our guess corresponding to the red line, which is the fit to the spectrum of 2A 1822-371 used by Iaria et al. (2015). The blue line is the input spectrum we have used, consisting of both a black body and a power law component.

compatible with recent spectral modelling performed by Niu et al. (2016) which discussed the possibility that the accretion disk corona around 2A 1822-371 is indeed optically thin.

The fit we created give a simple structure of the system, where the ADC is surrounding the pulsar, and reaching further out than the secondary star, making the pulsar light coming from an extended source, and thus both explaining the pulsations and the 50% depth of the eclipses. The structure of the system we suggest is initially very simple when compared to what White & Holt (1982) suggested. By analysing a spectrum that consists of both a power law and black body component, it is possible to eliminate the optically thick Comptonizing region, and thus explain the system only with an optically thin (or moderately thick; $\tau \approx 0.01 - 3$) ADC surrounding the pulsar. Another possibility for the geometry is that we could be seeing this system through an extended accretion stream. This stream scatters the light and pulsations just as an ADC would do. Assuming this as an explanation, simplifies the structure of the system even further.

2A 1822-371 is not the only suggested ADC systems. Another such system is MS 1603.3+2600. MS 1603.3+2600 was discovered by Morris et al. (1990) and has a 1.7 hr orbital period (Jonker et al. 2003b). The source shows both similarities and differences with 2A 1822-371. Both sources appear to be at a fairly high inclination, although the precise value for the inclination angle is not known for

MS 1603.3+2600. MS 1603.3+2600 is thought to be at a distance of about 6–24 kpc (Parmar et al. 2000; Jonker et al. 2003b; Hakala et al. 2005). Despite not showing accretion powered pulsations, MS 1603.3+2600 has a neutron star primary, since the source shows type I X-ray bursts (Jonker et al. 2003b; Hakala et al. 2005). The existence of an ADC around the source is supported by variations in the X-ray bursts. Hakala et al. (2005) looked at two XMM-*Newton* observations taken on 2003 January 20 and 22. They observed several Type I X-ray burst candidates. The bursts during the first observation have a count rate of about 6 counts s^{-1} whereas those seen during the second part of the observation only have a count rate of 2-3 counts s^{-1}. The variation suggests that the bursts are not directly observed, thus it is possibly only scattered X-rays that are observed, with the scattering medium forming an ADC (Hakala et al. 2005).

2.4.4   2A 1822-371 as a super Eddington source

A big weakness of the model that we have discussed so far is that it requires an Eddington limited accretion rate, despite the binary containing a low mass main sequence star that should transfer mass at a rate of about 10^{-10} M$_\odot$ yr^{-1}. Jonker et al. (2003a) performed detailed optical observations of 2A 1822-371 and suggested that one possible interpretation of the spectroscopic results is that the donor star is out of thermal equilibrium. Cowley et al. (2003) also suggested that the donor must be somewhat evolved since otherwise it would not fill its Roche lobe. Muñoz-Darias et al. (2005) also proposed that 2A 1822-371 is a LMXB which descends from an intermediate mass X-ray binary progenitor (initial $M \gtrsim 1\,M_\odot$), with the companion that has already lost a substantial amount of mass. In this case the mass transfer would not be driven by angular momentum loss via magnetic braking and/or gravitational radiation but would proceed on the thermal (Kelvin-Helmotz, KH) timescale of the companion (see e.g., King et al. 1996).

   The thermal timescale is $\tau_{KH} \approx GM_2^2/(2R\,L_{nucl})$ where G is the universal gravitational constant, M_2 is the companion mass, R_2 its radius and L_{nucl} the nuclear stellar luminosity. The stellar luminosity is not well known in 2A 1822-371 since the optical observations are usually dominated by the disk emission/irradiation. Furthermore, as shown by King et al. (1995), the thermal timescale changes when irradiation is present, since the stellar surface luminosity might exceed the nuclear luminosity. Since the observed X-ray luminosity is of the order of 10^{36} erg s^{-1} and assuming that all the irradiation luminosity is re-emitted by the stellar surface of the donor, the irradiation luminosity would, due to geometric effects, correspond to approximately 10^{34} erg s^{-1} and the KH timescale becomes $\tau_{KH} \gtrsim 10^7$ yr, using M$_2$=0.46 M$_\odot$ and R$_2$ corresponding to the Roche lobe radius, R$_L$=0.6 R$_\odot$. If the companion star evolved on the τ_{KH} timescale, then the mass transfer rate can be as high as $\sim 10^{-7}$ M$_\odot$ yr^{-1}

   We now try to interpret the observations of 2A 1822-371 in light of this hypothesis. In the following there is a big uncertainty on most parameters, thus the results could vary within an order of magnitude, and are only approximate. The orbital separation of 2A 1822-371 changes for two reasons: 1. the redistribution of angular momentum in the binary and 2. the loss of angular momentum via

magnetic braking/gravitational wave emission (see e.g., Frank et al. (2002)):

$$\frac{\dot{a}}{a} = \frac{2\dot{J}}{J} + \frac{-2\dot{M_2}}{M_2}(1-q) \quad (2.7)$$

here $q = M_2/M_{\mathrm{NS}}$ is the mass ratio between the companion (M_2) and neutron star mass (M_{NS}), a is the orbital separation, J is the angular momentum and the dot refers to the first time derivative. In J we include all effects, e.g. magnetic breaking, gravitational waves and mass loss (Tauris & van den Heuvel 2006). If the mass transfer $\dot{M_2} \approx 10^{-7} M_\odot \, yr^{-1}$ then, assuming to first order a conservative mass transfer scenario ($\dot{J} \approx 0$) we expect a relative variation of the orbit $\dot{a}/a \sim 10^{-14} \, s^{-1}$. The observations of the orbital period derivative $\dot{P}_{\mathrm{orb}} \approx 1.51 \times 10^{-10}$ (Iaria et al. 2011) provide a direct test of this hypothesis. Indeed from the 3-rd Kepler law we expect that $\dot{a}/a = 2\dot{P}_{\mathrm{orb}}/3P_{\mathrm{orb}}$ and the observed values give: $2\dot{P}_{\mathrm{orb}}/3P_{\mathrm{orb}} \approx 5 \times 10^{-15}\,\mathrm{s}^{-1}$ which is in good agreement with the hypothesis that 2A 1822-371 is evolving on a thermal timescale in a conservative mass transfer scenario.

Since the mass transfer is super-Eddington we can follow the line of reasoning of King & Lasota (2016), where they examine the case of the Ultra-Luminous X-ray source (ULX) M82 X-1. If that donor in M82 X-1 is in a super-Eddington mass transfer phase then the mass accretion rate, magnetic radius and the magnetic moment of the neutron star (μ) can be inferred from first principles. We argue here that one remarkable possibility to explain the phenomenology of 2A 1822-371 is that it is a mildly super-Eddington source.

In this case the accretion disk will be the standard Shakura-Sunyaev geometrically thin disk down to the so-called spherization radius (Shakura & Sunyaev 1973):

$$R_{\mathrm{sph}} = \frac{27}{4}\frac{\dot{M}_{\mathrm{tr}}}{\dot{M}_{\mathrm{Edd}}}R_{\mathrm{g}} \quad (2.8)$$

where $\dot{M}_{\mathrm{tr}}$ and $\dot{M}_{\mathrm{Edd}}$ are the mass transfer rate ($10^{-7}\,\mathrm{M_\odot\,yr^{-1}}$) and the Eddington limit for a neutron star (that we set equal to $\approx 2 \times 10^{-8}\,\mathrm{M_\odot\,yr^{-1}}$) and the $R_{\mathrm{g}} = GM/c^2 \approx 2 \times 10^5$ cm is the neutron star gravitational radius ($M_1 = 1.69\,\mathrm{M_\odot}$). This gives a spherization radius of $\sim 10^7$ cm. Beyond this radius the flow will become geometrically thick and generate a funnel flow that can produce beaming (see e.g., King (2009)).

If the innermost region of the accretion disk is truncated at the magnetospheric radius R_{M}, with $R_{\mathrm{M}} < R_{\mathrm{sph}}$, then the local mass accretion rate in any annulus of the disc with radius $R < R_{\mathrm{sph}}$ needs to be:

$$\dot{M}(R) = R/R_{\mathrm{M}}\dot{M}_{\mathrm{Edd}}. \quad (2.9)$$

Together with the expression for the magnetic dipole moment and spin up (Eq. 2.6), the spherization radius and the mass accretion rate equations (Eq. 2.8, 2.9) form a set of 4 equations with four variables, R_{sph}, $\dot{M}(R_{\mathrm{M}})$, μ and R_{M}. Following the method by King & Lasota (2016) one finds $R_{\mathrm{M}} \sim 10^6 - 10^7$ cm, $\mu \approx 1 \times 10^{28}\,\mathrm{G\,cm^3}$ (corresponding to a magnetic field of $\approx 2 \times 10^{10}\,\mathrm{G}$ at the poles and assuming a

$\dot{M}(R_{\mathrm{M}}) \approx 2 \times 10^{-8}\,\mathrm{M_\odot\,yr^{-1}}$). The fact that the spherization radius and the magnetospheric radius are very close suggests that only the innermost portions of the accretion disk must be geometrically thick and generate a strong outflow. Such outflow might be responsible for the observed ADC since it will surround the central X-ray source. The value of the magnetic field is somewhat smaller than the one inferred from the possible cyclotron line reported by Iaria et al. (2015) although it is of the same order of magnitude despite the large uncertainties involved. Indeed we suggest that:

- The donor star of 2A 1822-371 is irradiated by a luminosity of $\approx 10^{36}\,\mathrm{erg\,s^{-1}}$.

- The irradiation drives a thermal timescale mass transfer of the order of $10^{-7}\,\mathrm{M_\odot\,yr^{-1}}$.

- The super-Eddington mass transfer rate generates an outflow at the spherization radius, very close to the magnetospheric radius.

- The inner regions of the disk are geometrically thick and obscure the central source, as seen in Fig. 2.7.

Since the donor (and the observer) are nearly parallel to the accretion disk plane, even a very mild beaming will be sufficient to direct most of the radiation outside the line of sight of both the donor and the observer. Therefore the donor will not be irradiated by an X-ray luminosity much larger than the observed $L_{\mathrm{X}} \approx 10^{36}\,\mathrm{erg\,s^{-1}}$.

Finally, as a self-consistency check we need to verify whether the angular momentum loss due to the expulsion of material from the Roche lobe of the neutron star can alter significantly the orbit of the binary. As a limiting case we assume that all the material transferred in the neutron star Roche lobe is expelled and thus, following Postnov & Yungelson (2006):

$$\frac{\dot{J}_{\mathrm{orb}}}{J_{\mathrm{orb}}} = \beta \frac{\dot{M}_2\,M_2}{M_{\mathrm{NS}}M_{\mathrm{T}}} \approx 10^{-16}\,\mathrm{s^{-1}} \tag{2.10}$$

where $M_{\mathrm{T}} = M_2 + M_{\mathrm{NS}}$ is the total binary mass (assumed here to be approximately $2\,\mathrm{M_\odot}$) and J_{orb} and $\dot{J}_{\mathrm{orb}}$ are the total orbital angular momentum of the binary and its variation, and β is the fraction of the mass that is expelled. By inserting this value in Eq. 2.7 and by considering that $\dot{M}_2 \approx 10^{-7}\,\mathrm{M_\odot\,yr^{-1}}$ we see that the final value of $\dot{a}/a$ is still of the order of $10^{-14}\,\mathrm{s^{-1}}$ which, again, is compatible with the observations.

2.4.4.1   Possible Tests of the Proposed Model

If 2A 1822-371 is really a mildly super-Eddington source then:

- The neutron star magnetic field must be of the order of a few times 10^{10} G.

- The source should not show any torque reversal in the near future.

- An outflow from the neutron star must be present and possible radio emission from a jet/outflow should be expected.
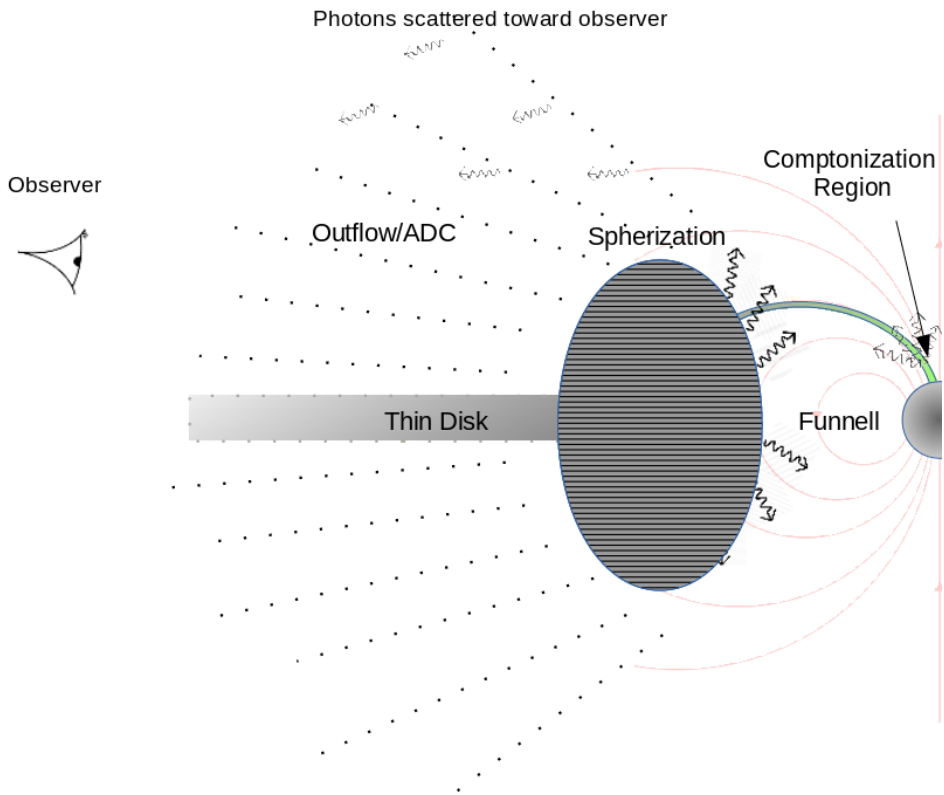
Figure 2.7: The illustrations show the geometry of the problem according to the super-Eddington scenario that we propose for 2A 1822-371 . The observer is located at an inclination angle $i = 82°$ and we have chosen an aligned rotator for simplicity. The thick part of the accretion disk begins at the spherization radius and ends at the magnetospheric radius where the plasma becomes channeled towards the neutron star poles. The accretion flow along the magnetic field lines is abruptly stopped a the neutron star surface and a shock forms close to the neutron star surface. It is in this shock that the Comptonization process takes place. The outflow generates instead an optically thin cloud around the neutron star that is responsible for the scattering of a small portion of the X-ray photons towards the direction of the observer.

2.5   Conclusion

We examined 13 years of data from *RXTE*, and conclude that the long-term spin frequency derivative and the two phase connected data sets, where we found short-term spin frequency derivatives, support an overall fast spin-up. The spin-up supports previous work by Jain et al. (2010); Iaria et al. (2015) and Chou et al. (2016). We tested if there was any flux-phase correlation present in this pulsar as there is in other systems, but found that there were no correlation.

   We propose that the 2A 1822-371 is a relatively young binary (age of $\sim 1 - 10\,\mathrm{Myr}$) in which the donor is in a thermal timescale mass transfer phase. The orbital variation observed can be explained by the effect of the redistribution of angular momentum in the binary with no need for a large mass outflow from the donor star. An outflow is instead expected from the Roche lobe of the neutron star as a consequence of the nearly Eddington mass accretion rate occurring close to the neutron star magnetospheric radius. We propose that the outflow generates a large scale optically thin corona with $\tau \approx 1$ that surrounds the system. The lack of variability in the fractional amplitude suggests however, that the central source is always partially obscured and thus an optically thick region must form close to the neutron star at the approximate location of the spherization radius. We propose that this optically thick region generates a mild beaming as a consequence of the super-Eddington mass transfer rate. The Eddington/super-Eddington luminosity is not seen directly since the observer is viewing the source nearly edge on, in a way similar to what happens in the black hole binary SS433 (King 2009).

Bibliography

Aly J. J., 1985, A&A, 143, 19

Bayless A. J., Robinson E. L., Hynes R. I., Ashcraft T. A., Cornell M. E., 2010, ApJ, 709, 251

Beri A., Jain C., Paul B., Raichur H., 2014, MNRAS, 439, 1940

Bhattacharya D., van den Heuvel E. P. J., 1991, Phys. Rep., 203, 1

Bildsten L., et al., 1997, ApJS, 113, 367

Bradt H. V., Rothschild R. E., Swank J. H., 1993, A&A, 97, 355

Burderi L., Di Salvo T., Riggio A., Papitto A., Iaria R., D'Aì A., Menna M. T., 2010, A&A, 515, A44

Cavecchi Y., et al., 2011, ApJ, 740, L8

Chakrabarty D., et al., 1997, ApJ, 474, 414

Chou Y., Hsieh H.-E., Hu C.-P., Yang T.-C., Su Y.-H., 2016, preprint, (arXiv:1608.04190)

Cowley A. P., Schmidtke P. C., Hutchings J. B., Crampton D., 2003, AJ, 125, 2163

D'Angelo C. R., Spruit H. C., 2010, MNRAS, 406, 1208

D'Angelo C. R., Spruit H. C., 2012, MNRAS, 420, 416

D'Angelo C., Giannios D., Dullemond C., Spruit H., 2008, A&A, 488, 441

Frank J., King A., Raine D. J., 2002, Accretion Power in Astrophysics: Third Edition

Ghosh P., Lamb F. K., 1979, ApJ, 234, 296

Giacconi R., Murray S., Gursky H., Kellogg E., Schreier E., Tananbaum H., 1972, ApJ, 178, 281

Giannios D., Spruit H. C., 2004, A&A, 427, 251

Goodson A. P., Winglee R. M., Böhm K.-H., 1997, ApJ, 489, 199

Griffiths R. E., Gursky H., Schwartz D. A., Schwarz J., Bradt H., Doxsey R. E., Charles P. A., Thorstensen J. R., 1978, Nature, 276, 247

Hakala P., Ramsay G., Muhli P., Charles P., Hannikainen D., Mukai K., Vilhu O., 2005, MNRAS, 356, 1133

Harlaftis E. T., Charles P. A., Horne K., 1997, MNRAS, 285, 673

Hartman J. M., et al., 2008, ApJ, 675, 1468

Haskell B., Patruno A., 2011, ApJ, 738, L14

Heinz S., Nowak M. A., 2001, MNRAS, 320, 249

Hellier C., Mason K. O., Smale A. P., Kilkenny D., 1990, MNRAS, 244, 39P

Iaria R., Di Salvo T., Burderi L., Robba N. R., 2001, ApJ, 557, 24

Iaria R., di Salvo T., Burderi L., D'Aí A., Papitto A., Riggio A., Robba N. R., 2011, A&A, 534, A85

Iaria R., Di Salvo T., D'Aì A., Burderi L., Mineo T., Riggio A., Papitto A., Robba N. R., 2013, A&A, 549, A33

Iaria R., et al., 2015, A&A, 577, A63

Jahoda K., Markwardt C. B., Radeva Y., Rots A. H., Stark M. J., Swank J. H.,

Strohmayer T. E., Zhang W., 2006, ApJs, 163, 401

Jain C., Paul B., Dutta A., 2010, MNRAS, 409, 755

Ji L., Schulz N. S., Nowak M. A., Canizares C. R., 2011, ApJ, 729, 102

Jonker P. G., van der Klis M., 2001, ApJL, 553, L43

Jonker P. G., van der Klis M., Groot P. J., 2003a, MNRAS, 339, 663

Jonker P. G., van der Klis M., Kouveliotou C., Méndez M., Lewin W. H. G., Belloni T., 2003b, MNRAS, 346, 684

King A. R., 2009, MNRAS, 393, L41

King A., Lasota J.-P., 2016, MNRAS, 458, L10

King A. R., Frank J., Kolb U., Ritter H., 1995, ApJ, 444, L37

King A. R., Frank J., Kolb U., Ritter H., 1996, ApJ, 467, 761

Lovelace R. V. E., Romanova M. M., Bisnovatyi-Kogan G. S., 1995, MNRAS, 275, 244

Maccarone T. J., Girard T. M., Casetti-Dinescu D. I., 2014, MNRAS, 440, 1626

Mason K. O., Cordova F. A., 1982, ApJ, 262, 253

Morris S. L., Liebert J., Stocke J. T., Gioia I. M., Schild R. E., Wolter A., 1990, ApJ, 365, 686

Muñoz-Darias T., Casares J., Martínez-Pais I. G., 2005, ApJ, 635, 502

Niu S., Yan S.-P., Lei S.-J., Nowak M. A., Schulz N. S., Ji L., 2016, Research in Astronomy and Astrophysics, 16, 57

Papitto A., D'Aì A., Motta S., Riggio A., Burderi L., di Salvo T., Belloni T., Iaria R., 2011, A&A, 526, L3

Parmar A. N., Oosterbroek T., Del Sordo S., Segreto A., Santangelo A., Dal Fiume D., Orlandini M., 2000, A&A, 356, 175

Patruno A., Wijnands R., van der Klis M., 2009, ApJ, 698, L60

Patruno A., Hartman J. M., Wijnands R., Chakrabarty D., van der Klis M., 2010, ApJ, 717, 1253

Patruno A., Alpar M. A., van der Klis M., van den Heuvel E. P. J., 2012a, ApJ, 752, 33

Patruno A., Alpar M. A., van der Klis M., van den Heuvel E. P. J., 2012b, ApJ, 752, 33

Podsiadlowski P., Rappaport S., Pfahl E. D., 2002, ApJ, 565, 1107

Postnov K. A., Yungelson L. R., 2006, Living Reviews in Relativity, 9, 6

Sasano M., Makishima K., Sakurai S., Zhang Z., Enoto T., 2014, PASJ, 66, 35

Shakura N. I., Sunyaev R. A., 1973, A&A, 24, 337

Somero A., Hakala P., Muhli P., Charles P., Vilhu O., 2012, A&A, 539, A111

Tauris T. M., van den Heuvel E. P. J., 2006, Formation and evolution of compact stellar X-ray sources. pp 623–665

Ustyugova G. V., Koldoba A. V., Romanova M. M., Lovelace R. V. E., 2006, ApJ, 646, 304

White N. E., Holt S. S., 1982, ApJ, 257, 318

White N. E., Becker R. H., Boldt E. A., Holt S. S., Serlemitsos P. J., Swank J. H., 1981, ApJ, 247, 994

Yi I., Wheeler J. C., Vishniac E. T., 1997, ApJ, 481, L51
van Straaten S., van der Klis M., Méndez M., 2003, ApJ, 596, 1155
van der Klis M., 2001, ApJ, 561, 943

CHAPTER

3

Coherent variability of GX 1+4

The accreting pulsar GX 1+4 is a symbiotic X-ray binary system with a M-type giant star companion. The system has a spin period of about 150 s and a proposed strong magnetic field of 10^{12}–10^{14} G. In this chapter we study the coherent variability of the source and attempt to find a phase-coherent solution for the pulsar. We also test for the presence of a pulse phase - flux correlation, similar to what is observed for the accreting millisecond X-ray pulsars, in order to test whether this feature is dependent on the magnetic field strength. We find that no phase coherent solution exists which suggests that the pulsar is accreting plasma from a wind rather than an accretion disc. We also find evidence that the pulse phase is not correlated with the X-ray flux, which strengthens the idea that such relation might be present only in weak magnetic field sources like accreting millisecond pulsars.

3.1   Introduction

The X-ray pulsar GX 1+4 was first discovered in 1970 by balloon X-ray obser-
vations at energies above 15 keV by Lewin et al. (1971). GX 1+4 is the first
discovered accreting pulsar in a low mass symbiotic X-ray binary system (SyXB)
and it is unique among the symbiotic binaries, due to the primary star being a
neutron star and not a white dwarf or a main sequence star (Davidsen et al. 1977;
Hinkle et al. 2006; Serim et al. 2017). The companion of GX 1+4 is V2116 Oph
(Chakrabarty et al. 1997), which is an M giant star, of about $1.2 M_\odot$ and the pulsar
is thought to have a mass of $1.35 M_\odot$ (González-Galán et al. 2012). The M giant
is probably not filling its Roche lobe, but the pulsar is instead accreting through a
stellar wind (Chakrabarty et al. 1997; Hinkle et al. 2006). The orbital period of GX
1+4 was originally proposed to be 304 days (Cutler et al. 1986; Pereira et al. 1999).
This value was, however, revised to be 1161 days and it remains to be confirmed
(Hinkle et al. 2006). The orbit is modestly eccentric with e=0.10 (Hinkle et al.
2006). Torque reversals are observed in GX 1+4, with the first observations show-
ing a clear neutron star spin-up (Nagase 1989) that, around 1987, when the pulsar
reappeared, turned into a clear spin-down. During the spin-up phase, the pulsar
had a spin frequency derivative of $\dot{\nu}$=6.0×10^{-12} Hz s^{-1}, whereas during spin down
the pulsar had a spin frequency derivative of $\dot{\nu}$=-3.7×10^{-12} Hz s^{-1} (Chakrabarty
et al. 1997). The spin period was about 159.9 s in 2010 (Yoshida et al. 2017).

Rea et al. (2005) observed a possible electron cyclotron feature in the energy
spectra, using *BeppoSAX*, at an energy of 32–37 keV. This would correspond to a
magnetic field of about 4×10^{12} G, which is lower than earlier magnetic field esti-
mates of order $B \sim 10^{13-14}$ G (Dotani et al. 1989; Mony et al. 1991; Cui & Smith
2004), inferred from spin-down episodes. It must be remarked, however, that the
proposed identification of the cyclotron line is still unconfirmed (Rea et al. 2005).

An open question about GX 1+4, as well as other slow accreting pulsars in low
mass X-ray binaries, is whether the presence of the neutron star magnetic field and
its interaction with the accretion flow could lead to phenomena similar to those
observed in accreting millisecond X-ray pulsars (AMXPs), which are much fainter
and with lower magnetic fields (see Patruno & Watts 2012 for a review). The
reason is that observing a similar phenomenology for example in the behaviour of
pulsations might shed some light on how accretion flows and neutron star magne-
tospheres interact and clarify the exact role of the strength of the magnetic field
and mass accretion rate. For example, a still unexplained correlation between the
X-ray flux and the pulse phases is observed in several AMXPs (Patruno et al.
2009), contrary to what is predicted by accretion torque theory, where it is the
spin frequency derivative and not the pulse phase that is expected to be correlated
with the X-ray flux. Iłkiewicz et al. (2017) discussed the variability of GX 1+4,
reporting large variations in the X-ray flux over several energy bands. The varia-
tions reach up to one to two orders of magnitude (Iłkiewicz et al. 2017; Serim et al.
2017). Due to these large variations in X-ray flux, we consider GX 1+4 an opti-
mal system to test whether corresponding large variations in the pulse phases are
present. Patruno et al. (2009) examined six known AMXPs based on the presence

of red timing noise in the pulse phases. They found that there was a correlation and in some cases an anti-correlation, between the flux and pulse phase. This was interpreted as due to the motion of the hot spot on the surface of the pulsar in response to mass accretion rate variations. It is currently not known whether a similar phenomenon exists in high field pulsars since the stronger magnetic field might prevent the movement of plasma on the neutron star surface. Bak Nielsen et al. (2017) and Patruno et al. (2012) found that such phase–flux correlation was not present in two moderately high field accreting pulsars, namely 2A 1822–371 and Terzan 5 X–2. Despite the lack of phase–flux correlations some timing noise was however observed in the pulse phase residuals of these systems. Furthermore the strength of their magnetic fields is only 1-2 orders of magnitude larger than what is seen in AMXPs, whereas their accretion rate is close to the Eddington limit. Therefore it remains to be verified whether higher magnetic field accreting pulsars show such correlation or not. Testing this hypothesis is very valuable for two reasons. On one hand, if the hot spot is moving on the surface then this effect must be taken into account when finding a pulsar timing solution. Second, the magnetic field of GX 1+4 is four to six orders of magnitude larger than those found in AMXPs and thus detecting (or not detecting) this phenomenon will help understand its origin.

In this chapter we examine long and short term fluctuations of the pulse time of arrivals, variations of the X-ray flux and we check whether there is any evidence for a pulse phase–flux correlation on the prototype system GX 1+4. In section 3.2 we go through the observations used, and in section 3.3 we present the results of our analysis. In section 3.4 we discuss the possible presence (or lack thereof) of a pulse phase–flux correlation, the observed short term variability of the source and we provide a physical interpretation of what is observed.

3.2   Observations

We have used data taken between March 6 to November 14, 2001 (ObsID=60060), thus using almost the same data range as Serim et al. (2017). We choose this dataset because Serim et al. (2017) claim to have phase connected the data and provide a timing solution for the source. The data was recorded with the Proportional Counter Array (PCA) which was on board of the Rossi X-ray Timing Explorer (*RXTE*). *RXTE*/PCA has five xenon/methane proportional counter units that are sensitive in the energy range of 2–60 keV (Jahoda et al. 2006). We use the event files with a resolution of 2^{-20} s (GoodXenon) for the timing analysis, and the Standard-2 data-mode, with a 16 s time resolution, to create the X-ray lightcurve. The lightcurve is created in the 2–16 keV energy range and the X-ray flux is averaged for each observation (ObsID) and normalized in Crab units (see top panel in Fig. 3.1). A detailed description of this procedure can be found in van Straaten et al. (2003). We perform the timing analysis by selecting the energy channels 9–67, which correspond to an energy range of about 3–20 keV, as specified by Serim et al. (2017). The data was barycentered using the FTOOL `faxbary`,
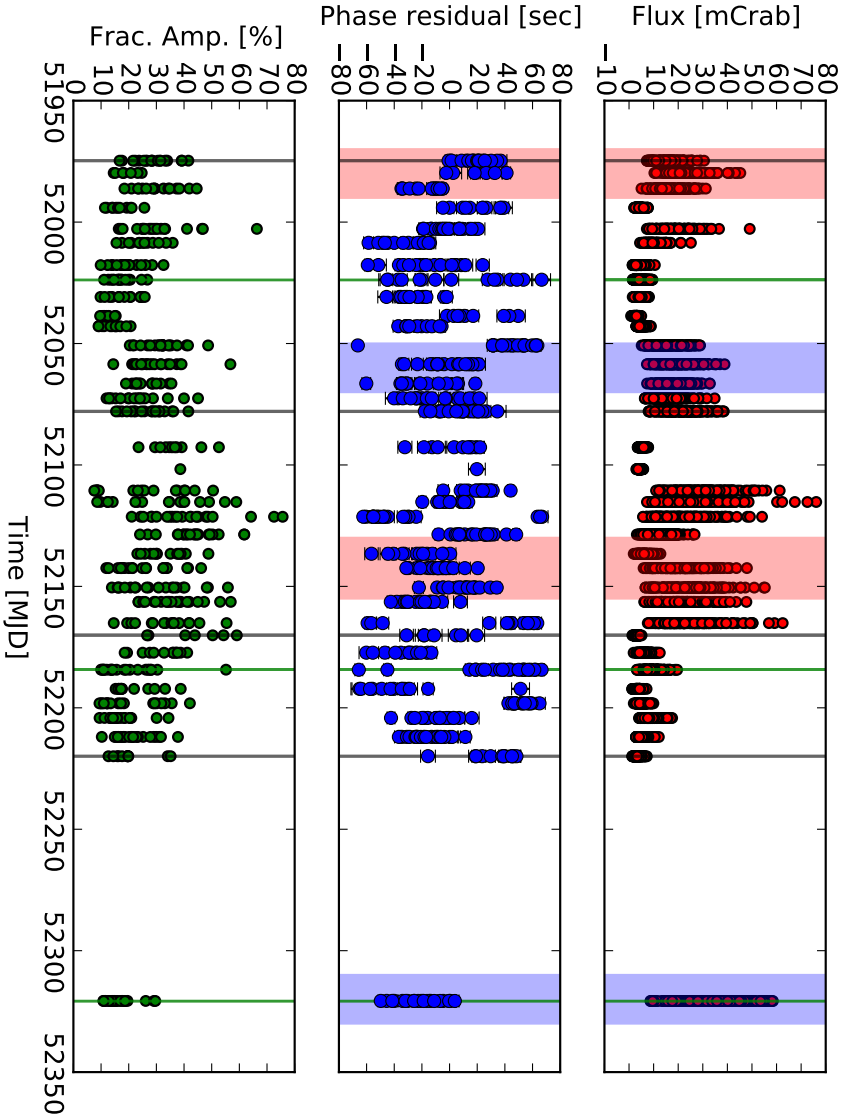
Figure 3.1: Top panel: The lightcurve for the *RXTE* data between March 6 to November 14 2001. Lower panel: The corresponding pulse phase. The red area marks the correlations between the flux and pulse phase, the blue area marks the anti-correlation and the green line marks the data segment that is zoomed in on in Fig. 3.2. The black lines mark the 4 times for which pulse profiles are shown in Fig. 3.3

Table 3.1: The parameters used in the epoch folding.

Parameter	Value
MJD	51974.7 - 52320.7
RA	17:32:02.16
DEC	-24:44:44.2
Epoch	51974.0
ν	0.007335526
$\dot{\nu}$	-2.0585×10^{-12}

using the JPL D405 Solar System coordinates and the source coordinates, from Cutri et al. (2003), RA: 17:32:02.16, DEC:-24:44:44.2. We then epoch folded the barycentered data in pulse profiles of 32 bins over the spin period, P_s=136.3228 s for segments of length ~ 2000–3500s. We cross-correlated each pulsation with a sinusoid at the spin frequency and generated the time of arrivals (TOAs) for this data set. We selected only pulsations with a signal-to-noise (S/N) larger than 3.3 σ in order to achieve less than one false detection in our ensemble (composed by a total of $N = 538$ pulse profiles). The S/N is defined as the ratio between the pulse amplitude and its 1σ statistical error. The ephemeris used during the epoch folding are taken from Serim et al. (2017). To phase connect the data we used TEMPO2 version 2012.6.1.

3.3   Results

In the following sections we will go though the flux variations of GX 1+4 and compare these to variations in the pulse phase, in order to test if there is a correlation or anti-correlation. We look at both the full data set and three small segments of the data.

3.3.1   Phase connection

We have used archival data from *RXTE* approximately corresponding to the data segment labelled "*a*" in Serim et al. (2017), and we used the coherent timing solution from the same paper (see Table 3.1). We do this in order to reproduce their results and inspect the pulse phase residuals in order to later look for a pulse-phase correlation in the data. When folding the data we clearly detect pulsations with high S/N, but the pulse phase residuals are scattered between -0.5 and +0.5 pulse phase cycles, which means that the pulsations are not phase connected. We thus cannot recover the same results of Serim et al. (2017) with their proposed timing solution.

We thus consider the possibility that the true spin frequency (and derivatives) of GX 1+4 might be off with respect to the solution proposed by Serim et al. (2017) To look for a phase connected solution we thus keep all parameters fixed and vary the pulse frequency to explore the χ^2 surface and select the value that minimizes the χ^2. We used 1000 different pulse frequencies, varying between 0.0071355 Hz

and 0.0075355 Hz in steps of 4×10^{-7} Hz. The pulse frequency corresponding to the minimum χ^2 found still did not give a phase-connected solution. We then considered also variations of the pulse frequency derivative $\dot{\nu}$, exploring values between -2.24585×10^{-12} Hz s^{-1} and -1.6585×10^{-12} Hz s^{-1} in steps of 8×10^{-16} Hz s^{-1} and again we were unable to find a phase-connected solution. To further investigate the reason of this, we considered also the presence of a $\ddot{\nu}$, since Serim et al. (2017) provide also a measured value for that parameter. However we found no improvement in our attempt to phase connect the data. This is not surprising since the contribution of $\ddot{\nu}$ to the pulse phase variation with time can be considered negligible when compared to ν and $\dot{\nu}$. A difference between our analysis and that of Serim et al. (2017) is that our dataset spans a time range slightly larger than theirs, by about 2 months. However, again this makes no difference with regards to the final solution since the phase connections is not achieved in any segment of the data. We do see pulsations with high signal to noise throughout the observations, which means that the solution is sufficiently accurate to fold the data. An example of the pulse phase residuals found when using for example the solution given in Table 3.1 is given in Fig. 3.1.

Finally, since we are using only the fundamental frequency for our coherent timing analysis, we tested the presence of a 2nd and 3rd harmonic in the pulse profiles. Both were present in the data with relatively high significance (S/N up to ~ 15). However, they did not behave differently from the 1st harmonic (i.e., the fundamental), and no phase connected solution could be found in this case.

3.3.2 Phase - Flux correlation

Another way to search for a phase connected solution is to try to maximize the strength of the phase–flux correlation, which has been observed so far in several accreting millisecond pulsars (for a more detailed discussion of this method see for example Patruno 2010). We thus tested whether there are similarities in the variations of the flux with the pulse phase residuals as seen in Patruno et al. (2009). To obtain the exact count rate we used only one PCU, namely PCU2, since this unit is always on during all observations. We use the count rate in this case because in this way we can create a lightcurve with the exact same time binning as the pulse phase time series. We then kept the Keplerian orbit fixed (see Table 1) and varied the pulse frequency and frequency derivative as explained in the previous section. We then fitted the data with the linear correlation

$$\phi = a + bF_x \tag{3.1}$$

where ϕ is the pulse phase, F_x is the X-ray count-rate and "a" and "b" are fitting parameters. We explored the χ^2 surface to find the value of ν that minimizes the χ^2 value. We explored a grid of 1000 values for ν and then fitted the phase residuals vs. flux with the linear relation in Eq. 3.1. We then found the minimum root-mean-squared (rms) value of the fit which gave us the best fit value of $\nu \sim 0.007417326$ Hz. We re-folded the data with the new value for ν and iterated this entire procedure for a few times, but the minimum χ^2 value did not converge. This means that we are unable to find a global χ^2 minimum corresponding to a phase-connected

solution of the data. We then repeated the entire procedure by adding also the pulse frequency derivative $\dot{\nu}$ (and using again 1000 guess values) to verify whether the lack of a phase connection could be ascribed to a rapid variation of the pulse frequency over the time span of the observations. However, we could not find a global minimum for the χ^2 even in this case.

In summary, when using both standard χ^2 minimization methods with the pulse phases alone and when using the pulse-phase correlation method we cannot phase connect the solution. We stress, however, that pulsations were detected throughout the observations, which means that a coherent signal is present in the data, at least on a short timescale (of the order of a few rotational periods of the pulsar). The coherence of the signal is then lost when looking at longer (>hours) timescales. We then went back and used the TOA solution given in table 3.1 (Serim et al. 2017), and inspected the resulting light curves and pulse phase residuals, showing the minimum rms. These are shown in Fig. 3.1. The reason for this choice is that if the pulse phases keep their coherence on short timescales then it should still be possible to see correlations between flux and pulse phases on these timescales (assuming that such an effect exists in GX 1+4). From the figure it is clear that there is no simple long-term correlation or shape that is similar in the top two panels, but there are indeed a few segments of the top two panels on Fig. 3.1 where the flux and pulse phase residuals are correlated or anti-correlated. These are respectively marked in blue (anti-correlation) and red (correlation). The green lines on Fig. 3.1 are the three sections that are zoomed in on in Fig. 3.2, and the grey lines are the times where the pulse profiles are plotted, as seen in Fig. 3.3.

3.3.3   Short-term variability

Since we do see pulsations in every data point plotted in Fig. 3.1 this means that we recover part of the coherent signal with the solution used. On Fig. 3.2 the three data segments marked in green (in Fig. 3.1) are shown. The three segments were chosen due to the variations in the flux and phase residuals, where segment 1 has almost no variation in the flux but a large variation in the phase residuals, segment 2 has small variations in the flux with larger variations in the phase residuals but not as large as segment 1, and the 3rd segment has a variation in both flux and phase of somewhat similar order. On Fig. 3.2 the average of the phase residuals are corresponding to an overall slope of zero, indicating that the frequency is correctly measured. When looking at Fig. 3.2 it is evident that there is no clear correlation between the flux and phase residuals on a short time scale.

3.4   Discussion

3.4.1   Pulse Profiles

The TOA solution we have used throughout this chapter, found by Serim et al. (2017), was found using a template pulse profile. As reported earlier by Cui & Smith (2004), and as shown on Fig. 3.3 we see that the pulse profiles vary
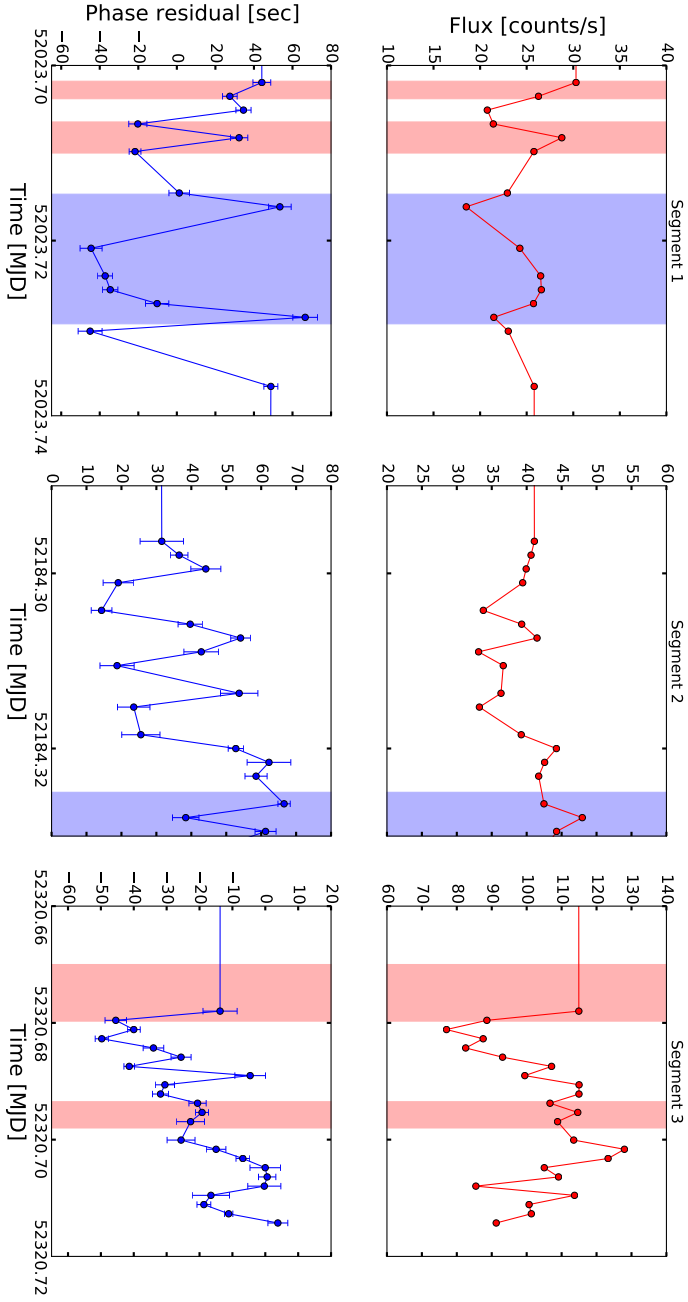
Figure 3.2: Top panel: Light curve of small data segment. Lower panel: Pulse Phase residuals for the same data segment. The data segment is marked on Fig. 3.1 in green. The red areas mark the correlations between pulse phase and flux and the blue are marks the anti-correlation between pulse phase and flux.

throughout the observation, so that it is not possible to use a single template high signal to noise pulse profile to perform the coherent timing analysis. Indeed, when the pulse shape variability is not properly taken into account there is the risk of introducing strong systematics in the results (Boynton et al. 1984; Hartman et al. 2008; Ibragimov & Poutanen 2009). We have, however, used the solution found by Serim et al. (2017) as our guess solution in order to find a phase connected solution of each harmonic separately (up to the 3rd harmonic), so to avoid the ambiguity in the definition of the pulse phase reference point. However, despite this precaution, we find that it is not possible to create a phase connected solution.

The pulse profiles seen on Fig. 3.3 show an example of the variability in the pulse shape.

3.4.2   Phase - Flux correlation – consequence for AMXPs

A proposed scenario for explaining the pulse phase and flux correlation in accreting millisecond pulsars was the movement of the hot spot, perhaps linked to movement of the magnetic field (Patruno et al. 2009). In this chapter and in the paper by Bak Nielsen et al. (2017) it has been tested if there is any such correlation in the pulsars with a higher magnetic field, which would possibly rule out movement of the hot spot. It is found in this chapter and in Bak Nielsen et al. (2017), concerning the LMXB pulsar 2A 1822-371, that it is not possible to find a phase - flux correlation. As described in section 3.3.2 in this chapter, it is also not possible to find any phase - flux correlation for GX 1+4. Because 2A 1822-371 and GX 1+4 are pulsars with a higher magnetic field than the AMXPs, it is possible that the pulse phase - flux correlation found in AMXPs (Patruno et al. 2009) is dependent on the magnetic field strength. If the magnetic field is strong enough this could prevent the movement of the hot spot on the neutron star surface, which was suggested to be a possible explanation for the phase - flux correlation (Patruno et al. 2009).

3.4.3   Short term flux variability

We can infer, from our attempts to phase connect the data, that the signal from GX 1+4 is not coherent over a time scale of days or longer. Furthermore, since we see short term variability in both the flux and the phase and we do not see a correlation between the flux and phase we infer that something is varying quickly on the neutron star surface. This is also supported by the change in the pulse profile shape. The variation could for example be the shape of the hot spot or perhaps the geometry of the beam. We observe pulsations throughout the observations, which does imply that even though we are not able to find a phase connected solution, we keep the coherence of the signal on a time scale of hours.

From the above, we would infer, that wind accretion is quite likely. The wind would attach to random field lines and thus create short term variability, pulse shape variability and make it impossible to find a phase coherent (long-term) solution (González-Galán et al. 2012; van den Eijnden et al. 2018). The short-term variability is similar to variability seen in Vela X-1, a HMXB, that accretes
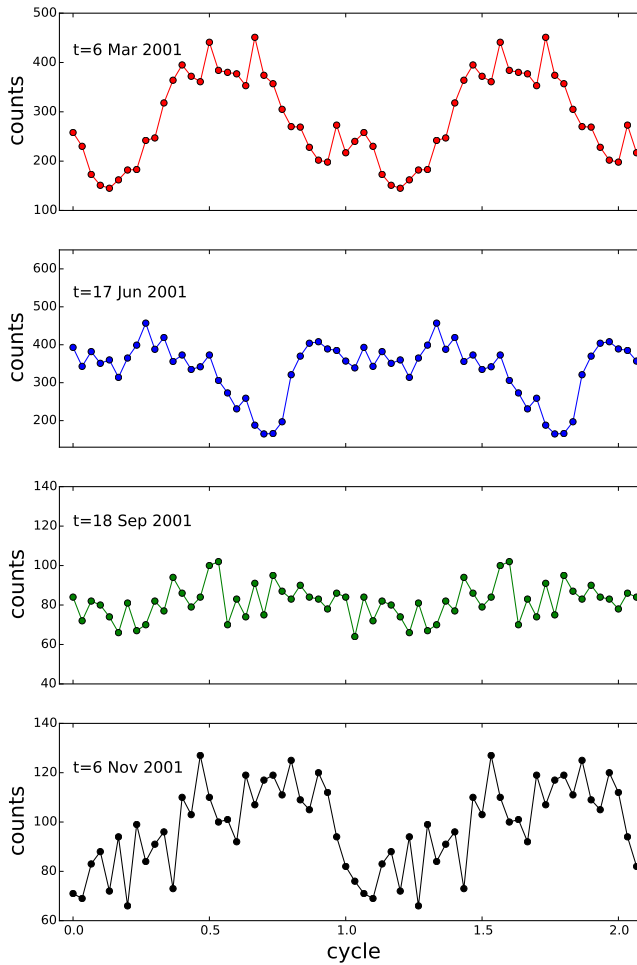
Figure 3.3: Four pulse profiles at different times. The first and last pulse profile in the Figure correspond to the initial and final epoch of the folded data. The two middle panels correspond to in-between times (marked in each panel).

through wind accretion (Boynton et al. 1986; Malacaria et al. 2016). However, it should be noted, that it is, at least on short timescales, possible to create coherent timing solutions to Vela X-1 (Nagase 1989). Due to the short-term variations, wind accretion seems to be the most likely accretion mechanism of GX 1+4, considering the variability on short time scales.

3.5   Conclusions

We examined about a year of *RXTE* data of GX 1+4, from March 2001 to February 2002. We conclude that it is not possible to phase connect the data due to the nature of the accretion process, which most likely proceeds via wind from the giant donor companion in the binary. We tested if a pulse phase - flux correlation was present in the data, similar to what is sometimes seen in the AMXPs and find that such a correlation does not appear to be present in GX 1+4. This might be due to the stronger magnetic field of the pulsar or, alternatively, to the different nature of the accretion process, which, in AMXPs, proceeds via an accretion disk interacting with the pulsar magnetosphere. The findings of this chapter, along with the findings of Bak Nielsen et al. (2017) does suggest that the phase - flux correlation is only present for pulsars with low magnetic fields of the order 10^8-10^9 G, as is the case for the AMXP. In this chapter we further suggest that there are some similarities between GX 1+4 and HMXBs such as for example VELA X-1, they both show variations in the pulse profile which is suggested to originate from wind accretion.

Bibliography

Bak Nielsen A.-S., Patruno A., D'Angelo C., 2017, MNRAS, 468, 824

Boynton P. E., Deeter J. E., Lamb F. K., Zylstra G., Pravdo S. H., White N. E.,
   Wood K. S., Yentis D. J., 1984, ApJ, 283, L53

Boynton P. E., Deeter J. E., Lamb F. K., Zylstra G., 1986, ApJ, 307, 545

Chakrabarty D., et al., 1997, ApJ, 481, L101

Cui W., Smith B., 2004, ApJ, 602, 320

Cutler E. P., Dennis B. R., Dolan J. F., 1986, ApJ, 300, 551

Cutri R. M., et al., 2003, VizieR Online Data Catalog, 2246

Davidsen A., Malina R., Bowyer S., 1977, ApJ, 211, 866

Dotani T., Kii T., Nagase F., Makishima K., Ohashi T., Sakao T., Koyama K.,
   Tuohy I. R., 1989, PASJ, 41, 427

González-Galán A., Kuulkers E., Kretschmar P., Larsson S., Postnov K., Ko-
   chetkova A., Finger M. H., 2012, A&A, 537, A66

Hartman J. M., et al., 2008, ApJ, 675, 1468

Hinkle K. H., Fekel F. C., Joyce R. R., Wood P. R., Smith V. V., Lebzelter T.,
   2006, ApJ, 641, 479

Ibragimov A., Poutanen J., 2009, MNRAS, 400, 492

Iłkiewicz K., Mikołajewska J., Monard B., 2017, A&A, 601, A105

Jahoda K., Markwardt C. B., Radeva Y., Rots A. H., Stark M. J., Swank J. H.,
   Strohmayer T. E., Zhang W., 2006, ApJS, 163, 401

Lewin W. H. G., Ricker G. R., McClintock J. E., 1971, ApJ, 169, L17

Malacaria C., Mihara T., Santangelo A., Makishima K., Matsuoka M., Morii M.,
   Sugizaki M., 2016, A&A, 588, A100

Mony B., et al., 1991, A&A, 247, 405

Nagase F., 1989, PASJ, 41, 1

Patruno A., 2010, ApJ, 722, 909

Patruno A., Watts A. L., 2012, preprint, (arXiv:1206.2727)

Patruno A., Wijnands R., van der Klis M., 2009, ApJ, 698, L60

Patruno A., Alpar M. A., van der Klis M., van den Heuvel E. P. J., 2012, ApJ,
   752, 33

Pereira M. G., Braga J., Jablonski F., 1999, ApJ, 526, L105

Rea N., Stella L., Israel G. L., Matt G., Zane S., Segreto A., Oosterbroek T.,
   Orlandini M., 2005, MNRAS, 364, 1229

Serim M. M., Şahiner Ş., ćerri-Serim D., Inam S. ć., Baykal A., 2017, MNRAS,
   469, 2509

Yoshida Y., Kitamoto S., Suzuki H., Hoshino A., Naik S., Jaisawal G. K., 2017,
   ApJ, 838, 30

van Straaten S., van der Klis M., Méndez M., 2003, ApJ, 596, 1155

van den Eijnden J., Degenaar N., Russell T. D., Miller-Jones J. C. A., Wijnands
   R., Miller J. M., King A. L., Rupen M. P., 2018, MNRAS, 474, L91

CHAPTER *4*

The low luminosity behaviour of the 4U 0115+63 Be/X-ray transient

The Be/X-ray transient 4U 0115+63 exhibited a giant, type-II outburst in October 2015. The source did not decay to its quiescent state but settled in a meta-stable plateau state (a factor $\sim$10 brighter than quiescence) in which its luminosity slowly decayed. We used *XMM-Newton* to observe the system during this phase and we found that its spectrum can be well described using a black-body model with a small emitting radius. This suggests emission from hot spots on the surface, which is confirmed by the detection of pulsations. In addition, we obtained a relatively long ($\sim$7.9 ksec) *Swift*/XRT observation $\sim$35 days after our *XMM-Newton* one. We found that the source luminosity was significantly higher and, although the spectrum could be fitted with a blackbody model the temperature was higher and the emitting radius smaller. Several weeks later the system started a sequence of type-I accretion outbursts. In between those outbursts, the source was marginally detected with a luminosity consistent with its quiescent level. We discuss our results in the context of the three proposed scenarios (accretion down to the magnestospheric boundary, direct accretion onto neutron star magnetic poles or cooling of the neutron star crust) to explain the plateau phase.

4.1 Introduction

Be/X-ray transients harbour high-magnetic field (B$\sim$10$^{12-13}$ G) neutron stars (NSs) that move around Be-type stars in eccentric orbits. Typically, these binaries can exhibit two types of transient activity: more common, short-lived (i.e., small fraction of the orbital period) type-I outbursts that typically occur at the periastron passage of the NSs, and giant, type-II outbursts that can last significantly longer than an orbital period. In the first case, the NSs accrete matter from the Be-star decretion disks (e.g., Okazaki & Negueruela 2001) and reach X-ray luminosities of L$_X$ $\sim$10$^{36-37}$ erg s^{-1}. In the second case, during the type-II outbursts the luminosities usually reach the Eddington limit for a NS but the exact physical mechanism(s) causing these outbursts is not understood (Moritani et al. 2013; Monageng et al. 2017).

Most studies of Be/X-ray transients have been performed at high luminosities (i.e., >10^{36} erg s^{-1}; e.g., see the review by Reig 2011) and consequently not much is known about their behaviour when they accrete at lower X-ray luminosity. However, several Galactic systems have been detected at luminosities of L$_X$ $\sim$10$^{34-35}$ erg s^{-1} (e.g., Motch et al. 1991; Campana et al. 2002; Rutledge et al. 2007) indicating that they are still accreting but at relatively low rates. In addition, detailed X-ray studies (using the *Chandra* and *XMM-Newton* observatories) of the Be/X-ray binary populations in the Magellanic Clouds (i.e., the Small Magellanic Cloud; Laycock et al. 2010; Haberl & Sturm 2016) have showed that a significant number of the Be/X-ray transients in those galaxies, can be detected at similar low luminosities in between their outbursts. This fact indicates that such low-luminosity states are a common property of Be/X-ray transients.

At these low rates, the NS spin period is a key component in determining how the accretion proceeds. For slow spinning NSs (spin periods of hundreds of seconds) matter may still be directly accreted onto the stellar surface (i.e., at the magnetic poles) but for the fast spinning systems (with spin periods of only a few seconds) matter is likely ejected from the inner part of the system due to the pressure of the rotating NS magnetic field (the so-called propeller effect; e.g., Illarionov & Sunyaev 1975; Stella et al. 1986; Romanova et al. 2004; D'Angelo & Spruit 2010; Tsygankov et al. 2016). In the latter case, one would expect that the observed flux is not pulsed. However some sources still exhibit pulsations in this regime, probably because matter is able to leak through the field lines and reach the surface at the magnetic poles, thus creating hot spots (e.g., Elsner & Lamb 1977; Ikhsanov 2001; Lii et al. 2014).

Some sources are detected at even lower luminosities of L$_X$ $\sim$10$^{32-34}$ erg s^{-1} (e.g., Mereghetti et al. 1987; Roberts et al. 2001; Campana et al. 2002; Reig et al. 2014; Elshamouty et al. 2016), but the cause of this faint emission is still unclear. One possibility is the accretion down to the magnetosphere although it is likely that this emission would not peak in the X-rays but at longer wavelengths (e.g., UV; Tsygankov et al. 2016). However, the pulsed emission seen in some systems at those luminosities (e.g., Rothschild et al. 2013; Doroshenko et al. 2014; Table 2 of Reig et al. 2014) suggests that, for at least those systems, the matter does reach the surface at the magnetic poles, supporting the idea of leakage of matter through

the magnetospheric barrier (Orlandini et al. 2004; Mukherjee & Paul 2005).

Although low level accretion onto the magnetic poles could be the physical mechanism behind these low luminosities in some sources, it is also possible that in other systems the accretion has fully halted and we see a cooling NS. During outburst the accreted matter might heat up the NS (due to the pycnonuclear reactions deep in the crust; Brown et al. 1998) and, when the accretion has stopped, the deposited heat is radiated away. This explanation has been proposed for several sources but it remains to be confirmed (Campana et al. 2002; Wijnands et al. 2013; Reig et al. 2014; Elshamouty et al. 2016; Tsygankov et al. 2017).

In the heating and cooling scenario, one would expect that after a long and strong period of accretion (i.e., after type-II outbursts), the crust might be heated very significantly and it might have become hotter than the core. When the accretion has stopped, the crust would then slowly cool down until equilibrium is reached again. This process would be similar to what has been observed for several low-magnetic field NS systems (for recent discussions see Degenaar et al. 2015 and Parikh et al. 2017). Wijnands & Degenaar (2016) attempted to test this hypothesis in two Be/X-ray transients (4U 0115+63 and V0332+53) after the end of their type-II outbursts. They found that after those bright outbursts both sources showed elevated emission in a meta-stable state above their known quiescent levels (e.g., Elshamouty et al. 2016; Tsygankov et al. 2017). Wijnands & Degenaar (2016) suggested that this "plateau phase" could indeed be consistent with the slow cooling of the crust, although they could not exclude accretion scenarios. Here we further investigate this plateau phase for 4U 0115+63.

4.2   Observations, Analysis and Results

After the *Swift*/X-Ray Telescope (XRT) data reported in Wijnands & Degenaar (2016), we obtained several extra *Swift*/XRT observations as well as an *XMM-Newton* one of 4U 0115+63 (Table 4.1 and Table 4.3). This source harbours a magnetized NS (B$\sim$1.3$\times$10^{12} G; Raguzova & Popov 2005), with a spin period of P$_s$ $\sim$3.62 s (Cominsky et al. 1978) and an orbital period of P$_{orb}$ $\sim$24.3 days (Rappaport et al. 1978). 4U 0115+63 was monitored with the XRT in the Photon Counting (PC) mode and observed by *XMM-Newton* with the EPIC detectors in the full frame (pn) and large window (MOS) modes. The *Swift*/XRT PC mode only allows for a time resolution of $\sim$2.5 s which is insufficient to study possible pulsations due to the NS spin. For *XMM-Newton*, we used the pn to search for and study the pulsations (time resolution 73.4 ms; section 4.2.3) due to its higher count rate.

4.2.1   Light curve

The 2015 type-II outburst was monitored using the *Swift*/BAT and *Swift*/XRT (see Figure 4.1). In particular, the decay of this outburst was intensively mon-
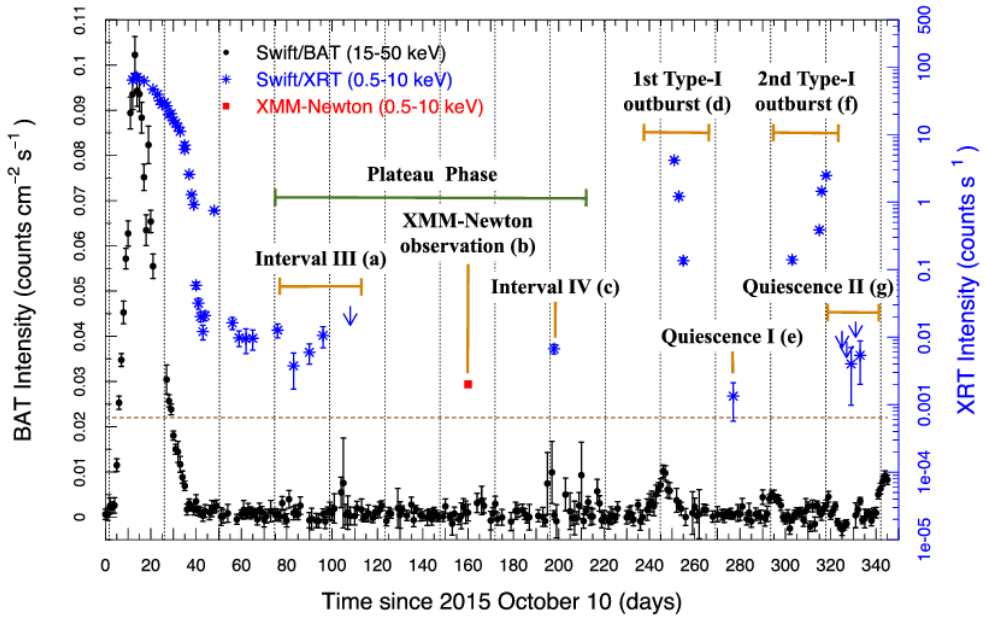
Figure 4.1: *Swift*/XRT (blue) and *Swift*/BAT (black) light curves during and after the 2015 type-II outburst of 4U 0115+63. The time of our *XMM-Newton* observation is given as a red symbol converted in *Swift*/XRT count rate (section 4.2.1). The dotted brown line corresponds to the quiescent level of 4U 0115+63. Vertical dotted lines indicate the time of periastron passages. We label our results in the different source phases as a continuation of the ones used in Wijnands & Degenaar (2016). Errors are 3σ.

itored using the *Swift*/XRT which also allowed to observe the transition of the source into the low-luminosity state (see also Wijnands & Degenaar 2016). This was the first time such a state was detected for this system but very likely it was present after the end of the previous type-II outbursts as well. However, those possible occurrences were missed because no sensitive X-ray observations after the end of those outbursts were obtained in the past.

We obtained the *Swift*/BAT data from the hard X-ray transient monitor web page[1] (Krimm et al. 2013) and the *Swift*/XRT light curve from the interface build *Swift*/XRT products[2] (Evans et al. 2009). For a direct comparison the source count rate during the *XMM-Newton* observation was converted to XRT count rate (for the energy range 0.5-10 keV) applying the WEBPIMMS[3] tool and the spectral parameters obtained from the first observation during the low luminosity state (hereafter "plateau phase") in our chapter. From Figure 4.1 (see also Wijnands & Degenaar 2016), we can see that after the type-II outburst the source did not go directly to quiescence (Campana et al. 2002; Tsygankov et al. 2017) but settled down at a plateau that is a factor of $\sim$10 brighter. Almost $\sim$240 days after the type-II outburst, the source experienced several type-I outbursts (e.g., Nakajima et al. 2016a,b,c).

After the episodes reported by Wijnands & Degenaar (2016), the *Swift*/XRT count rate continued to decrease until our "*XMM-Newton* observation (b)" (see Figure 4.1): from $\sim$0.015 counts s^{-1} during "Interval I" of Wijnands & Degenaar (2016, i.e., at the start of the plateau phase) to $\sim$0.002 counts s^{-1} during *XMM-Newton* observation (b). A similar decreasing trend is seen in the X-ray luminosities (Figure 4.2, top panel) obtained from our spectral analysis (see section 4.2.2). Despite that a general decreasing trend is seen in the *Swift*/XRT count rate, it unexpectedly increased slightly again to $\sim$0.007 count s^{-1} ("Interval IV (c)") after the *XMM-Newton* observation (b). During the plateau phase the *Swift*/BAT count rate appears to have brief excursions above the background possible indicating occasional enhanced activity (Figure 4.1). However, those variations are consistent with statistical fluctuations and do not represent detections of the source (see Krimm et al. 2013 for a detailed description about the *Swift*/BAT data processing). The monitoring campaign stopped for $\sim$53 days after our Interval IV (c) *Swift*/XRT observation until the source exhibited a type-I outburst ("1st Type-I outburst (d)") during which the *Swift*/XRT count rate reached $\sim$4 counts s^{-1}. The decay during this outburst was monitored with the *Swift*/XRT and 26 days after the peak of the outburst we obtained a 8.8 ksec observation in which the source only showed 8 photons ("Quiescence I (e)"; see Figure 4.1). This level is consistent with the quiescent level of the source (Figure 4.1; Tsygankov et al. 2017).

The *Swift*/BAT continued to monitor the source and 17 days later another type-I outburst was detected (Figure 4.1; Nakajima et al. 2016b). We monitored the source using the XRT to determine how it would transit to quiescence. Surprisingly during the first observation the source was not in quiescence but at relatively high count rate ($\sim$0.15 counts s^{-1}) and 12 days later the source increased again in

---

[1] http://swift.gsfc.nasa.gov/results/transients/weak/4U0115p634/
[2] http://www.swift.ac.uk/user_objects/
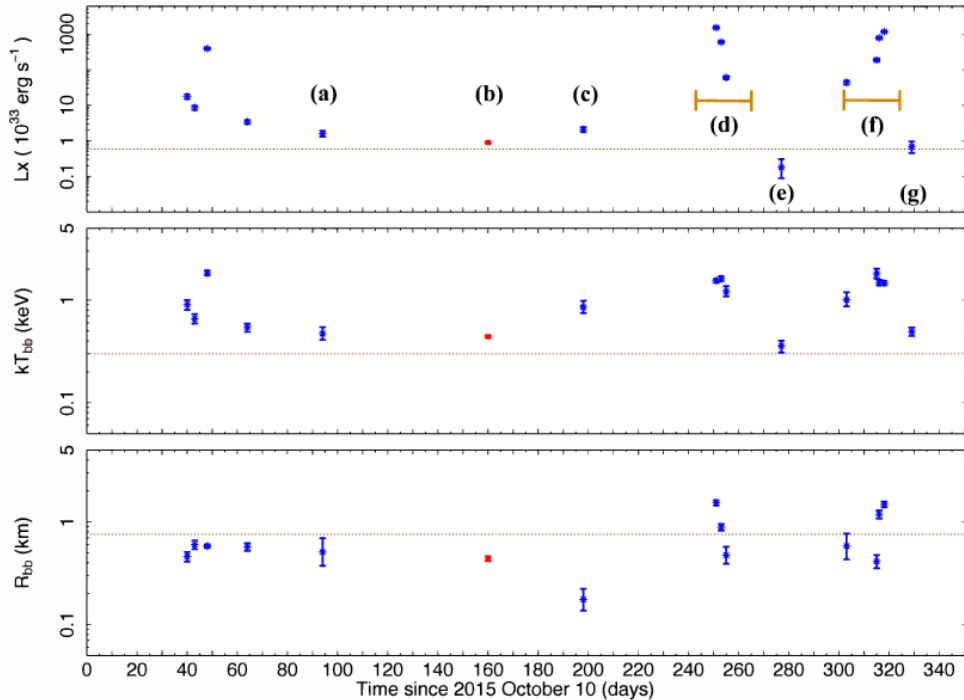[3] http://heasarc.gsfc.nasa.gov/cgi-bin/Tools/w3pimms/w3pimms.pl

Figure 4.2: Evolution (using a black-body model) of the luminosity (top; 0.5-10 keV), temperature (middle) and emission radius (bottom; fixed values not shown). The blue points are the *Swift*/XRT observations and the red point is the *XMM-Newton* one. The dotted brown line corresponds to parameters in quiescence (Tsygankov et al. 2017). Labels as in Figure 4.1. Errors are 1σ.

count rate indicating the start of the next type-I outburst ("2nd Type-I outburst (f)"; Figure 4.1). Already within 7 days of the peak , the source was back in quiescence; we obtained 5 observations ("Quiescence II (g)") during which the source was not detected or only marginally. The stacking of these observations shows a weak (9 photons in 4.7 ksec) but clear detection.

4.2.2   Spectral analysis

For the spectral analysis, we only used *Swift*/XRT observations obtained after those already analyzed by Wijnands & Degenaar (2016) (ObsID 000311720[42-59]) and used the results obtained by these authors for the earlier observations. The data extraction and analysis have been performed in the same way as in Wijnands & Degenaar (2016) so that the results can be directly compared. Due to the very low count rates in the observations with ObsIDs 000311720[42-45] (a) and 000311720[55-59] (g), we stacked those ones. The data were analysed with HEASOFT v.6.17. After reprocessing the raw data with the XRTPIPELINE, we extracted source and background spectra using XSELECT. The source infor-

mation (count rates, spectra) was obtained from a circular region with a radius
of 15 pixels centered around the source position (Reig & Fabregat 2015), and
background information from a surrounding annulus with an inner-outer radius
of 60-110 pixels. Only during the type-I outbursts observations the source count
rate was $\geq 0.5\,\mathrm{counts\,s^{-1}}$ causing piled-up. Therefore, those data were corrected
following the standard thread[4]. The exposure maps were obtained through XRT-
PIPELINE and were used to create ancillary response files using XRTMKARF. We
employed the response matrix files (version 14) from the *Swift* calibration database.

For the *XMM-Newton* data, we used SAS (version 1.2) for reducing and analysing
them. The EMPROC and EPPROC tasks produced calibrated event lists, which
were filtered against background flaring (determined in the 10-12 keV range with
a threshold rate$\geq$0.5 counts s^{-1} for pn; in the $>10\,\mathrm{keV}$ range with a threshold
rate$\geq$0.3 counts s^{-1} for MOS). Source counts and spectra were obtained from a
circular region with a 20 arcsec radius, and the background ones from a circular
region free of sources with a 50 arcsec radius on the same CCD. The data were
not piled-up. The response matrix files were generated using RMFGEN and the
ancillary response files by ARFGEN.

In Figure 4.2 we show the evolution of the source during the plateau phase
plotting our new results with those of Wijnands & Degenaar (2016). Due to the
often very few counts in the spectra we rebinned the data (with GRPPHA for
Swift and SPECGROUP for *XMM-Newton* data) to 1 count per bin and we used
C-statistics to fit the spectra. The data were fitted in the 0.5-10 keV energy range
using XSPEC v.12.9.0. The pn, MOS1 and MOS2 spectra were fitted simulta-
neously, with all parameters tied between the spectra. We fitted the data with
either an absorbed power-law model (PEGPWRLW) or an absorbed blackbody
model (BBODYRAD). We note that we cannot exclude other single component
models or spectral models with multiple components (e.g., a blackbody model plus
a power-law contribution; potentially describing multiple emission mechanisms).
However, the quality of our spectra is typically rather poor and we cannot dis-
tinguish between different single component model (except for the *XMM-Netwon*
spectrum, see below), let alone that we can obtain constraining results when fit-
ting multiple components. Therefore, we have opted to only report on the spectral
results obtained with two of the most basic models used in the fitting of X-ray
binary spectra: the blackbody model and the power-law model. This will allow
us to determine general trends in the data (i.e., softening of the spectra in time)
which will help in the interpretation of the results.

We included absorption by the interstellar medium (TBABS) with abundances
set to WILM (Wilms et al. 2000) and cross-sections to VERN (Verner et al. 1996).
The column density was fixed to the same value as in Wijnands & Degenaar
(2016, i.e., $\mathrm{N}_H{=}9{\times}10^{21}\,\mathrm{cm^{-2}}$). We adopted a distance of D=7 kpc (Negueruela &
Okazaki 2001). In the PEGPWRLW model we set the energy boundaries to 0.5
and 10 keV, so that the model normalization gives the unabsorbed flux for that
energy range (see Table 4.3). For the BBODYRAD fits, we left the emitting ra-
dius as a free parameter and determined the unabsorbed 0.5-10 keV flux by using
CFLUX (see Table 4.1).

---

[4]`http://www.swift.ac.uk/analysis/xrt/pileup.php`

The results of our spectral analysis are given in Tables 4.1 and 4.3. Although we cannot statistically prefer one of the models over the other during the plateau phase because of the *Swift* data quality, the *XMM-Newton* spectrum is of high enough one that the black-body model is preferred. The PEGPWRLW fits suggest that the spectra of the plateau phase are softer (typical photon indices of 1.5-3.6) than those of the type-I outbursts (indices of 0.5-1.2; Table 4.3). The spectra of the plateau phase can be adequately described by a BBODYRAD model with temperatures of $kT_{bb} \sim 0.4\text{-}0.8$ keV with radii $R_{bb} \sim 0.1\text{-}0.5$ km (Table 4.1; Figure 4.2), smaller than the radius of a NS. This suggests that the emission comes from hot spots on the surface (likely at the magnetic poles). This is confirmed by the detection of pulsations in the *XMM-Newton* data (section 4.2.3). The (c) state shows a higher luminosity ($L_X \sim 2.1 \times 10^{33}$ erg s^{-1}; Figure 4.2) than during (b), as well as a higher temperature (from ~ 0.44 keV to ~ 0.85 keV) but a significantly smaller emission radius (from ~ 0.51 to ~ 0.18 km; Table 4.1). The source is detected at $L_X \sim 10^{32-33}$ erg s^{-1} (0.5-10 keV) during the low luminosity state, whereas during the type-I outbursts it increases to $L_X \sim 10^{34-36}$ erg s^{-1}. The (e) and (g) states are consistent with quiescence (Figure 4.2).

4.2.3   Timing analysis

The *XMM-Newton* pn data were barycentric corrected using the task BARYCEN and the region selection applied was the same as used in the spectral analysis. We rebinned the data to 0.1 s time resolution and then used 16384 points (thus 1638.4 s of data) to make a FFT. This resulted in a power-density spectrum in the frequency range of 6.104×10^{-4} Hz to 5 Hz (the Nyquist frequency). No background subtraction was performed prior to the calculation of the FFTs. The Poisson level was removed from the final power spectrum, which was then normalized using an rms normalization, where the power density units are (rms/mean)^2 Hz^{-1}. The power spectrum in Figure 4.3 shows a peak close to the known NS spin frequency (~ 0.3 Hz).

The light curve was then folded using PRESTO (Ransom 2001) to determine the precise spin frequency. The best results were obtained using a frequency of $(27677600.0 \pm 9.2) \times 10^{-7}$ Hz yielding a period of $(361300.0 \pm 1.5) \times 10^{-5}$ s. The pulse profile (see inset in Figure 4.3) was fitted with a sinusoid using the procedure described in Patruno et al. (2010) to obtain the pulse fractional amplitude. We fitted one harmonic and two harmonics (to only one cycle but for clarity two cycles are shown in Figure 4.3). When one harmonic is fitted we find the fractional amplitude to be FA$_1$=83.3$\pm$9.5 per cent, with a χ^2_ν=1.3 for 46 degrees of freedom. This indicates that the fit is marginally acceptable with a p-value of 7%. To explore the option that the profile might contain multiple harmonics, we fitted the profile with two harmonics. We found FA$_1$=83.3$\pm$8.7 and FA$_2$=28.4$\pm$7.6 per cent with χ^2_ν=1.09 for 44 degrees of freedom. Therefore, fitting two harmonics to the profile only yielded a marginally better χ^2_ν and consequently we cannot conclude that the second harmonic is real. If it would be real, it might be due to slight beaming of the emission (e.g., by Compton scattering due to low-level accretion) or because
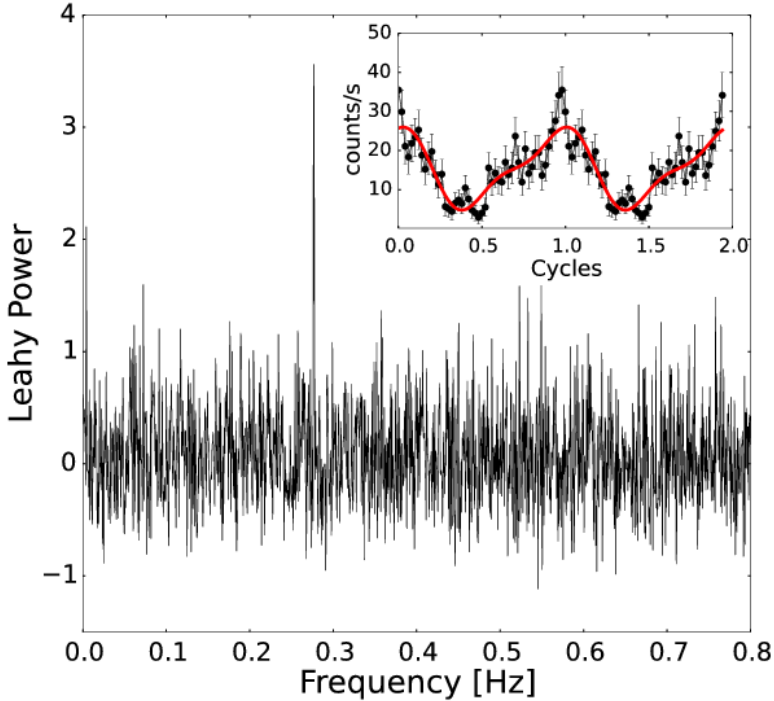
Figure 4.3: Power spectrum obtained from the EPIC-pn data showing a clear signal at ~0.277 Hz that corresponds to the NS spin frequency. Inset: folded (using the detected frequency) pulse profile. Two cycles are shown for clarity. The red curve is a fit to the profile using two harmonically related sinusoids.

there are two hot spots contributing to the observed emission. However, because of the low significance of this second harmonic we will not discuss it or its potentially consequences on the interpretation further in our chapter.

4.3 Discussion

We have presented additional *Swift*/XRT and *XMM-Newton* observations (Figure 4.1) during the low-luminosity plateau phase previously identified for 4U 0115+63 (Wijnands & Degenaar 2016). From our *Swift* data we can infer that the plateau phase lasted between 160 and 200 days. The exact duration cannot be estimated due to the lack of monitoring during the final state of this state and because the system started to exhibit type-I outbursts. Wijnands & Degenaar (2016) proposed three models to explain the plateau phase: accretion down to the NS magnetosphere, cooling of an accretion heated NS crust and direct low-level accretion onto the NS magnetic poles. The magnetospheric accretion model can likely be excluded because no pulsations are expected in this scenario (Campana et al. 2002),

contrary to our *XMM-Newton* results where we detect a clear pulsation at the NS spin frequency. This assumes that pulsations were also always present during the XRT observations in the plateau phase. The data do not allow this to be tested, but if they were not present during (some of) these XRT observations, it might still be possible that magnetospheric accretion could still have happened during some of those observations. Moreover, it is indeed possible that multiple emission mechanisms were active during different observations in the plateau phase (or even during a specific observation; e.g., cooling emission during some observations and accretion emission during others; i.e., at periastron), but the current data set is of too low quality to further investigate this. In the following two sections we, for simplicity, assume that only one emission mechanisms is active during the full duration of the plateau phase. This will allow us to investigate if indeed one single mechanism is sufficient to explain this enigmatic state and what the possible problems are with this hypothesis.

4.3.1   Cooling of the neutron star heated crust

The accretion-induced heating of the NS crust and its subsequent cooling has been studied extensively for accreting low-magnetic field (B$\leq 10^8$ G) NSs, but not for high magnetic-field NSs (B$\sim 10^{12-13}$ G). The strong magnetic field could alter the heating and cooling processes significantly. Wijnands & Degenaar (2016) suggest that the magnetic field configuration in the crust might be such that the cooling process could take place through hot spots, an idea supported by the small radii of the emission regions found in our spectral analysis. Such interpretation might be consistent with the detection of pulsations during our *XMM-Newton* observation.

Our *Swift*/XRT monitoring campaign during the plateau phase is consistent with the cooling hypothesis, except for the last observation (Interval IV in Figure 4.1). During that observation the luminosity increases compared to the previous *XMM-Newton* one, concurrently, we detect a significant increase in the fit temperature (Figure 4.2; Table 4.1). The emitting region notably decreased in size but this was not enough to compensate the rise in temperature so that the observed luminosity increased. This indicates that the energy release at the hot spots increases significantly and this cannot straightforwardly be explained in the cooling hypothesis.

Interval IV was obtained after a periastron passage which could lead to matter transfer from the Be disk or from the wind of the companion to the NS. This matter could leak through the magnetosphere barrier and potentially cause an increase in luminosity. The lack of monitoring after Interval IV does not allow us to determine if this observation was part of an overall trend or a special event on top of a general decay curve. Nevertheless, the spectral shape is difficult to explain in this scenario (section 4.3.2) and therefore we suggest an explanation for this enigmatic behaviour in the cooling scenario.

One possible explanation, which we call the "Phase Transition model" (Figure 4.4), is based on the possible phase transitions the crust matter might undergo during the cooling process. Two matter states likely are present: a solid state in
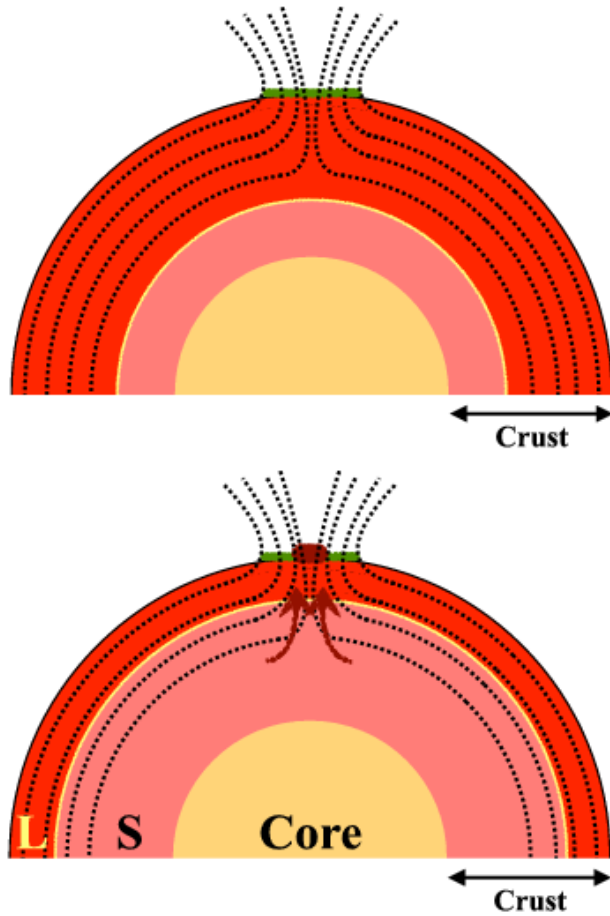
Figure 4.4: Phase Transition model (not to scale). Colour code: red (liquid crustal layer, so-called "ocean"), pink (solid crustal layer), yellow (core), green (hot spot region at the magnetic pole), garnet (hot spot central emission region) and dashed black lines (magnetic field lines). *Upper Panel*: Initial state configuration of the crust once the accretion has halted. *Bottom Panel*: Configuration after the cooling has proceeded. The inner layers of the ocean have become solid and the magnetic field lines that are placed in this region conduct the heat faster towards the magnetic pole. As a consequence, the central region of the hot spot emits higher heat flux.

the inner part and the liquid one, also called "ocean", that formed on top of the solid crust due to the heat generated by the accretion. When the accretion has halted, the liquid ocean slowly becomes solid again as the temperature decreases. Since we see pulsations during our *XMM-Newton* observation (assuming pulsations were also present during the *Swift*/XRT observations), the heat stored in the crust must be preferably released at hot spots, likely at the magnetic poles. Therefore, it is plausible to assume that the magnetic field in the crust might be parallel to the surface and only exits the crust at the poles (Figure 4.4).

Once the cooling starts, the bottom parts of the ocean become solid. At this point, some magnetic field lines that were first in the liquid ocean are now in the new solid layer. It has been shown that in a solid crust layer the thermal conductivity is larger than when this layer is liquid (Horowitz et al. 2007; Brown & Cumming 2009; Mckinven et al. 2016). As a consequence, the heat flux toward the hot spots increases significantly in the layer that solidified. Therefore, we can distinguish two regions in the hot spots: one in the outer part that is produced by those field lines guiding heat from the liquid layers, and other in the central part of the hot spots that is produced by the magnetic field located in the solid crustal layer and shows a higher heat flux. If originally all the field lines were located in the liquid layers, then when part of those layers become solid, the inner part of the hot spot can suddenly rise in temperature. Thus the hot spot does not physically shrink in size, but its core becomes significantly hotter and the observed emission is dominated by this central region. Therefore we observe an artificially smaller size for the emitting region with higher temperature and luminosity. In addition, an extra amount of energy may be released due to the phase transition which would heat the inner part of the hot spot.

This model could in principle explain what we observed in Interval IV, but we stress that detailed calculations should be performed to determine if this is also physically possible. In addition, one prediction of the model is that after the initial artificial observed decrease in size of the hot spot, it should appear to grow again when the cooling proceeds because most of the liquid layers will solidify and thus the region with enhanced heat flux will increase. We do not have additional observations after this enigmatic *Swift*/XRT observation so we cannot test this prediction.

4.3.2   Direct accretion onto neutron star magnetic poles

In the direct accretion scenario, the matter is guided by the magnetic field to the poles forming hot spots. Although it remains unknown how the accretion works at low accretion rate and what type of spectra would be produced, it might be possible that it would produce softer spectra than those obtained in higher accretion rate states (Zampieri et al. 1995). The Be/X-ray transient 1A 0535+26 was observed at similar low luminosities and it showed clear accretion features (source detection at $> 100\,\mathrm{keV}$ and aperiodic variability in the light curve; Orlandini et al. 2004, Rothschild et al. 2013; Doroshenko et al. 2014), so low-level accretion can definitely occur in these systems. However, its spectrum was harder than what we

observe for 4U 0115+63 indicating that the emission is not formed in the same way in both systems. Two possibilities are left: either low-level accretion onto strongly magnetized NSs could give two types of spectra, or the physical mechanisms are widely different and we indeed could see cooling emission in 4U 0115+63.

When assuming that the plateau phase in 4U 0115+63 is due to low-level accretion down to the surface of the NS, the behaviour seen during Interval IV could be due to some increase in accretion triggered by the periastron passage. However, if the direct accretion scenario is the right model to explain the source behaviour during this observation, there are still some caveats to be clarified. A temperature increase can naturally be explained if the accretion rate onto the pole increases, but it is not clear why the size of the emitting region would suddenly decrease significantly. This could signal a change in accretion geometry (e.g., disk like to wind like, or vice versa) but it is unclear if this is realistic. One key ingredient that needs to be explained is why we observe such a soft spectra in the plateau phase compared to the type-II and the mini-type I outbursts (Wijnands & Degenaar 2016) where the source is definitely accreting. Detailed models are needed that calculate the expected spectral shape during these different accretion states in order to make any further conclusive statements.

4.4   Conclusions

We have presented the latest results of our monitoring campaign using *Swift* and *XMM-Newton* on the Be/X-ray transient 4U 0115+63 during its low-luminosity state observed after its 2015 type-II outburst. The aim of our study was to investigate the possible physical mechanism or mechanisms behind this low-luminosity state that lasted for $\sim$200 days. The three previously proposed mechanisms (Wijnands & Degenaar 2016) to explain this state are: accretion down to the NS magnetosphere, accretion onto the magnetic poles of the NS, or cooling emission from a NS heated due to the accretion of matter during the type-II outburst. The low number of photons detected during the low-luminosity state only allowed for simple, single component models (i.e., a power-law or blackbody models) to be fitted to the X-ray spectra. The spectra were relatively soft and were well described by the blackbody model. In addition, we detected pulsations in our *XMM-Newton* observation, indicative of emission from the NS magnetic poles. As a consequence, the hypothesis of emission from the magnetospheric boundary is ruled out because pulsations are not expected in this scenario (assuming that pulsations were presented during the whole low-luminosity state; this could not be tested with the available data). However, we cannot conclusively reject the other two scenarios (or a combination of them), although both cannot straight forwardly explain our results. More dense monitoring of Be/X-ray transients after their type-II outbursts is needed to further determine the mechanism behind the low-luminosity state they can exhibit after those outbursts.

Bibliography

Brown E. F., Cumming A., 2009, ApJ, 698, 1020

Brown E. F., Bildsten L., Rutledge R. E., 1998, ApJ, 504, L95

Campana S., Stella L., Israel G. L., Moretti A., Parmar A. N., Orlandini M., 2002, ApJ, 580, 389

Cominsky L., Clark G. W., Li F., Mayer W., Rappaport S., 1978, Nature, 273, 367

D'Angelo C. R., Spruit H. C., 2010, MNRAS, 406, 1208

Degenaar N., et al., 2015, MNRAS, 451, 2071

Doroshenko V., Santangelo A., Doroshenko R., Caballero I., Tsygankov S., Rothschild R., 2014, A&A, 561, A96

Elshamouty K. G., Heinke C. O., Chouinard R., 2016, MNRAS, 463, 78

Elsner R. F., Lamb F. K., 1977, ApJ, 215, 897

Evans P. A., et al., 2009, MNRAS, 397, 1177

Haberl F., Sturm R., 2016, A&A, 586, A81

Horowitz C. J., Berry D. K., Brown E. F., 2007, Phys. Rev., 75, 066101

Ikhsanov N. R., 2001, A&A, 375, 944

Illarionov A. F., Sunyaev R. A., 1975, A&A, 39, 185

Krimm H. A., et al., 2013, ApJS, 209, 14

Laycock S., Zezas A., Hong J., Drake J. J., Antoniou V., 2010, ApJ 10.1088/0004-637X/716/2/1217, 716, 1217

Lii P. S., Romanova M. M., Ustyugova G. V., Koldoba A. V., Lovelace R. V. E., 2014, MNRAS, 441, 86

Mckinven R., Cumming A., Medin Z., Schatz H., 2016, ApJ, 823, 117

Mereghetti S., Bignami G. F., Caraveo P. A., Goldwurm A., 1987, ApJ, 312, 755

Monageng I. M., McBride V. A., Coe M. J., Steele I. A., Reig P., 2017, MNRAS, 464, 572

Moritani Y., et al., 2013, PASJ, 65, 83

Motch C., Stella L., Janot-Pacheco E., Mouchet M., 1991, ApJ, 369, 490

Mukherjee U., Paul B., 2005, A&A, 431, 667

Nakajima M., et al., 2016a, The Astronomer's Telegram, 9149

Nakajima M., et al., 2016b, The Astronomer's Telegram, 9291

Nakajima M., et al., 2016c, The Astronomer's Telegram, 9512

Negueruela I., Okazaki A. T., 2001, A&A, 369, 108

Okazaki A. T., Negueruela I., 2001, A&A, 377, 161

Orlandini M., et al., 2004, Nuclear Physics B Proceedings Supplements, 132, 476

Parikh A. S., et al., 2017, MNRAS, 466, 4074

Patruno A., Hartman J. M., Wijnands R., Chakrabarty D., van der Klis M., 2010, ApJ, 717, 1253

Raguzova N. V., Popov S. B., 2005, Astronomical and Astrophysical Transactions, 24, 151

Ransom S. M., 2001, PhD thesis, Harvard University

Rappaport S., Clark G. W., Cominsky L., Li F., Joss P. C., 1978, ApJ, 224, L1

Reig P., 2011, Ap&SS, 332, 1

Reig P., Fabregat J., 2015, A&A, 574, A33

Reig P., Doroshenko V., Zezas A., 2014, MNRAS, 445, 1314

Roberts M. S. E., Michelson P. F., Leahy D. A., Hall T. A., Finley J. P., Cominsky L. R., Srinivasan R., 2001, ApJ, 555, 967

Romanova M. M., Ustyugova G. V., Koldoba A. V., Lovelace R. V. E., 2004, ApJ, 616, L151

Rothschild R., et al., 2013, ApJ, 770, 19

Rutledge R. E., Bildsten L., Brown E. F., Chakrabarty D., Pavlov G. G., Zavlin V. E., 2007, ApJ, 658, 514

Stella L., White N. E., Rosner R., 1986, ApJ, 308, 669

Tsygankov S. S., Lutovinov A. A., Doroshenko V., Mushtukov A. A., Suleimanov V., Poutanen J., 2016, A&A, 593, A16

Tsygankov S. S., Wijnands R., Lutovinov A. A., Degenaar N., Poutanen J., 2017, MNRAS, 470, 126

Verner D. A., Ferland G. J., Korista K. T., Yakovlev D. G., 1996, ApJ, 465, 487

Wijnands R., Degenaar N., 2016, MNRAS, 463, L46

Wijnands R., Degenaar N., Page D., 2013, MNRAS, 432, 2366

Wilms J., Allen A., McCray R., 2000, ApJ, 542, 914

Zampieri L., Turolla R., Zane S., Treves A., 1995, ApJ, 439, 849

Table 4.1: Results of our spectral analysis using the blackbody model.

obsID	State	Exposure (ksec)	kT_{bb} (keV)	R_{bb} (km)	F_X (10^{-12} erg cm^{-2} s^{-1})	L_X (10^{33} erg s^{-1})
0790180301	XMM-Newton observation (b)	~20.8	0.44 ± 0.01	$0.44^{+0.03}_{-0.02}$	0.15 ± 0.01	0.90 ± 0.03
00311720+[42,45]	Interval III (a)	~5.8	$0.47^{+0.07}_{-0.06}$	$0.51^{+0.19}_{-0.13}$	$0.27^{+0.06}_{-0.05}$	1.6 ± 0.3
+46	Interval IV (c)	~7.9	$0.85^{+0.13}_{-0.11}$	$0.18^{+0.05}_{-0.04}$	$0.35^{+0.06}_{-0.05}$	$2.1^{+0.4}_{-0.3}$
+47	1st Type-I outburst (d)	~1.0	1.5 ± 0.1	1.5 ± 0.1	260 ± 9	1525^{+51}_{-50}
+48	"	~1.0	1.6 ± 0.1	0.89 ± 0.07	102 ± 5	599^{+27}_{-26}
+49	"	~0.9	$1.2^{+0.2}_{-0.1}$	$0.47^{+0.10}_{-0.08}$	10 ± 1	60 ± 6
+50	Quiescence I (e)	~8.8	$0.36^{+0.04}_{-0.05}$	0.3^*	0.03 ± 0.02	$0.18^{+0.13}_{-0.09}$
+51	2nd Type-I outburst (f)	~1.0	$1.0^{+0.2}_{-0.1}$	$0.58^{+0.19}_{-0.15}$	$7.5^{+1.0}_{-0.9}$	44^{+6}_{-5}
+52	"	~0.8	1.8 ± 0.2	0.41 ± 0.06	32 ± 2	186 ± 14
+53	"	~0.8	1.5 ± 0.1	1.2 ± 0.1	134 ± 7	783^{+42}_{-41}
+54	"	~1.0	1.5 ± 0.1	1.5 ± 0.1	201 ± 8	1177^{+45}_{-44}
+[55,59]	Quiescence II (g)	~4.7	0.49 ± 0.05	0.3^*	$0.12^{+0.05}_{-0.04}$	$0.68^{+0.29}_{-0.23}$

Table 4.2: Notes: the unabsorbed X-ray fluxes and X-ray luminosities are given in the 0.5-10 keV energy range assuming a fixed $N_H \sim 9\times10^{21}$ cm^{-2} and a source distance of ~7 kpc. The errors are 1σ. (*)The fit parameter was fixed to this value.

Table 4.3: Results of our spectral analysis using the power-law model.

obsID	Γ	F_X $(10^{-12}$ erg cm^{-2} s$^{-1})$	L_X $(10^{33}$ erg s$^{-1})$
0790180301	2.6±0.1	0.26±0.01	1.5±0.1
000311720+[42,45]	2.6±0.4	$0.55^{+0.10}_{-0.08}$	$2.6^{+0.6}_{-0.5}$
+46	1.5±0.3	$0.53^{+0.10}_{-0.09}$	$3.1^{+0.6}_{-0.5}$
+47	0.53±0.07	358^{+17}_{-16}	2096^{+98}_{-93}
+48	0.59±0.09	$130.1^{+7.6}_{-7.2}$	762^{+45}_{-42}
+49	1.2±0.3	15±2	86^{+10}_{-9}
+50	$3.6^{+3.0}_{-1.8}$	$0.08^{+0.52}_{-0.05}$	$0.47^{+3.03}_{-0.30}$
+51	1.6±0.5	13±2	73^{+12}_{-9}
+52	0.60±0.19	39^{+4}_{-3}	230^{+22}_{-20}
+53	0.70±0.12	181^{+13}_{-12}	1058^{+75}_{-70}
+54	0.69±0.08	270^{+14}_{-13}	1581^{+80}_{-76}
+[55,59]	2.1±1.4	$0.22^{+0.29}_{-0.08}$	$1.3^{+1.7}_{-0.4}$

Table 4.4: Notes: the unabsorbed X-ray fluxes and X-ray luminosities are given in the 0.5-10 keV energy range assuming a fixed $N_H \sim 9\times10^{21}$ cm^{-2} and a source distance of $\sim$7 kpc. The errors are 1σ. (*)The fit parameter was fixed to this value.

5

A study of timing stability of Black Widow pulsars

We study the timing stability of three black widow pulsars, both in terms of long-term variation as well as shorter-term changes in their orbital parameters. The erratic timing behaviour and radio eclipses of the first two black widow pulsar systems discovered (PSRs B1957−20 and J2051+0827) was assumed to be representative for this class of pulsars. With several new black widow systems added to this population in the last decade, there are now several systems known that do not show the typical orbital timing variations or radio eclipses. We present timing solutions using 7−8 yrs of observations, using data from four of the European Pulsar Timing Array telescopes for PSRs J0023+0923, J2214+3000 and J2234+0944, and confirm that these pulsars do not show any significant variations over our observing time span, both in terms of secular or orbital parameters. Our results from the long-term timing of these pulsars provide several new or improved parameters compared to earlier work. We discuss our results regarding the stability of these pulsars, and the stability of the class of black widow pulsars in general, in context of the binary parameters, and discuss the potential of the Roche lobe filling factor of the companion star being an indicator of stability of these systems.

A. Bak Nielsen, G. Janssen, G. Shaifullah, J. Verbiest, L. Guillemot,
B. Stappers, A. Possenti, and the EPTA collaboration

Paper in prep.

5.1   Introduction

The first radio pulsar was discovered in 1967 by Jocelyn Bell (Hewish et al. 1968) and since then more than 2600 radio pulsars have been found (Manchester 2017). Those ~ 2600 radio pulsars include both isolated pulsars and pulsars in binary systems, and slow and millisecond pulsars (MSPs). The millisecond pulsars are thought to have formed through the recycling scenario, which implies that MSPs have spun up and decreased their magnetic field through X-ray binary evolution (Alpar et al. 1982; Bhattacharya & van den Heuvel 1991). Pulsars are spun up in binary systems through accretion, which transfers angular momentum onto the pulsar. During the X-ray pulsar phase, the magnetic field of the pulsar decreases (Chen et al. 2013). When accretion stops, the newly formed MSPs in binary systems include the so called 'spiders'. These are the 'redback' pulsars (RBPs), which have companion star masses of $M_2 \simeq 0.1 - 0.4\,M_\odot$, and the 'black widow' pulsars (BWPs), with $M_2 \ll 0.1\,M_\odot$ (Chen et al. 2013). The low mass companions of BWPs are often thought to be degenerate stars, similar to brown dwarfs (see section 4.4 in Lazaridis et al. (2011)). The companions of RBPs are non-degenerate stars, as suggested by a few cases where the optical counterpart was discovered (Roberts 2011, 2013). The fate of the companion star in the BWP systems is unclear. However, one discussed scenario is that the companion could be fully ablated, creating an isolated MSP. Alternatively, tidal effects could play a significant role in destroying the companion (Stappers et al. 1998; Chen et al. 2013).

Since the discovery of PSR B1957+20 and J2051−0827, the population of BWPs and RBPs have increased greatly with recent surveys, using either radio surveys which were optimised to find MSPs, or targeted surveys at high energies using e.g. *Fermi*. At least 30+ MSPs were found using such surveys over the past few years (Roberts 2011). The two original BWP systems show eclipses of the radio emission from the pulsar, which are thought to originate from the companion star and be broadened by material being ablated off of the companion star by a strong pulsar wind (Fruchter et al. 1988; Stappers et al. 1996; Chen et al. 2013). The BWPs are, due to the ablated material, often complicated systems to use for precision timing. The companion stars are often bloated, and they exert small torques on the system, which will then cause small changes in the orbit. The changes in the orbit increase the number of parameters that is required in timing models, and their variability could reduce the sensitivity of the timing solution to the gravitational wave (GW) signals (Bochenek et al. 2015). By observing multiple stable pulsars in different parts of the sky, an array of pulsars, and cross-correlating the timing residuals from the different pulsars, it should be possible to obtain the sensitivity to measure the expected quadrapolar signature of a GW. This is the general idea behind the pulsar timing arrays (PTAs) (Lentati et al. 2015).

With new BWPs being discovered, Bochenek et al. (2015) tested the feasibility of using BWPs in the pulsar timing arrays, by testing if fitting for multiple orbital frequency derivatives was significantly reducing the sensitivity to the GW signal. Bochenek et al. (2015) used simulated data sets of five different pulsars to constrain how sensitive to a GW signal a timing solution would be, if several orbital period derivatives were fitted for. They found that the sensitivity to the GW signals were

not reduced significantly, partly due to GW signals spanning several years and the typical BWP orbit spans 2 to 20 hr. It was thus concluded that some BWPs could be used in pulsar timing arrays, and PSR J0610−2100 is already used by the PTAs (Desvignes et al. 2016). There are three other BWPs that are stable and which are candidates for the PTAs: PSRs J0023+0923, J2214+3000 and J2234+0944. All three are currently observed by the North American Nanohertz Observatory for Gravitational Waves (NANOGrav) (Arzoumanian et al. 2018) and the European Pulsar Timing Array (EPTA) (this work).

PSR J0023+0923 was discovered with the Green Bank Telescope (GBT) through the survey of *Fermi* γ-ray sources (Hessels et al. 2011). PSR J0023+0923 is a millisecond pulsar with a spin period of $\sim$3 ms, an orbital period of about 3.3 hr and a companion mass of 0.016 $M_\odot$. The optical counterpart to PSR J0023+0923 was discovered by Breton et al. (2013) with the *Gemini North* telescope. By combining measurements of the filling factor with the estimated distance from the dispersion measure value they inferred that the companion star never fills its Roche lobe. Their results show that when taking the small filling factor into account, the companion star could be as small as 0.05 $R_\odot$. PSR J0023+0923 has also been observed in X-rays, but no pulsations were detected (Ransom et al. 2011).

PSR J2214+3000 was discovered with the GBT, searching for radio pulsars among unassociated sources in the *Fermi*-LAT list of sources (Ransom et al. 2011). It was discovered to be a BWP system, with a low mass companion ($\sim 0.02\,M_\odot$) and an orbital period of about 10 hr. The companion star of PSR J2214+3000 was detected in optical by Schroeder & Halpern (2014)

PSR J2234+0944 has an orbital period of about 10 hr, with a companion star of $\sim$0.015 $M_\odot$, and a spin period of $\sim$3.36 ms. The pulsar was found with the Parkes telescope as a part of the search for radio sources that could be associated with unidentified *Fermi*-LAT sources (Ray et al. 2012).

The three pulsars have all been observed in γ-ray and they all show γ-ray pulsations[1] (Ransom et al. 2011).

In this chapter we present updated timing solutions for the three BWPs J0023+0923, J2214+3000 and J2234+0944. In section 5.2 we present the observations of the three BWPs, in section 5.3 we present our timing solutions and in section 5.4 we discuss the stability of these pulsars and compare their properties with other BWPs.

---

[1] `https://confluence.slac.stanford.edu/display/GLAMCOG/`
`Public+List+of+LAT-Detected+Gamma-Ray+Pulsars`

5.2   Observations

The data in this chapter consists of time of arrivals (TOAs), derived from data from four telescopes that are all part of the European Pulsar Timing Array (EPTA). The EPTA is a collaboration of scientists working with five different telescopes around Europe, the Westerbork Synthesis Radio Telescope (WSRT) in the Netherlands, the Effelsberg Radio Telescope (EFF) in Germany, the Lovell Radio Telescope (JBO) in the UK, the Nançay Radio Telescope (NRT) in France and The Sardinia Radio Telescope (SRT) in Italy (Desvignes et al. 2016). As SRT is a more recent telescope, data from this telescope is not used in this chapter. The aim of the EPTA, like other PTAs, is to enable the detection of the stochastic gravitational wave background (Lee et al. 2011; Desvignes et al. 2016). The three data sets for PSR J0023+0923, J2214+3000 and J2234+0944 respectively span about 7.5, 8 and 7 years of data, see Fig. 5.1. The data used is from several pulsar recording instruments, see Table 5.1 (Karuppusamy et al. 2008; Desvignes et al. 2011; Lazarus et al. 2016; Shaifullah et al. 2016; Guillemot et al. 2016).

The data was collected using different pulsar timing backends (see table 5.1) and was recorded using coherent dedispersion and online folding. Specific parts of the data that were affected by RFI were zapped using standard PSRCHIVE tools. The cleaned data was frequency and time scrunched, meaning the time and frequency of the data cubes were collapsed. For PSR J0023+0923, some observations were taken with a total integration time of several hours, to cover the full orbital period. We split observations that were more than 1 hr long, into smaller subsets of 30 min each, to avoid smearing due to a non-optimal folding solution. The data for PSR J0023+0923 was also refolded, to correct for orbital signatures in the long observations of this source.

The TOAs were created by cross-correlating the time integrated and frequency scrunched data using the total intensity profile analytical templates, which were constructed by fitting von Mises functions to the high signal to noise pulse profiles, using the `paas` tool. The TOAs were generated using the `pat` tool[2], which creates TOAs with a Fourier domain with Markov chain Monte Carlo algorithm (van Straten et al. 2012). Our standard procedure of integrating over the full available bandwidth was insufficient for the NUPPI data from NRT. Since the ISM is not only magnetised and ionised, but is also a turbulent medium and very inhomogeneous, the irregularities cause the observed radio emission to fluctuate over different bandwidths and timescales, which lead to interstellar scintillation (Tielens 2009; Lorimer & Kramer 2012). This is strongly affecting the TOAs derived from the NUPPI backend of NRT, with its large bandwidth of 512 MHz, showing strong scintillation for the PSR J2234+0944, as shown on Fig. 5.2, and less strong scintillation for PSR J0023+0923 and J2214+3000. We refer the calculated TOA to the center of the observing band. However, in case of strong scintillation, this may lead to an apparent time-offset in the calculated TOA due to the reference

---

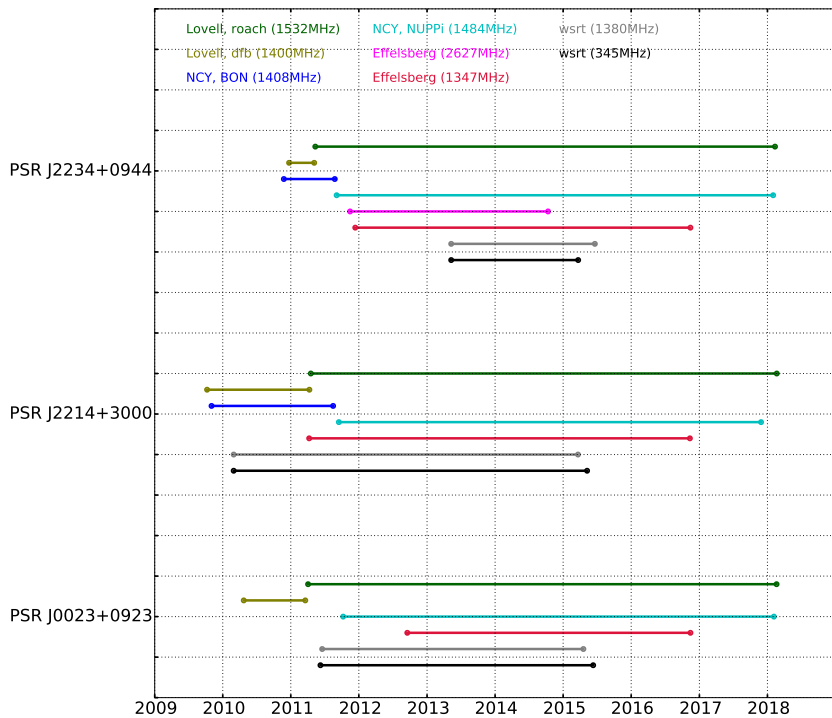[2]See also `psrchive.sourceforge.net`

Figure 5.1: Plot showing the timing baselines per backend for the three BWPs discussed in this chapter. The colours correspond to backend and observing frequnecy band combinations. The dark green lines represent the time span covered by the ROACH-based backend, observing at a centre frequency of 1532 MHz, and the light green line represents the AFB at 1400 MHz, both at the Lovell radio telescope. The dark blue line represents the BON backend at 1408 MHz, and the light blue the NUPPI backend at 1404 MHz, both at the Nançay Radio Observatory. The pink and red lines represent timing spans of the PSRIX backend at 2627 and 1347 MHz, respectively at the Effelsberg 100-m radio telescope. Finally, the grey and black lines represent timing baselines for the PuMa-II backend at the Westerbork Synthesis Radio Telescope. More details for the backends and telescopes can be found in the text and Table 5.1.

frequency not reflecting the data itself. To correct the TOAs for scintillation, we divided the bandwidth in two, which for PSR J0023+0923 and J2214+3000 improved the timing solution. For PSR J2234+0944 only splitting the bandwidth in two improved half of the band, but the other half of the band still showed variations due to scintillation. We thus split the band in half again. This process resulted in TOAs that were only marginally affected by scintillation. We adopt this workaround for this work, reserving a full 2D-template matching method for future work.

The TOAs were measured with reference to a local clock at each observatory, and corrected to the Solar system barycentre using the NASA-JPL DE421 planetary ephemerides (Folkner et al. 2009). The reference clock used was the Terrestrial Time standard, which is derived from the "Temps Atomique International" time standard, TT(TAI) (Hobbs et al. 2006) and the ELL1 (T2) model was used in fitting the TOAs (Lange et al. 2001). Data sets generated by different telescopes were aligned by using constant offsets (JUMPS; following the procedure as described in Verbiest et al. (2016)) and a few clock or timing offsets were applied where necessary.

`Tempo2`[3] error scaling factors were calculated for each telescope backend, using the timing model derived in the previous steps and taking the square root of the reduced χ^2, giving a `T2EFAC` vale. The `T2EFAC` value corrects the weight of the data by rescaling the error bars to correct for under estimation.

5.3 Results

We found a stable timing solution to the three pulsars PSR J0023+0923, J2214+3000 and J2234+0944 over the time span $7-8$ years, using data from four of the EPTA telescopes. In table 5.2 the best fit timing solutions to the three pulsars are shown and in Fig. 5.3 the timing residuals of the three BWPs are shown.

5.3.1 New parameter measurements

For the timing solution we have used the ELL1 model, which is valid only for small eccentricities. The ELL1 model use Laplace parameters, $\epsilon_1 = e\,sin(\omega)$ and $\epsilon_2 = e\,cos(\omega)$, instead of the eccentricity and omega. For low eccentricities the location of periastron is not well defined and a strong correlation between ω and T_0 occur. This leads to very large uncertainties in the estimate of χ^2 of these parameters. By using the ELL1 model this is corrected (Lange et al. 2001). In this chapter we introduce and measure a first order derivative of the dispersion measure ($\dot{DM}$) for PSR J2214+3000, of $3.5(5) \times 10^{-4}$cm^{-3} pc yr^{-1}. This accounts for the DM variations we show in Fig. 5.4 (for more details see section 5.3.2). We measure ϵ_1 and ϵ_2, which are effectively the eccentricity, of the three pulsars. The eccentricity is given by $e = \sqrt{\epsilon_1^2 + \epsilon_2^2}$ and the eccentricities of the pulsars are thus $e = 4.8(10) \times 10^{-5}$, $e = 3.0(11) \times 10^{-5}$, $e = 5.2(31) \times 10^{-6}$ respectively for PSR

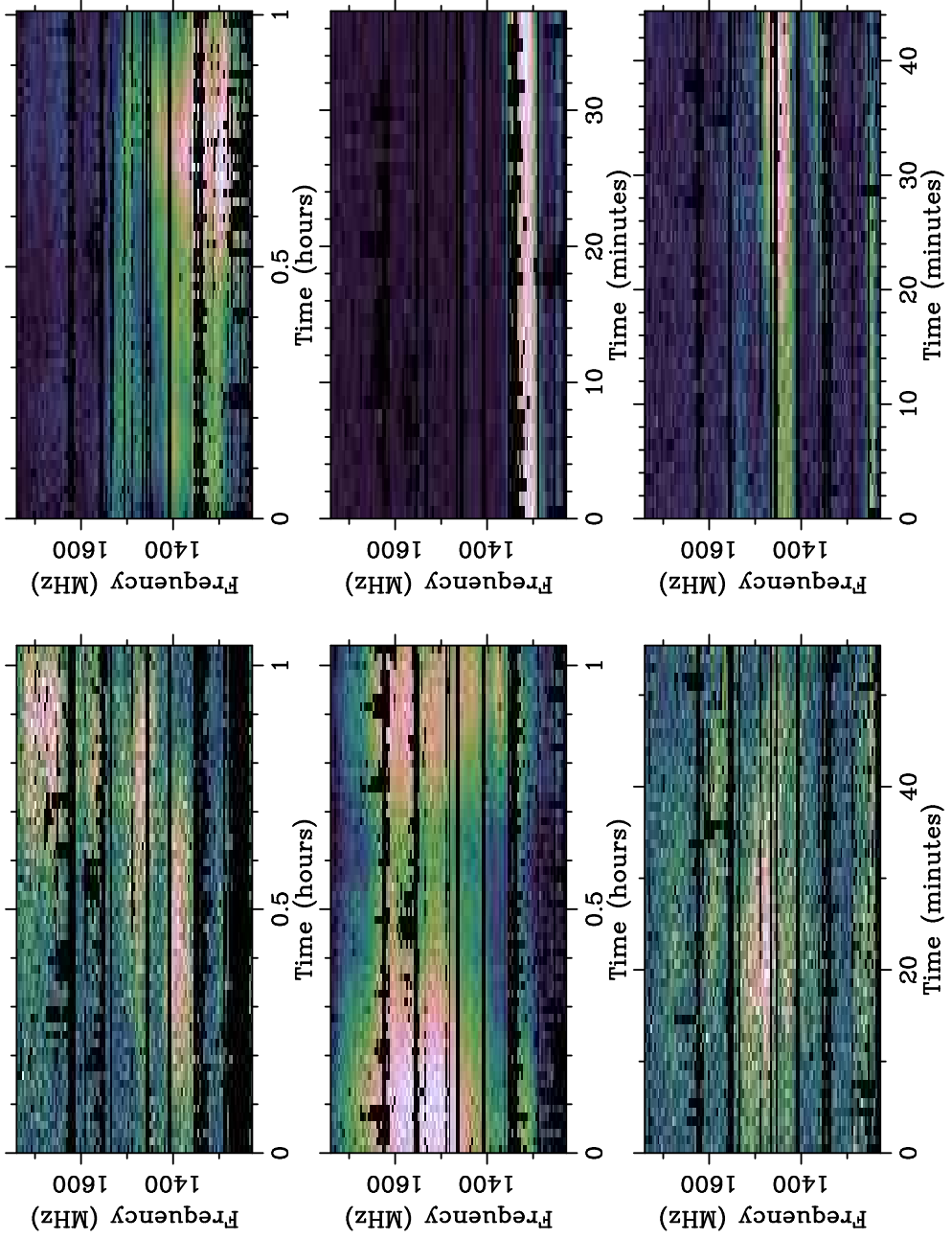[3]Throughout this work `Tempo2` version 2014.2.1 was used.

Figure 5.2: On the dynamical spectra, the scintillation over bandwidth is clearly seen for the pulsar J2234+0944. The variation affects the precision timing of the Nançay data with the NUPPI backend.

Table 5.1: Telescope backends, centre frequency, bandwidth, and number of TOAs for the different pulsars. The four telescopes used are a part of the EPTA and they are the Westerbork telescope (WSRT), Effelsberg, Nançay, and Lovell at Jodrell Bank. *The data from Nançay, NUPPI, is affected by scintillation, and the frequency bands have thus been split into smaller bands, of 256MHz for PSR J0023+0923 and J2214+3000, for PSR J2234+0944 we have split the band in three, so we have one band of 256MHz and two bands of 128MHz.

Telescope (Backend)	f_c (MHz)	BW (MHz)	No. of TOAs (J0023+0923)	No. of TOAs (J2214+3000)	No. of TOAs (J2234+0944)
WSRT (PuMaII)	345	70	55	51	27
Effelsberg (PSRIX)	1380	160	36	61	44
	1347.5	200	59	25	31
	2627	200	-	-	27
Nançay (NUPPI)	1484	512/256/128*	784	193	486
Nançay (BON)	1408	128	-	108	31
Lovell (DFB)	1400	16	25	108	48x
Lovell (ROACH)	1532	400	115	126	147

Table 5.2: Timing solutions for the three BWPs discussed in this chapter; PSRs J0023+0923, J2214+3000 & J2234+0944. In the timing solutions we used TT(TAI) as the Clock correction procedure, DE421 as the Solar system ephemeris model and T2(ELL1) as the binary model.

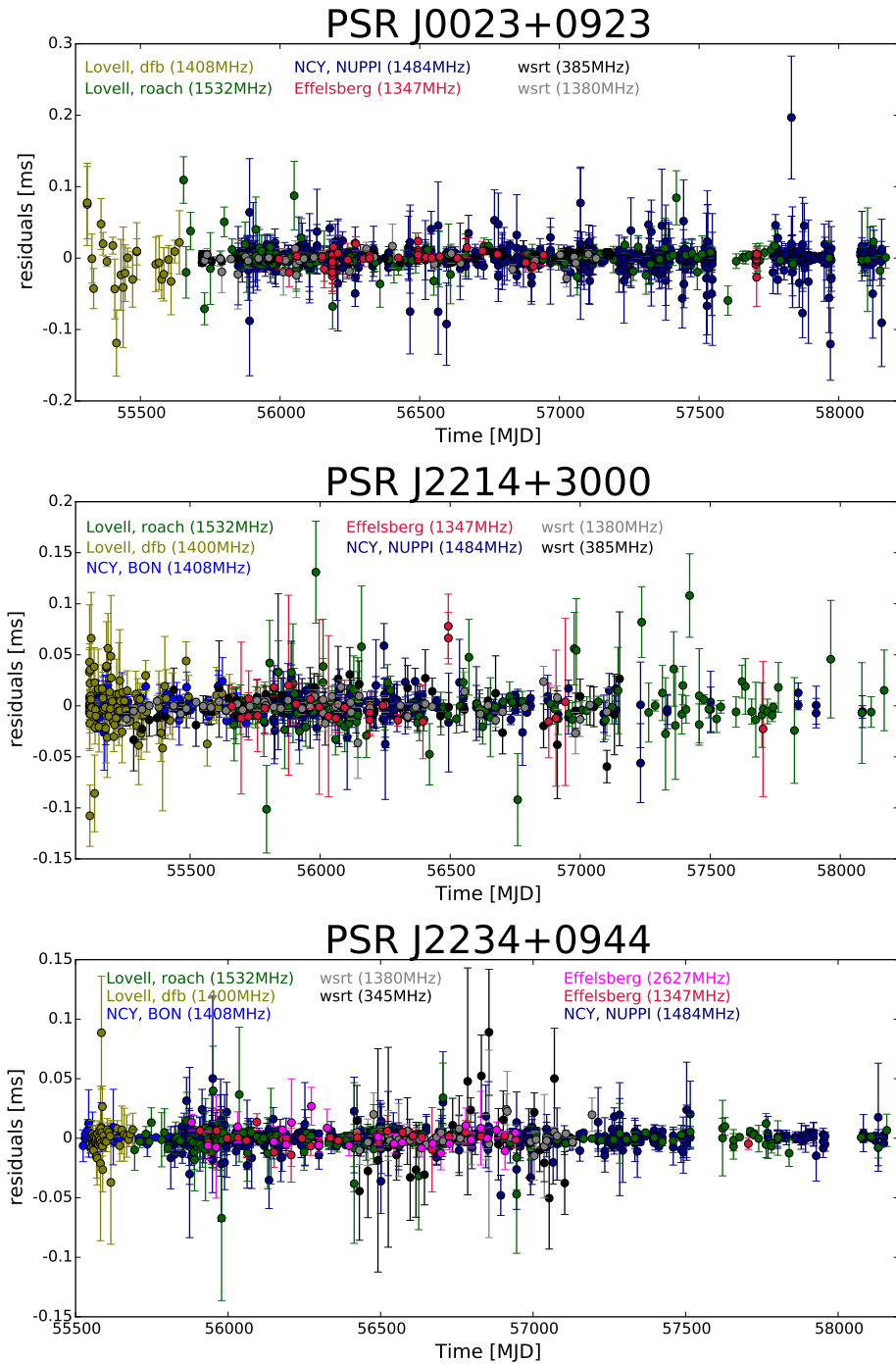|	J0023+0923	J2214+3000	J2234+0944
Fit and data-set			
Pulsar name	J0023+0923	J2214+3000	J2234+0944
MJD range	55309.6–58167.8	55112.9–58168.8	55524.7–58159.5
Data span (yr)	7.83	8.37	7.21
Number of TOAs	1074	660	841
Rms timing residual (μs)	3.7	5.3	1.8
Reduced χ^2 value	1.0	1.0	1.0
Measured Quantities			
Right ascension, α (hh:mm:ss)	00:23:16.877776(19)	22:14:38.852766(18)	22:34:46.853751(6)
Declination, δ (dd:mm:ss)	+09:23:23.8623(7)	+30:00:38.1968(4)	+09:44:30.25618(18)
Pulse frequency, ν (s^{-1})	327.84701548913 65(8)	320.592287390235(3)	275.707828394594 2(6)
First derivative of pulse frequency, $\dot{\nu}$ (s^{-2})	$-1.22767(3) \times 10^{-15}$	$-1.51364(6) \times 10^{-15}$	$-1.527891(19) \times 10^{-15}$
Dispersion measure, DM (cm^{-3}pc)	14.322(3)	22.565(4)	17.8292(9)
First derivative of dispersion measure, DM (cm^{-3}pc yr^{-1})		$3.5(5) \times 10^{-4}$	
Proper motion in right ascension, $\mu_\alpha \cos \delta$ (mas yr^{-1})	$-12.79(16)$	20.64(10)	7.08(6)
Proper motion in declination, μ_δ (mas yr^{-1})	$-5.0(4)$	$-1.35(16)$	$-32.50(10)$
Orbital period, P_b (d)	0.1387991469 7(13)	0.4166329525(3)	0.4196600431(3)
Projected semi-major axis of orbit, x (lt-s)	0.03484151(19)	0.0590819(6)	0.06842971(12)
First derivative of orbital period, $\dot{P}_b$	$-1.23(7) \times 10^{-12}$		$4.7(17) \times 10^{-13}$
First derivative of x, $\dot{x}$ (10^{-12})		$-1.7(7) \times 10^{-14}$	
TASC (MJD)	55186.1136004(7)	55094.1380394(7)	55517.4822997(3)
EPS1 (ϵ_1)	$4.7(11) \times 10^{-5}$	$3.0(11) \times 10^{-5}$	$-4.8(31) \times 10^{-6}$
EPS2 (ϵ_2)	$-1.0(10) \times 10^{-5}$	$-3.7(118) \times 10^{-6}$	$-2.0(31) \times 10^{-6}$
Upper Limits			
Parallax, π (mas)	0.4(4)		
First derivative of x, $\dot{x}$ (10^{-12})	$4.1(32) \times 10^{-15}$		
Set Quantities			
Epoch of frequency, position and DM determination (MJD)	56738	56640	56842

Figure 5.3: The timing residuals of PSRs J0023+0923, J2234+0944 and J2214+3000 after fitting the timing models presented in Table 5.2. The residuals show stability over the collective length of all the observations.

J0023+0923, J2214+3000 and J2234+0944. The eccentricity of J0023+0923 is significant, however, for the two other pulsars they are counted as marginally significant and an upper limit. Any value below a 2σ significance has been set to be an upper limit, and values around or a bit more than a 2σ significance have been set to be marginally detected, in table 5.2. The upper limits stated in table 5.2 are not used in the final timing solution. We found an upper limit on the parallax of PSR J0023+0923, of PX$\leq$0.4(4) mas, which differs from a previous measurement of 0.93(15) mas (Arzoumanian et al. 2018). We further find a marginal detection of the first order derivative of the semi major axis, of $-1.7(7)\times10^{-14}$ for PSR J2214+3000 and an upper limit for the first order derivative of the orbital period, of 4.7(17)$\times10^{-13}$ for PSR J2234+0944. Furthermore, we found a significant value of $\dot{P}_b$ for PSR J0023+0923, of $-1.23(7)\times10^{-12}$, which is significantly different from previous measurements (see section 5.4.2) (Arzoumanian et al. 2018).

5.3.2 Dispersion Measure

We also tested for DM variations along the lines of sight to the three pulsars. The effects on the DM are inversely proportional to the observing frequency, and are therefore more easily detectable at lower frequencies. In Fig. 5.4 we see an example of the DM variations in PSR J2214+3000. The DM measurements on Fig. 5.4 were created by fitting the DM and first order derivative of DM to segments of data that were around 100 days long. The top panel of Fig. 5.4 show the total frequency range of the WSRT data, where we do not detect any DM variations. However, if we only look at the low frequency of the WSRT data, lower panel, we see DM variations. We here detected a first order DM derivative of 3.5(5)$\times10^{-4}$cm^{-3} pc yr^{-1}. For PSRs J0023+0923 and J2234+0944 we did not detect any DM variations.

5.4 Discussion

In the following section we will discuss some of the features that the three sources show and relate these to the long term stability of the three BWPs. We will furthermore compare the properties of stable and unstable BWPs.

5.4.1 Stability

The first BWP found, PSR B1957+20, is unstable over long durations of time, implying that it was not possible to create a valid timing solution for more than a few months to maybe a year (Arzoumanian et al. 1994). The pulsar also showed radio eclipses due to the bloated companion and material surrounding the companion, which is blocking the line of sight towards the pulsar. The second BWP found, PSR J2051−0827, showed similar behavior, including timing solutions that were only stable for short periods of time, of about 3 yrs (Lazaridis et al. 2011; Shaifullah et al. 2016). There are several other BWPs known that show variations. Amongst these is PSR J1731−1847, which shows clear radio eclipses similar to the eclipses seen in the first two observed BWPs. PSR J1731−1847 also shows
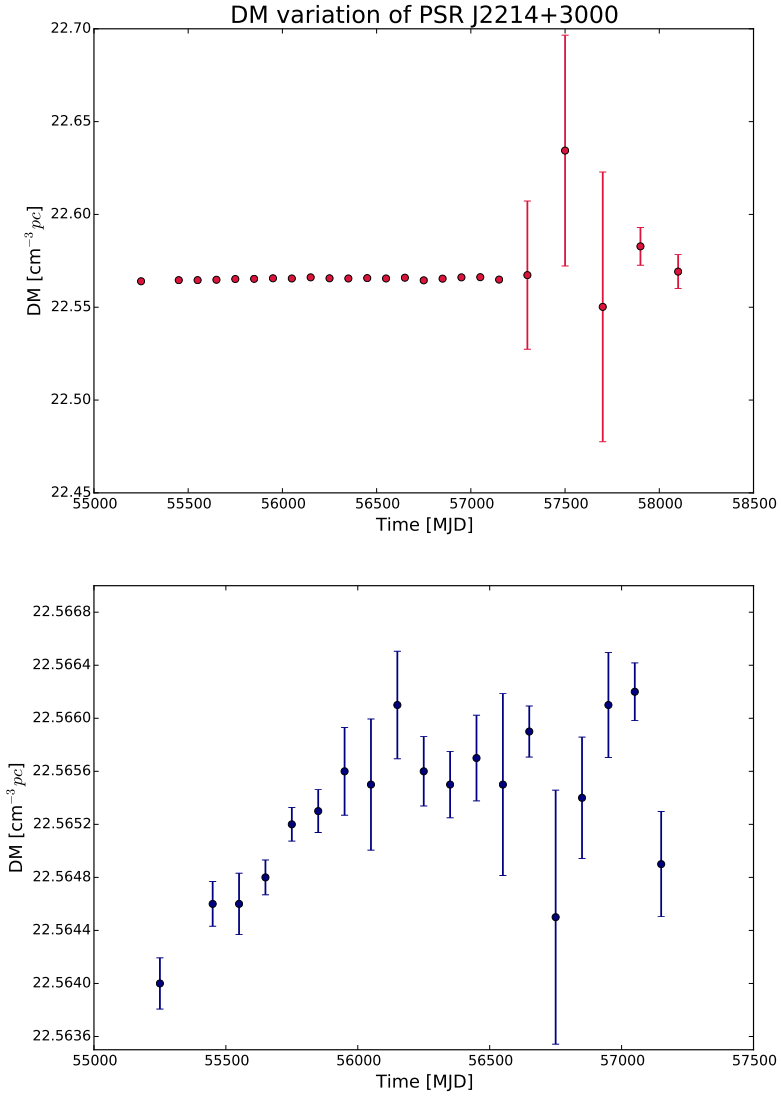
Figure 5.4: Dispersion measure variations are evident for PSR J2214+3000. The dispersion measure derivative in the data is clearly visible in the low frequency data, as shown by the DM time-series derived from those data plotted in the lower panel. The top panel include both high and low frequency data, whereas the lower panel only include 345 MHz data, from the Westerbork telescope.

orbital period variations on relatively short timescales, ~ 3 yrs, comparable to PSR B1957+20 and J2051−0827 (Bates et al. 2011; Ng et al. 2014). The three BWPs in this chapter are very different from the first two BWPs. None of the three BWPs show radio eclipses and it is possible to find a coherent timing solution for each of the three systems that is valid over a 7−8 year period. Furthermore, there is one other BWPs system, aside from the three pulsars in this chapter, that show a stable timing solution. This is PSR J0610−2100, which was already included in the EPTA data set (Desvignes et al. 2016).

5.4.2   Different orbital period derivatives

In section 5.3 we mentioned that there was a difference between the value presented in Arzoumanian et al. (2018) and our measurement of the orbital period derivative, $\dot{P}_b$, of PSR J0023+0923. Orbital period changes are due to e.g. gravitational wave emission, acceleration of the binary system, mass loss from the system or tidal interactions in the system (see e.g. Lorimer & Kramer (2012)). One of the differences between this work and the work by Arzoumanian et al. (2018) is that the aim of this chapter is to understand the physical difference of the stable and unstable BWPs, whereas the aim of Arzoumanian et al. (2018) is to reduce the white noise of an array of pulsars, in order to be sensitive to an eventual GW signal. We therefore believe the difference in the parameter can be explained by a different approach towards including additional orbital derivatives in the fitting procedure.

5.4.3   Eclipses

We examined our data sets for the three pulsars for eclipses, and do not find any evidence for radio eclipses for any of the three pulsars at any of our observed frequencies. This indicates that there is indeed not enough material around the companion to create the eclipses, as is also suggested for J0023+0923 from X-ray observations by Gentile et al. (2014). The lack of radio eclipses can be an indication that the companion stars are not filling their Roche lobe (see section 5.4.4).

5.4.4   Roche lobe filling factors

The companion stars for the first two black widow pulsars, B1957+20 and J2051−0827, are suggested to be Roche lobe filling (Stappers et al. 2001; van Kerkwijk et al. 2011). This means that the outer layers of the companion star are less gravitationally bound to the star and it is thus easier to expel material from, or ablate the companion star. This is one of the essential details of the geometry of the BWPs, as it is the ablated material that causes the radio eclipses (van Kerkwijk et al. 2011). The Roche lobe filling factors for PSR B1957+20 and J2051−0827 are about 0.9, i.e. the Roche lobe is almost filled. The filling factors are determined from fitting the optical light curve of the companion stars (Stappers et al. 2001; Reynolds et al. 2007; van Kerkwijk et al. 2011). The same applies to the recently

found BWP J1810+1744, which also shows radio eclipses and instabilities (Breton et al. 2013; Polzin et al. 2018).

The filling factor of the companion star of PSR J0023+0923 was found to be ∼0.3, from fitting the light curve of the companion star, which means that the companion star is far from filling its Roche lobe (Breton et al. 2013). Binary systems where the companion is not filling its Roche lobe typically show less variability in their orbits and a consequence for the system may thus be that the BWP system PSR J0023+0923 is a stable system (Breton et al. 2013). If the Roche lobe of a BWP system is not filled, eclipses would not be expected, which coincide with what is observed for PRS J0023+0924, J2214+3000 and J2234+0944. It is thus possible that the filling factors could be used as an indicator of whether systems are stable or unstable.

5.4.5   PSR J2234+0944 as a possible transitional system

Transitional millisecond pulsars are a relatively new class of binary pulsars, that show changes between emitting in radio and X-ray, and are believed to switch states between having an active accretion disc and an inactive or no accretion disc (Archibald et al. 2009). Since the first transitional millisecond pulsar, PSR J1023+0038, was discovered to switch states, two more have been found, and all three systems are RBPs (Papitto et al. 2013; Bassa et al. 2014; Roy et al. 2015). The companion stars of BWPs and RBPs are very different, as RBPs have non-degenerate companions with a higher mass than the semi-degenerate companions of BWPs (Chen et al. 2013). However, variations in their orbit and that some systems show radio eclipses are shared between the BWPs and the transitional systems (Fruchter et al. 1988; Stappers et al. 1996; Archibald et al. 2009; Papitto et al. 2013; Chen et al. 2013; Roy et al. 2015). Torres et al. (2017) suggested that the pulsar PSR J2234+0944 could be a potential transitional system, based on variations in the γ-ray spectrum, which is similar to what is seen in the transitional millisecond pulsar PSR J1227−4853. However, PSR J2234+0944 has a timing solution that is stable over 8 yrs, with no obvious irregularities, and no obvious eclipses. This system is thus different from the variable transitional systems, which would seem to suggest that PSR J2234+0944 is not a transitional system.

5.5   Conclusions

We studied three BWPs, PSR J0023+0923, J2234+0944 and J2214+3000, all of which showed a different behaviour than the two first discovered pulsars PSR B1957+20 and J2051−0827. The first two discovered pulsars show unstable timing solutions, where it is only possible to create a stable solution over a few months to years. We present timing solutions for PSR J0023+0923, J2214+3000 and J2234+0944, that are stable over a time span of 7−8 yrs. Compared to earlier work, our timing solution is sensitive to a few new parameters and we present upper limits

on other parameters: we find an upper limit of the parallax of PSR J0023+0923 which differs significantly from a previous measurement (Arzoumanian et al. 2018). Furthermore we set limits and introduce significant measurement of the eccentricity of the BWPs in this chapter. We also measure an orbital period derivative for PSR J0023+0923, of $-1.23(7)\times10^{-12}$, which also differs significantly from previous measurements (Arzoumanian et al. 2018). The BWPs in this study are all stable, and we discuss their properties to find out what causes these differences in timing behaviour. It is possible that it is due to their companion star not filling the Roche lobe. This would make the systems more tightly bound, resulting in a cleaner system with less material to interfere with, or affect the radio signal and the orbital parameters. Since the three pulsars show stability over long timescales it is possible to use the systems as a part of the pulsar timing arrays. For future work we will further fine tune our fitting procedure, which will improve the measurement of all timing parameters. It furthermore remains to be seen if the lack of stability in some of these gravitationally tightly bound systems are tied to specific high-energy signatures. However, as discussed in the preceding sections, while all three systems discussed in this chapter are detected in high-energy data, such signatures have not yet emerged in those data. The improved timing solutions presented in this work will also be useful in new investigations of possible high-energy signatures. Comparing with more BWPs and other pulsar systems will give a clearer picture of what is the most important factor for why a BWP system is stable or unstable.

Bibliography

Alpar M. A., Cheng A. F., Ruderman M. A., Shaham J., 1982, Nature, 300, 728

Archibald A. M., et al., 2009, Science, 324, 1411

Arzoumanian Z., Fruchter A. S., Taylor J. H., 1994, ApJ, 426, 85

Arzoumanian Z., et al., 2018, preprint, (arXiv:1801.01837)

Bassa C. G., et al., 2014, MNRAS, 441, 1825

Bates S. D., et al., 2011, MNRAS, 416, 2455

Bhattacharya D., van den Heuvel E. P. J., 1991, Phys. Rep., 203, 1

Bochenek C., Ransom S., Demorest P., 2015, ApJ, 813, L4

Breton R. P., et al., 2013, ApJ, 769, 108

Chen H.-L., Chen X., Tauris T. M., Han Z., 2013, ApJ, 775, 27

Desvignes G., Barott W. C., Cognard I., Lespagnol P., Theureau G., 2011, in Burgay M., D'Amico N., Esposito P., Pellizzoni A., Possenti A., eds, American Institute of Physics Conference Series Vol. 1357, American Institute of Physics Conference Series. pp 349–350,

Desvignes G., et al., 2016, MNRAS, 458, 3341

Folkner W. M., Williams J. G., Boggs D. H., 2009, Interplanetary Network Progress Report, 178, 1

Fruchter A. S., Stinebring D. R., Taylor J. H., 1988, Nature, 333, 237

Gentile P. A., et al., 2014, ApJ, 783, 69

Guillemot L., et al., 2016, A&A, 587, A109

Hessels J. W. T., et al., 2011, in Burgay M., D'Amico N., Esposito P., Pellizzoni A., Possenti A., eds, American Institute of Physics Conference Series Vol. 1357, American Institute of Physics Conference Series. pp 40–43 (arXiv:1101.1742)

Hewish A., Bell S. J., Pilkington J. D. H., Scott P. F., Collins R. A., 1968, Nature, 217, 709

Hobbs G. B., Edwards R. T., Manchester R. N., 2006, MNRAS, 369, 655

Karuppusamy R., Stappers B., van Straten W., 2008, PASP, 120, 191

Lange C., Camilo F., Wex N., Kramer M., Backer D. C., Lyne A. G., Doroshenko O., 2001, MNRAS, 326, 274

Lazaridis K., et al., 2011, MNRAS, 414, 3134

Lazarus P., Karuppusamy R., Graikou E., Caballero R. N., Champion D. J., Lee K. J., Verbiest J. P. W., Kramer M., 2016, MNRAS, 458, 868

Lee K. J., Wex N., Kramer M., Stappers B. W., Bassa C. G., Janssen G. H., Karuppusamy R., Smits R., 2011, MNRAS, 414, 3251

Lentati L., et al., 2015, MNRAS, 453, 2576

Lorimer D. R., Kramer M., 2012, Handbook of Pulsar Astronomy

Manchester R. N., 2017, in Journal of Physics Conference Series. p. 012001 (arXiv:1801.04323)

Ng C., et al., 2014, MNRAS, 439, 1865

Papitto A., et al., 2013, Nature, 501, 517

Polzin E. J., et al., 2018, MNRAS, 476, 1968

Ransom S. M., et al., 2011, ApJ, 727, L16

Ray P. S., et al., 2012, preprint, (arXiv:1205.3089)

Reynolds M. T., Callanan P. J., Fruchter A. S., Torres M. A. P., Beer M. E., Gibbons R. A., 2007, MNRAS, 379, 1117

Roberts M. S. E., 2011, in Burgay M., D'Amico N., Esposito P., Pellizzoni A., Possenti A., eds, American Institute of Physics Conference Series Vol. 1357, American Institute of Physics Conference Series. pp 127–130 (arXiv:1103.0819)

Roberts M. S. E., 2013, in van Leeuwen J., ed., IAU Symposium Vol. 291, Neutron Stars and Pulsars: Challenges and Opportunities after 80 years. pp 127–132 (arXiv:1210.6903)

Roy J., et al., 2015, ApJ, 800, L12

Schroeder J., Halpern J., 2014, ApJ, 793, 78

Shaifullah G., et al., 2016, MNRAS, 462, 1029

Stappers B. W., Bessell M. S., Bailes M., 1996, ApJ, 473, L119

Stappers B. W., Bailes M., Manchester R. N., Sandhu J. S., Toscano M., 1998, ApJ, 499, L183

Stappers B. W., van Kerkwijk M. H., Bell J. F., Kulkarni S. R., 2001, ApJ, 548, L183

Tielens A. G. G. M., 2009, Astrophysics and Space Science Proceedings, 10, 271

Torres D. F., Ji L., Li J., Papitto A., Rea N., de Oña Wilhelmi E., Zhang S., 2017, ApJ, 836, 68

Verbiest J. P. W., et al., 2016, MNRAS, 458, 1267

van Kerkwijk M. H., Breton R. P., Kulkarni S. R., 2011, ApJ, 728, 95

van Straten W., Demorest P., Oslowski S., 2012, Astronomical Research and Technology, 9, 237

Nederlandse Samenvatting

De mensheid is altijd geïntrigeerd geweest door de nachtelijke hemel. We keken omhoog en verwonderden ons. Vroege astronomen brachten de hemel in kaart en stelden zich een universum voor waarin wij centraal stonden. Met de uitvinding van de telescoop veranderde ons beeld van de wereld en verbreedde zich onze horizon. Sindsdien is de astronomie ver gekomen en kijken we vandaag de dag niet alleen naar planeten in ons Zonnestelsel, maar ook naar sterrenstelsel hier ver, ver vandaan en naar kleine exotische objecten zoals de overblijfselen van ontplofte sterren. Dit proefschrift gaat over sommige van deze restanten.

In 1934 werd voorgesteld dat neutronensterren de overblijfselen zijn van supernova's, maar het eerste bewijs voor het bestaan van neutronensterren deed zich pas voor bij de ontdekking van pulsars in 1967. Pulsars kunnen gevonden worden in veel verschillende soorten systemen, van allerlei dubbelster configuraties, tot eenzame neutronensterren. Het onderzoek naar pulsars omvat observaties in meerdere golflengtegebieden, waarbij het mogelijk is om niet alleen de eigenschappen en het ontstaan van pulsars te onderzoeken, maar ook om deze pulsars te gebruiken als laboratoria voor extreme natuurkunde zoals extreem sterke magnetische velden, accretieschijven en zwaartekrachtgolven.

Wat is een pulsar?

Pulsars zijn neutronensterren die zeer snel rond om hun eigen as draaien en een sterk magnetisch veld hebben. Ze stoten straling uit vanaf hun magnetische polen en het gebied daaromheen, waarbij we deze emissie als pulsaties waarnemen wanneer de magnetische as niet overeenkomt met de rotatieas. De straling wordt vastgelegd als een korte detectie met grotendeels constante tijdsinterval tussen opeenvolgende detecties, zoals te zien is in Fig. 5.5 , de opname van de eerste ontdekking van een pulsar (genaamd CP 1919).

De benaming "pulsar"verscheen voor het eerst in 1968 in een artikel over de ontdekking door Jocelyn Bell Burnell en Anthony Hewish. De term staat voor 'pulserende ster', wat een accuratere beschrijving is dan de eerste naam die Bell Burnell en Hewish eraan gaven namelijk Little Green Men-1 (LGM-1).

Verschillende soorten pulsars

Er bestaan veel verschillende soorten pulsars; ze kunnen waargenomen worden in golflengtes van gammastraling tot radiostraling, en worden zowel gevonden als
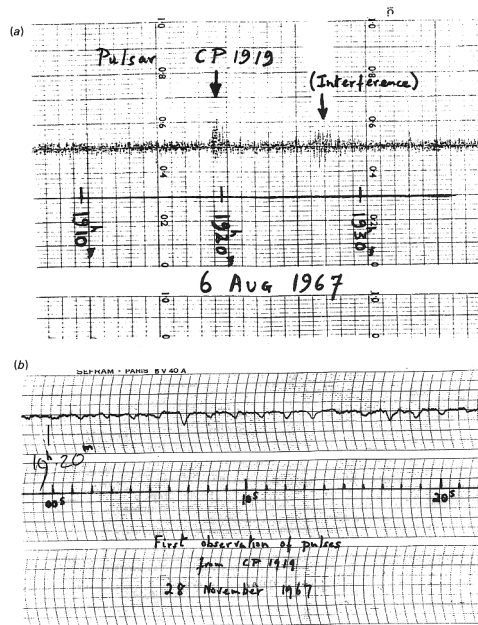
Figuur 5.5: In het bovenste figuur worden de miniscule variaties weergegeven die op een scintillator plaat zijn opgenomen. Het onderste figuur komt van snellere opname apparatuur waardoor de pulsen van CP 1919 veel beter zichtbaar worden. Bron: Jocelyn Bell Burnell en Antony Hewish.

geïsoleerde objecten als in dubbelster configuraties. The Röntgenstraling die van Röntgen-pulsars komt, worden geproduceerd door opwarming van materiaal bij de magnetische polen, de zogenaamde 'hot spots'. De magnetische polen worden opgewarmd door accretie van materiaal dat van de begeleidende ster komt, via een accretieschijf dan wel via accretie gedreven door sterrenwind. Deze mechanismen horen respectievelijk bij een pulsar met een begeleidende ster van kleine massa, of van grote massa. Beiden soorten pulsars wordt in dit proefschrift beschreven. Een ander type pulsar dat in dit proefschrift aan de orde komt zijn zogenaamde 'black widow' ('zwarte weduwe') pulsars. Dit zijn pulsars die tijdens een Röntgenstraling-fase sneller zijn gaan roteren met als gevolg dat ze een periode van milliseconden hebben. Daarbij hebben ze een semi-ontaarde partner ster - vergelijkbaar met een bruine dwergster - die door de wind die van de pulsar komt vanaf de buitenkant van zijn materie wordt ontdaan.

Waarom onderzoeken we pulsars?

Er zijn vele redenen om pulsars te bestuderen. Het is mogelijk om ze te gebruiken als laboratoria voor natuurkunde in extreme omstandigheden die op aarde onmogelijk na te bootsen zijn. Onder andere worden hiermee sterke magnetische velden, de toestandsvergelijkingen van een neutronenster en plasma- en accretie fysica onderzocht. Veel pulsars zijn daarnaast zeer precieze klokken, waardoor het mogelijk zou moeten zijn om een reeks pulsars te gebruiken om zwaartekrachts-golven mee te detecteren. Tenslotte worden ook de eigenschappen onderzocht die direct iets te maken hebben met gedrag van pulsars en hun partner sterren zoals de lange-termijns veranderingen van hun rotatie snelheid, en de evolutie van de

partner sterren. Het doel in dit proefschrift was om de evolutie van de rotatie en de eigenschappen van de interacties tussen pulsars en hun partner sterren te onderzoeken.

Dit proefschrift

In dit proefschrift bestudeer ik zes pulsars die zich allemaal net anders gedragen dan wat we normaal gesproken zouden verwachten van deze systemen. We hebben het over verschillende Röntgen pulsars, en drie radio pulsars waarvan het nodig was om ze zowel in Röntgenstraling als in radiostraling te onderzoeken. De zes systemen worden in de volgende vier hoofdstukken behandeld.

Hoofdstuk 2: In dit hoofdstuk hebben we gekeken naar de pulsar 2A 1822−371, die Röntgenstraling uitzendt en zich ophoudt in een dubbelstersysteem met een begeleidende ster van lage massa waarbij de twee sterren tijdens hun omloopbanen eclipsen veroorzaken langs de gezichtslijn. De omlooptijd van de pulsar is ongeveer 5.57 uur, en de rotatieperiode is 0.59 seconde. Deze pulsar vertoond een grote toename in de omlooptijd, iets wat niet verklaard wordt door de gebruikelijke theorieën over het verloop van de omlooptijden in dit soort systemen. We hebben onderzocht of deze toename verklaard kan worden door zogenaamde super-Eddington massaoverdracht van de begeleidende ster naar de neutronenster. De sterkte van het magnetische veld van de pulsar is onzeker voor dit systeem. Tot op heden bestaan er twee gerapporteerde detecties van cyclotron resonantie verstrooiing signalen die een magnetisch veld van 10^{10} G dan wel 10^{12} G impliceren. Onze voorspellingen voor de massaoverdracht geeft ook een schatting van het magnetisch veld, in dit geval dichter bij de 10^{10} G. In dit hoofdstuk is 13 jaar aan data van de RXTE telescoop gebruikt om de toename in rotatiesnelheid van de pulsar over deze 13 jaar te meten.

Hoofdstuk 3: We hebben het symbiotische Röntgen dubbelstersysteem GX 1+4 bestudeerd, een pulsar met een periode van ongeveer 150 s. Het doel van dit hoofdstuk is om te testen of deze pulsar tekenen vertoond van een puls fase - flux correlatie. Deze correlatie wordt waargenomen in veel Röntgen pulsars met periodes van enkele tot honderden milliseconden waar accretie plaatsvindt, maar het is nog niet onderzocht of deze correlatie zich ook bij Röntgen dubbelstersystemen met lange rotatietijden en sterke magnetische velden (10^{7-9} G), en met begeleidende sterren van lage massa. Het bleek niet mogelijk om een puls fase - flux correlatie te vinden in deze pulsar. Dit kan mogelijk als bewijs geïnterpreteerd worden voor de stelling dat de aanwezigheid van deze correlatie in pulsars met een sterk magnetisch veld onmogelijk is.

Hoofdstuk 4: Voor dit hoofdstuk hebben we 4U 0115+63 bestudeerd, een tijdelijke Röntgenbron in een dubbelstersysteem met een begeleidende Be-type ster van hoge massa. Deze bron heeft een type II uitbarsting ondergaan, maar in plaats van een opvolgende uitdoving, blijft de bron kort na de uitbarsting tijdelijk in een fase van vrij constante helderheid. De bron werd geobserveerd door de XMM-Newton telescoop, en het spectrum kan gemodelleerd worden als zwarteli-

chaamsstraling uitgezonden door een klein gebied, wat suggereert dat de straling van 'hot spots' op het oppervlak van de neutronenster komt. Deze interpretatie werd bevestigd met de detectie van pulsaties. In dit hoofdstuk hebben we geprobeerd om zowel de emissie zelf, als de trage afname van de helderheid te verklaren via accretie van materiaal aan de magnetische polen, of via het afkoelen van de neutronenster (deze is tenslotte in de eerste plaats reeds opgewarmd door het accretie materiaal tijdens de type II uitbraak). Beide modellen blijken plausibel, waarbij geen van beiden de voorkeur boven de ander genoot.

Hoofdstuk 5: In dit hoofdstuk bestuderen we drie zogenaamde 'zwarte weduwe' pulsars; PSR J0023+0923, J2214+3000 en J2234+0944. We hebben bestaande modellen voor de puls aankomsttijden aangevuld met nieuwe observaties. Deze pulsars zijn stabiel over de observatie periode van $7-8$ jaar. Wij buigen ons over de vraag waarom deze drie pulsars stabiel zijn terwijl vorige bestudeerde zwarte weduwen (PSR B1957$-$20 en J2051+0827) zeer onstabiel waren. Een mogelijkheid die wij bespreken is dat de begeleidende ster anders is de stabiele systemen, aangezien in de instabiele systemen de begeleidende ster de Roche lobe vult terwijl dit niet het geval is bij het ene stabiele systeem waarvoor dit gemeten kon worden. Met het vullen van de Roche lobe wordt bedoeld dat de ster minder sterk intern gebonden is, waardoor het makkelijker wordt materiaal ervan af te halen. Doordat het materiaal makkelijk af te vangen is door de pulsar veroorzaakt dit een dubbelstersysteem dat omgeven wordt door een grote hoeveelheid materiaal dat invloed kan hebben op de omloopbanen van beide sterren waardoor het systeem onstabiel kan worden.

English Summary

Humanity has always been intrigued by the night sky. We looked up and wondered. The early astronomers mapped the sky and imagined a universe revolving around us. With the invention of the first telescopes our image of the world changed and our horizons broadened. Since then, astronomy has come a long way and today we do not only look at the planets in our Solar system, we look at galaxies far, far away and at small exotic objects such as the remnants of stellar explosions. It is some of these remnants this thesis is on.

In 1934 it was proposed that neutron stars were the remnants of supernovae. The first proof of the existence of neutron stars came with the discovery of pulsars in 1967. Pulsars are found in many different systems, from various binary configurations to single neutron stars. Pulsar research spans multiple wavelengths and it is possible to study not only the nature of pulsars, but also to use them as extreme laboratories for studying e.g. strong magnetic fields, accretion discs and gravitational waves.

What is a pulsar?

Pulsars are neutron stars that spin very fast around their own axis and have a strong magnetic field. Pulsars emit radiation from or around their magnetic poles and we observe the emission as pulsations when the magnetic field axis is misaligned with the rotation axis. The emission is recorded as a short detection with a mostly constant time interval between each observation, as seen on Fig. 5.6 which is the recording of the first pulsar discovered (named CP 1919).

The name "Pulsar" first appeared in 1968 in an article about the discovery by Jocelyn Bell Burnell and Anthony Hewish. The term pulsar meaning pulsating star. This was somewhat more accurate than the first name Bell Burnell and Hewish gave the discovery, which was LGM-1 (Little Green Men-1).

The different types of pulsars

There are many different types of pulsars, spanning wavelengths from γ-ray to radio, and both isolated and binary systems. In this thesis I have worked on both X-ray and radio pulsars in binary systems. The X-rays from X-ray pulsars originate from heating of the magnetic poles, from the so called hot spots. The magnetic poles are heated through accretion of material from the companion star, either via an accretion disc or through wind accretion. This is respectively the
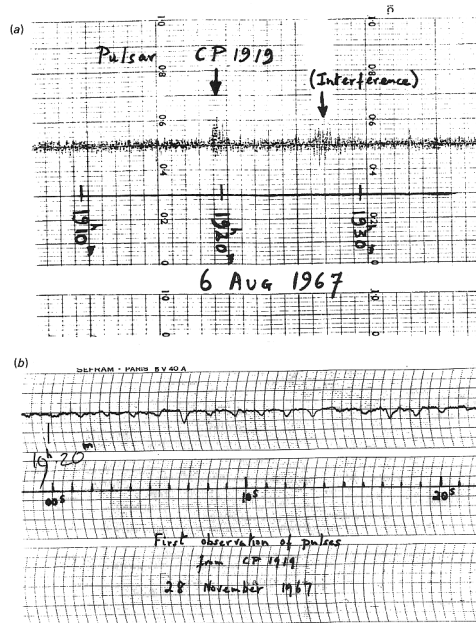
Figure 5.6: The top panel show the almost indistinguishable variations on a scintillation chart recorder and the lower image show a results from a higher speed recorder, now with the pulsations of CP 1919 visible. Image credit: Jocelyn Bell Burnell and Antony Hewish

emission mechanism of a pulsar in a low mass X-ray binary or a high mass X-ray binary. Both low mass X-ray binaries and high mass X-ray binaries are included in this thesis.

Another type of pulsars found in this thesis are black widow pulsars, a type of radio pulsars in binary systems. These are millisecond pulsars that have been spun up during an X-ray pulsar phase. They have semi-degenerate companion stars, somewhat similar to brown dwarfs, which are being ablated by the pulsar wind.

Why do we study pulsars?

There are many reasons to study pulsars. It is possible to use pulsars as extreme laboratories to study extreme physics that we cannot recreate on earth. We e.g. study strong magnetic fields, the equation of state of a neutron star and plasma and accretion physics. Many pulsars are furthermore very precise clocks, and it should be possible to use their stability to detect gravitational waves, using an array of pulsars. It is also possible to study properties directly linked to the pulsars themselves or to their binaries e.g. their spin evolution and binary stellar evolution. In this thesis it was the aim to study spin evolution and properties of interactions between the stars in binary systems.

In this thesis

In this thesis I study six pulsars that all behave slightly differently from what we would normally expect for the types of systems in question. I have studied different X-ray binary systems, and three radio pulsars, which required using both X-ray

and radio telescopes. The six systems are treated in the following four chapters.

Chapter 2: In chapter 2 we looked at the eclipsing low mass X-ray binary 2A 1822-371, a pulsar with a spin period of 0.59 s and an orbital period of 5.57 hr. This pulsar showed a large orbital period increase which was not explained by the usual theories of orbital period evolution, and we therefore tried to see if we could explain the evolution via super Eddington mass transfer from the companion star to the neutron star. The magnetic field of the pulsar is uncertain for this system. There are two previous claims of cylotron resonance scattering features (crsf) yielding a magnetic field of either $\sim 10^{10}$ G or $\sim 10^{12}$ G. Our prediction for the mass transfer also yielded a possible magnetic field, which was closer to the field of 10^{10} G. In this chapter we used 13 years of *RXTE* data and determined the spin-up of the pulsar over those 13 years.

Chapter 3: We studied the symbiotic X-ray binary GX 1+4, a pulsar with a spin period of about 150 s. The aim with this chapter was to test if the pulsar showed any pulse phase – flux correlation. The pulse phase – flux correlation is widely seen in accreting millisecond X-ray pulsars, but it had not been tested if it was present in the low mass X-ray binaress hosting slow rotating pulsars with high magnetic fields ($>10^{7-9}$G). It was not possible to find a pulse phase – flux correlation. This could be taken as evidence for the correlation to be impossible in pulsars with high magnetic fields.

Chapter 4: For this chapter we studied the Be/high mass X-ray transient 4U 0115+63. This source experienced a type II outburst, but instead of decaying to quiescence, the source settled in a temporary meta-stable plateau state. The source was observed with *XMM-Newton*, and its spectrum was fitted with a blackbody model with a small emitting region, suggesting a emission from hot spots on the surface of the neutron star. This was confirmed with the detection of pulsations. In this chapter we tried to explain the emission and slow luminosity decay via either accretion onto the magnetic field poles or with cooling of the neutron star, which was heated due to accreted material during the type II outburst that was observed. Both models are plausible and we do not find a conclusive best model.

Chapter 5: In this chapter we studied three black widow pulsars, PSR J0023+0923, J2214+3000 and J2234+0944. We updated the timing solutions, using new observations, for these pulsars, and found long term stable timing solutions over an observation period of 7-8 years. The first two black widow systems found, PSRs B1957 − 20 and J2051+0827, are very unstable systems. We discuss the possibility that the stability is due to the companion star in the stable systems being slightly different from the companion star in unstable systems. The companion star is found to not fill the Roche lobe in the stable system (where it is possible to measure the Roche lobe filling) while it fills the Roche lobe in both of the unstable systems. Not filling the Roche lobe means that the star is more tightly bound to it self, and thus harder to ablate. If the companion star is

bloated, and the Roche lobe is filled, then the outer layers of the companion star are loosely bound to the companion star and thus easy to ablate. The ablated material creates a binary with a lot of material surrounding it, thus affecting the binary orbit and making the systems unstable.

Dansk resumé

Menneskeheden har altid været fascineret af nattehimmelen. Vi kiggede op og var forundrede. De første astronomer kortlagde himmelen og forestillede sig et univers med os som centrum. Opfindelsen af de første teleskoper ændrede vores verdensbillede. Siden er astronomien kommet langt. I dag kigger vi ikke kun på planeterne i vores eget solsystem, vi kigger på gallakser langt, langt væk og på små eksotiske objekter, så som resterne af eksploderede stjerner. Det er disse rester som denne afhandling beskæftiger sig med.

I 1934 blev det forslået at neutronstjerner var den rest, der var tilbage efter en supernovaeksplosion. Neutronstjernes eksistens blev bevist ved opdagelsen af pulsarer i 1967. Pulsarer befinder sig i mange forskellige stjernesystemer, fra forskellige dobbeltstjernesystemer til isolerede neutronstjerner. Pulsar forskning strækker sig over mange bølgelængder og det er, udover at studere pulsarerne selv, også muligt at bruge pulsarerne som ekstreme laboratorier hvor man undersøger stærke magnetfelter, accretion diske og gravitationelle bølger.

Hvad er en pulsar?
Pulsarer er neutronstjerner der roterer meget hurtigt rundt om deres egen akse og yderligere har et stærkt magnetfelt. Pulsarer udsender stråling fra eller omkring deres magnetfelts pol og vi observere strålingen som pulsationer når magnetfeltets akse er forskudt fra rotationsaksen. Udstrålingen er observeret som en kort detektion, med et tidsinterval mellem hver detektion, som ofte er konstant. Det kan ses på Fig. 5.7, hvilket er observationen af den første pulsar der blev opdaget (navnet på pulsaren var CP 1919).

Navnet "Pulsar"blev første gang brugt i 1968 i en artikel om Jocelyn Bell Burnell og Anthony Hewish opdagelse. Pulsar står for "pulserende stjerne". Dette var et noget mere korrekt navn, end det Bell Burnell og Hewish først gav deres opdagelse, hvilket var LGM-1 (little green men-1 eller små grønne mænd-1).

De forskellige typer af pulsarer
Der er flere forskellige typer af pulsarer. De strækker sig over bølgelængder fra gammastråling til radiostråling og findes i både isolerede og binære systemer. I denne afhandling har vi arbejdet med både røntgen og radio pulsarer i binære systemer. Røntgenstråling fra røntgenpulsarer er varme fra magnetfelt polerne, de såkaldte varme pletter. Magnetfelt polerne bliver opvarmet når material fra ledsa-
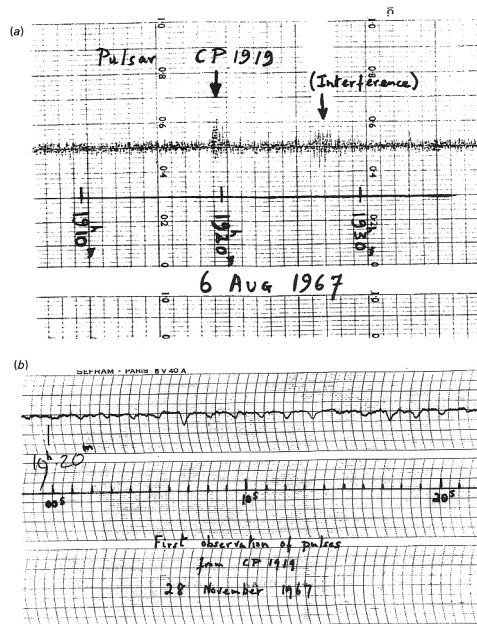
Figur 5.7: Øverste panel viser de utydelige variationer på en scintillations detektor og det nederste billede viser et resultat med en højhastigheds optager, hvor pulsationerne fra CP 1919 nu er synlige. Billede reference: Jocelyn Bell Burnell and Antony Hewish

ger stjernen falder ned på polen, dette kaldes accretion. Det sker enten ved en accretion disk eller ved vind accretion. Dette er respektivt emissions mekanismen i en lav masse røntgen binære systemer eller høj masse røntgen binære systemer. I denne afhandling har vi arbejdet med både høj og lav masse binære systemer.

En anden type pulsarer behandlet i denne afhandling er sorte enker (black widows), en type af radio pulsarer der findes i binære systemer. Disse pulsarer har en rotations hastighed som har været stigende, pga. at de har været igennem en røntgen pulsar fase. De har semi-degenerede ledsager stjerner, som minder om brune dværge, og deres ledsager stjerner bliver blæst i stykker af pulsarens vind.

Hvorfor studere vi pulsarer?

Der er mange grunde til at studerer pulsarer. Det er som tidligere nævnt muligt at bruge pulsarer som ekstreme laboratorier, hvor vi kan undersøge ekstrem fysik som det ikke er muligt at genskabe på Jorden. Vi studerer fx stærke magnetfelter, tilstandsligningen for neutronstjerner, plasma og accretion fysik. Mange pulsarer er derudover meget præcise ure og det burde være muligt at bruge deres stabilitet til at detekterer gravitationelle bølger. Det kan gøres ved at bruge et antal pulsarer fordelt på himmelen, kaldet pulsar timing array. Det er også muligt at studere enkelte pulsarers egenskaber eller de binære systemers egenskaber, fx deres rotations udvikling og udviklingen af det binære system. Det var målet med denne afhandling at undersøge rotationsudviklingen og interaktions egenskaberne i binære systemer.

I denne afhandling

I denne afhandling studerer vi seks pulsarer der alle opføre sig lidt anderledes end hvad vi ville forvente. Vi har studeret forskellige binære røntgen systemer og tre radiopulsarer. Dette har krævet brugen af både røntgen- og radioteleskoper. De seks systemer er behandlet i disse fire kapitler.

Kapitel 2: I kapitel 2 kiggede vi på det eklipsende lav masse røntgen binære system, 2A 1822-371, som har en pulsar med en rotations hastighed på 0.59 s og en omløbstid på 5.57 timer. Denne pulsar viste en stor tiltagen i omløbstiden, hvilket ikke kunne forklares med normale teorier omkring omløbsperiodens udvikling. Vi prøvede derfor at forklare udviklingen gennem super Eddington masse overførsel fra ledsager stjernen til neutronstjernen. Pulsarens magnetfelt er meget usikkert for dette system. Der er to tidligere påstande om cyklotron resonans sprednings linjer, som giver et magnet felt af enten $\sim 10^{10}$ G eller $\sim 10^{12}$ G. Vores ide om masse overførslen giver også et muligt magnetfelt, der var tættere på feltet på 10^{10} G. I kapitlet bruger vi 13 års *RXTE* data og måler også rotation af pulsaren over disse 13 år.

Kapitel 3: Vi studerede det symbiotiske røntgen binære system GX 1+4, en pulsar med en rotations periode på omkring 150 s. Målet var at teste om pulsaren viste en puls fase – flux korrelation. Denne puls fase – flux korrelation - er udbredt hos millisekund røntgen pulsarerne, men det er ikke før testet om den var tilstede i de systemer der har en langsom roterende pulsar med et stærkt magnetfelt ($>10^{7-9}$G). Det var ikke muligt at finde en puls fase – flux korrelation. Dette kunne antages at være bevis for at korrelationen er umulig ved stærke magnetfelter.

Kapitel 4: I dette kapitel studerede vi Be/høj-masse røntgen systemet 4U 0115+63, med en pulsar. Dette system oplevede et type II udbrud, men i stedet for at falde til hviletilstanden forblev pulsaren i en midlertidig plateau fase. Pulsaren blev observeret med *XMM-Newton* og dets spektrum blev fittet med en sortlegme strålingsmodel, der havde et lille område, der udsendte stråling, hvilket tyder på at udstrålingen kommer fra varme pletter på overfladen af neutronstjernen. Dette blev bekræftet da man fandt pulsationer. I dette kapitel forsøgte vi at forklare udstrålingen og den langsomme aftagende lysstyrke gennem enten accretion på magnetfelt polerne eller med afkøling af neutronstjernen. Neutronstjernen opvarmes når den optager materiale ved type II udbruddet. Begge modeller giver en mulig forklaring og det har ikke været muligt at finde en endelig model.

Kapitel 5: I dette kapitel kigger vi på de tre sorte enke pulsarer, PSR J0023+0923, J2214+3000 og J2234+0944. Vi opdaterer timing løsningerne for disse tre pulsarer, ved brug af nye observationer, og finder lang tids gyldige stabile timing løsninger over en observations periode på en 7-8 år. De første sorte enke pulsarer der blev opdaget, PSRs B1957−20 og J2051+0827, er meget ustabile. Vi diskuterer muligheden for at stabiliteten skyldes at ledsager stjernen i de stabile systemer er lidt anderledes end ledsager stjernen i de ustabile systemer. Ledsager stjernen i et af de stabile systemer udfylder ikke deres Roche lobe (det var kun muligt at observerer Roche lobe udfyldningen i en af e stabile systemer), men det gør den i begge de

ustabile systemer. Det ikke at udfylde Roche lobe betyder, at ledsager stjernen er tættere bundet til sig selv, og derfor sværE at blæse i stykker. Hvis ledsager stjernen er oppustet og udfylder Roche lobe, er den løst bundet til sig selv, og den vil være lettere at blæse i stykker. Materialet der blæses af ledsager stjernen er årsag til meget materiale omkring det binære system, og det påvirker kredsløbet af det binære system og gør dem ustabile.

Publications

Refereed Publications

The X-ray pulsar 2A 1822-371 as a super-Eddington source
A. Bak Nielsen, A. Patruno, C. D'Angelo, 2017, Mon. Not. R.l Astron. Soc., **468**, 824.

The low-luminosity behaviour of the 4U 0115+63 Be/X-ray transient
A. Rouco Escorial, **A. Bak Nielsen**, R. Wijnands, Y. Cavecchi, N. Degenaar, A. Patruno, 2017, Mon. Not. R. Astron. Soc., **472**, 1802.

Coherent variability of GX 1+4
A. Bak Nielsen, A. Patruno, 2018, Mon. Not. R. Astron. Soc., **479**, 353.

Early gray dust formation in the type IIn SN 2005ip
A. B. Nielsen, J. Hjorth, C. Gall, 2018, A&A, **611**, 67.

Publications in Preparation

A study of timing stability of Black Widow pulsars
A. Bak Nielsen, G. Janssen, G. Shaifullah, J. Verbiest, L. Guillemot,
B. Stappers, A. Possenti, and the EPTA collaboration , *In prep.*

Curriculum Vitae

I was born on 14 November 1990 in Odense, Denmark. I always looked up at the night sky in fascination, although I had no ambition to become a physicist as a kid, I wanted to be a vet and live in Kenya. That quickly changed when I had my first physics lesson in 7th grade. The lesson was about Niels Bohr's model of the atom, which, to my 14 year old self, seemed to make perfect sense. After I finished school in 2006 I went on to attend Gymnasium at Odense Katedral skole. There I further developed a taste for physics and science in general, and upon graduating I applied to continue my education at University of Copenhagen studying physics. I began my university education, in Copenhagen, in 2009. I was planning on becoming a particle physicist, but quickly found out that my interests were in astronomy and not particle physics. I decided to take the astronomy courses offered, and I graduated with a bachelor degree in physics & astronomy in 2012. I did my bachelor thesis on the evolution of dust in the Milky Way under supervision of then Dr. and now Prof. Anja C. Andersen. I then went on to doing my Master thesis at the University of Copenhagen, graduating in 2014, where I worked with Prof. Jens Hjorth on early dust formation in type IIn supernovae.

I was still intrigued with astronomy and wanted to learn more, so I embarked on the process of applying to PhD positions. In the fall of 2014 I was fortunate enough to begin my PhD at Leiden Observatory under supervision of Dr. Alessandro Patruno. It is the result of that PhD which you can read in this thesis. During my PhD I have present my work at various conferences in the US, Italy, England and Russia.

The next step in my academic life will be as a PostDoc at Bielefeld University, in Germany, in collaboration with the Max Planck Institute for Radio Astronomy, working on radio pulsars.

Acknowledgements

Sofie, thank you for our movie nights and for making Copenhagen a friendly place with a fellow fynbo, and for continuing to do so. Marie Louise we have know each other for something like 20 years, how did time pass this fast? I still remember the movie nights. I am so happy to have been able to call you my friend for so long and even happier to continue so for the next many years.

Susanne, Mark, Lucas and Sebastian, thank you for always being there to help when I needed it and for inviting me to your amazing Sunday roasts.

Til min familie i Danmark, Farmor tak, du er en fantastisk farmor! Til Far, tak fordi du altid har støttet mig også selvom jeg har valgt en karierer uden for Danmark. Mor, hvad kan jeg næsten skrive, du er min inspiration hver dag, du er der altid for mig, og uden dig ville jeg ikke være nået så langt som jeg er, så tak!

Not long after starting my PhD, I meet someone who is calm, kind and patient, thank you, Jeroen.